University of Évora

ARCHMAT

(ERASMUS MUNDUS MASTER IN ARCHaeological MATerials Science)

<u>Miróbriga: Study of Roman Mortars</u>

<u>Alvin Sern Hao, CHUA</u>

Paula Cristina Gonçalves Pereira Galacho
Universidade de Évora

(Supervisor)

Patrícia Sofia Martins Moita
Universidade de Évora

(Co-Supervisor)

José Carlos Quaresma
Universidade Nova de Lisboa

(Co-Supervisor)

ARISTOTLE
UNIVERSITY OF
THESSALONIKI

UNIVERSIDADE
DE ÉVORA

SAPIENZA

Acknowledgements

Abstract

Mirobriga is a Roman site located in the municipality of Santiago do Cacém, in Setúbal, a district in the southwest of Portugal. This settlement is mentioned in the ancient literature, and the archaeological evidence suggests that the city was developed by the Romans as an urban centre around the 1st century AD. For this study, 17 mortar samples were collected from various buildings – the Western *Thermae*, *Domus* 3, *Domus* 4, *Taberna* 1, *Taberna* 2, the 'Hospedaria', the m*acellum*, and the *forum*. The chemical, mineralogical, and microstructural characterisation of the samples was performed using a number of complementary techniques – stereomicroscopy, polarised light microscopy, chemical and granulometric analysis, thermogravimetric analysis (TGA), powder X-ray diffraction (XRD), and variable pressure scanning electron microscopy-energy dispersive spectrometry (SEM-EDS). The results show that the aggregates consist mainly of quartz, whereas the binder was lime-based. The sand for the aggregates was sourced locally (within a 20 km radius), whilst the limestone for the binder may have been obtained from local quarries (within a 20 km radius), or imported from further afield (possibly from São Brissos). Most of the samples have a binder to aggregate ratio of 1 : 3, and display some degree of hydraulicity. From the results, it may be said that most of the samples are similar, indicating the contemporaneity of the buildings. Nevertheless, several samples (MRBT-1E, MRBT-2E, MRBH7-12E, MRBH7-13BE, MRBH7-13VE, and MRBF-16E) are different, which may be attributed to their function.

Keywords: *Mirobriga*, Roman mortars, stereomicroscopy, polarised light microscopy, SEM-EDS, TGA, XRD, raw materials, provenance.

Resumo

O sítio arqueológico de Mirobriga localiza-se junto à cidade de Santigo do Cacém (distrito de Setúbal) no sudoeste de Portugal. Este sítio é mencionado na literatura antiga e as evidências arqueológicas sugerem que a cidade foi desenvolvida pelos romanos, como um centro urbano, por volta do século I dC. Para este estudo, foram recolhidas 17 amostras de argamassa de vários edifícios, nomeadamente, Termas Ocidentais, *Domus* 3 e 4, Taberna 1 e 2, a Hospedaria, *macellum* e fórum. A caracterização química, mineralógica e microestrutural das amostras foi realizada por recurso a técnicas complementares – estereomicroscopia, microscopia de luz polarizada, análise química e granulométrica, análise termogravimétrica (ATG), difração de raios-X (DRX), microscopia eletrónica de varrimento com espectroscopia de raios X por dispersão de energias (MEV-EDS). Os resultados mostram que a maioria das amostras são similares, nomeadamente, no que respeita ao tipo de agregados, com predomínio de quartzo e ao tipo de ligante, cal calcítica. A areia para os agregados era de proveniência local (num raio de 20 km) enquanto que o calcário para o ligante pode ter sido obtido em pedreiras locais (num raio de 20 km) ou transportado de mais longe (provavelmente de São Brissos). A maioria das amostras apresenta uma razão ligante agregado de 1:3 e um grau de hidraulicidade análogo., indicando a contemporaneidade dos diferentes edifícios estudados. As diferenças observadas em algumas amostras (MRBT-1E, MRBT-2E, MRBH7-12E, MRBH7-13BE, MRBH7-13VE, and MRBF-16E) podem ser atribuídas à função desempenhada pelas mesmas.

Palavras-chave: *Mirobriga*, argamassas romanas, esteromicroscopia, microscopia de luz polarizada, MEV-EDS, ATG, DRX, matérias primas, proveniências.

Index

List of Figures

List of Tables

List of Annexes

1. Introduction

1.1. Historical Context

The archaeological site of Chãos Salgados (more commonly known as *Mirobriga*) is located in the municipality of Santiago do Cacém, in Setúbal, a district in the southwest of Portugal. Situated on the western slope of the Grândola mountain range, the ruins of this Roman settlement are close to the present town of Santiago do Cacém.

Reference to *Mirobriga* in the ancient sources can be found in Pliny's *Natural History*. In Book IV, Chapter XXII, Pliny lists 'Mirobricenses surnamed Celtici' (*Mirobricenses qui Celtici cognominantur*) as one of the tributary towns (*stipendiaria*) of Lusitania. *Mirobriga* is also mentioned in Ptolemy's *Geography*, as well as in the *Antonine Itinerary* (Alarcão, 1976, p. 584). Be that as it may, apart from these passing references, the ancient authors are silent about *Mirobriga*. It may be added that although the site has been long known and identified, it was only in 1957 that *Mirobriga*'s identity was confirmed, in the form of inscriptions found at the site that named the settlement (Alarcão, 1967, p. 175).

Archaeology has contributed greatly to the current understanding of the site, more so than the writings of ancient authors and the epigraphic evidence. The archaeological evidence indicates that the site of *Mirobriga* was already occupied by the indigenous Celtici population during the Iron Age. This is apparent on the hill known as Castelo Velho, where the *forum* now stands. Fernando de Almeida speculated that this was where the pre-Roman settlement was situated, and was proven to be right by Tavares da Silva and Joaquina Soares, who studied the unstratified ceramics from the site (Biers et al., 1983, p. 38). Additionally, it was in this area that a "proto-Roman temple of the Celtic type", believed to have belonged to the Late / Second Iron Age, i.e. the 4th century BC, was discovered in 1982 (Biers et al., 1983, p. 40; Slane et al., 1984, pp. 55-56). In the following year, an earlier temple, dated to the Early / First Iron Age, i.e. the 8th / 9th century BC was discovered beneath the 4th century temple (though separated by a gap, i.e. "a layer of dark earth filled with charcoal, pebble-sized schist, feldspar, quartz and small rounded pink limestones), suggesting that a settlement was already in existence during this period (Slane et al., 1984, pp. 54-56).

In the stratigraphic layer designated as the final phase of the Iron Age "Celtic Temple", i.e. around 100 BC, Roman pottery appears for the first time, a sign that contact between the indigenous Celtic population and the Romans had been established during that time (Slane et al., 1984, p. 58). The "Roman urban development program" (Slane et al., 1984, p. 58) is reckoned to have occurred in the 1st century AD, during the reign of either Claudius or Nero, as evidenced by the "Pottery excavated from

1

beneath the foundations for paving slabs in the south corner of the *forum* and from beneath street paving slabs in front of the South Building" (Biers et al., 1983, p. 36). This fits the general trend that occurred in the Iberian Peninsula. The Roman provinces of Hispania Citerior and Ulterior were created in 197 BC, though it was only from the reign of Augustus onwards, i.e. the end of the 1st century BC and the beginning of the 1st century AD, that the adoption of Roman architecture can be seen in the archaeological evidence (Keay, 1995, cited in Revell, 2013, p. 386).

The settlement continued to develop during the Roman period, with new structures added or existing ones enlarged over time. As an example, the excavation of the *thermae*, which consists of the East Baths and West Baths, indicated that the two structures were built at different times. Pottery form the former provides a *terminus post quem* of the Flavian period (i.e. the second half of the 1st century AD) for its construction, whilst the building of the latter has been dated to the 2nd century AD. *Mirobriga* was abandoned several centuries later. Different dates, however, have been proposed regarding the abandonment of the site. The Luso-American team, for instance, point to the coins and pottery lying on the floor of one of the excavated houses as potential markers for the abandonment of the area during the 3rd / 4th century AD (Slane et al., 1985, p. 35). On the other hand, the excavation of three structures in residential area by Filomena Barata has led to the proposition that the site was abandoned during the middle of the 5th century AD (Quaresma, 1999b, cited in Quaresma, 2010, p. 350), whilst a piece of Phocaean red slip (Hayes form 3) in the abandonment layer of '*Domus* 3' may be an indication that the site continued to be occupied up until the first half of the 6th century AD (Quaresma, 2010, p. 351).

The first modern description of *Mirobriga* was made during the 16th century by a Portuguese Dominican friar from Évora, André de Resende (Quaresma, 2012, p. 25). It was, however, only during the 19th century that the site was first excavated, under the direction of Frei Manuel do Cenáculo, an Archbishop of Évora (Quaresma, 2012, p. 25). The excavation of the site continued in the following century, under the direction of various archaeologists. Of note are the campaigns of Fernando de Almeida (between 1959 and 1979), during which the first monograph of the site was produced (Quaresma, 2012, p. 25; Soren & Soren, 1996, p. 76), and those of the Luso-American team during the 1980s. The latter was a collaboration between the University of Missouri-Columbia, the University of Évora, and the Southern Regional Archaeological Services of the Portuguese Institute of Cultural Heritage (*Serviços Regionais de Arqueologia do Sul do Instituto Português do Património Cultural*), which is noteworthy for being the first systematic investigation of the site (Quaresma, 2012, pp. 12, 25).

Whilst *Mirobriga* continued to be excavated during the 1990s, it was also during this time that its development into a tourist destination commenced. During this decade, management of the site was taken over by the Portuguese Institute of Architectural Heritage (*Instituto Português do Património Arquitectónico*), the lands surrounding the site were acquired, and the construction of a Reception and Interpretation Centre (*Centro de Acolhimento e Interpretação*) was approved (Direção-Geral do Património Cultural, Ministério da Cultura, 2011).

The excavation of *Mirobriga* is ongoing, and the latest project, 'TabMir. Tabernae of Mirobriga, Chãos Salgados, Santiago do Cacém: A Study-Case on Roman and Late Antique Economy in Lusitania' (*As tabernae de Mirobriga, Chãos Salgados, Santiago do Cacém: um estudo de caso da economia romana e tardo-antiga na Lusitania*), which is under the direction of José Carlos Quaresma, runs from 2016 to 2019 (J. C. Quaresma, pers. comm., 19 May 2018).

The excavations at *Mirobriga* over the decades have brought a variety of structures to light. The public structures, such as the *forum* and *thermae*, no doubt received the most attention due to their prominence. Nevertheless, a number of domestic structures, including several *domus*, and the 'Hospedaria' (which in fact is another *domus*) (J. C. Quaresma, pers. comm., 24 May 2018), have been investigated. Moreover, the commercial structures of the site are currently being studied, as part of the TabMir project. A *taberna* was excavated during the 2017 season, whilst a second one, as well as part of the *macellum*, were the focus of the 2018 season (J. C. Quaresma, pers. comm., 23 April 2018).
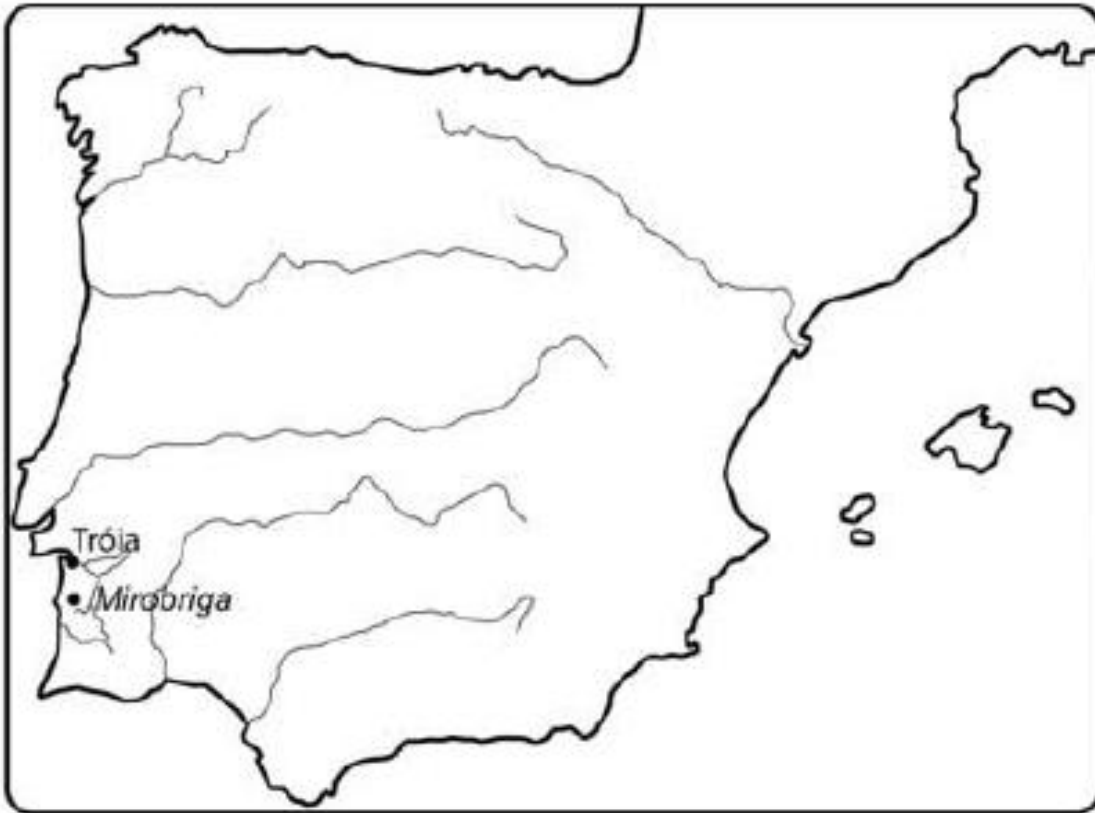
Figure 1.1. The location of *Mirobriga* in the Iberian Peninsula (taken from Quaresma, 2010, p. 348).

a. The Western *Thermae*	b. *Taberna* 1 (left) and 2 (right)	c. *Domus* 4
d. *Domus* 3	e. The *macellum (cryptoporticus*?)	f. The *forum* (temple podium)

Figure 1.2. The various archaeological structures at *Mirobriga.*

Figure 1.3. Location of the mortar samples in the general plan of the site (plan taken from Quaresma, 2012, p. 29, Fig. 4).

1.2. Mortar

Mortar is a building material that has been widely used in various parts of the world throughout history. Due to its workability, this material has been employed for a range of purposes in the construction of buildings. Amongst other things, mortar is used to fill the gaps between bricks or stones, thereby joining them, as a render to cover the external surface of walls, and as plaster for the painting of frescoes. In general, mortar is composed of three elements – an aggregate, a binder, and water, which are combined to form a paste (Borelli, 1999, p. 3; Schnabel, 2008, p. 1).

The aggregate forms the bulk of any mortar, volumetrically speaking, and its main function is to minimise the shrinkage that may occur in the mortar paste as it sets (Schnabel, 2008, p. 1). In most instances, the aggregate is an inert material, such as sand or crushed rocks, though in some cases, chemically reactive materials, including crushed bricks or ceramics, may be used. The most regularly used aggregate in mortars is natural sand, normally in one of its two most common forms, *i.e.* quartz or carbonate. Through the observation of the size and shape of the sand grains, as well as the identification of trace constituents, much information about the source of the aggregate may be obtained (Schnabel, 2008, p. 2).

The binder is the material that holds the aggregate together, and may be divided into two main types – non-hydraulic and hydraulic binders. The former solidifies through dehydration (the loss of water) and carbonation (the absorption of carbon dioxide), whilst the latter uses up water during the process of solidification. Non-hydraulic binders used in the past include clay, gypsum, and lime, whilst hydraulic lime and Portland cement are some examples of hydraulic binders (Borelli, 1999, pp. 4-9; Schnabel, 2008, p. 2).

Apart from the aggregate and binder, some mortars may also contain additives and admixtures. A wide range of materials fall in this category, and includes not only inorganic materials (*e.g.* iron filings and crushed ceramics), but also organic ones (*e.g.* blood and egg whites) (Schnabel, 2008, p. 3; Sickels, 1982, cited in Schnabel, 2008, p. 3). The addition of such substances serves to modify the properties of the mortar, either aesthetically (*e.g.* to give colour to the mortar), or physically (*e.g.* to improve the strength of the mortar) (Borelli, 1999, p. 4; Schnabel, 2008, p. 3).
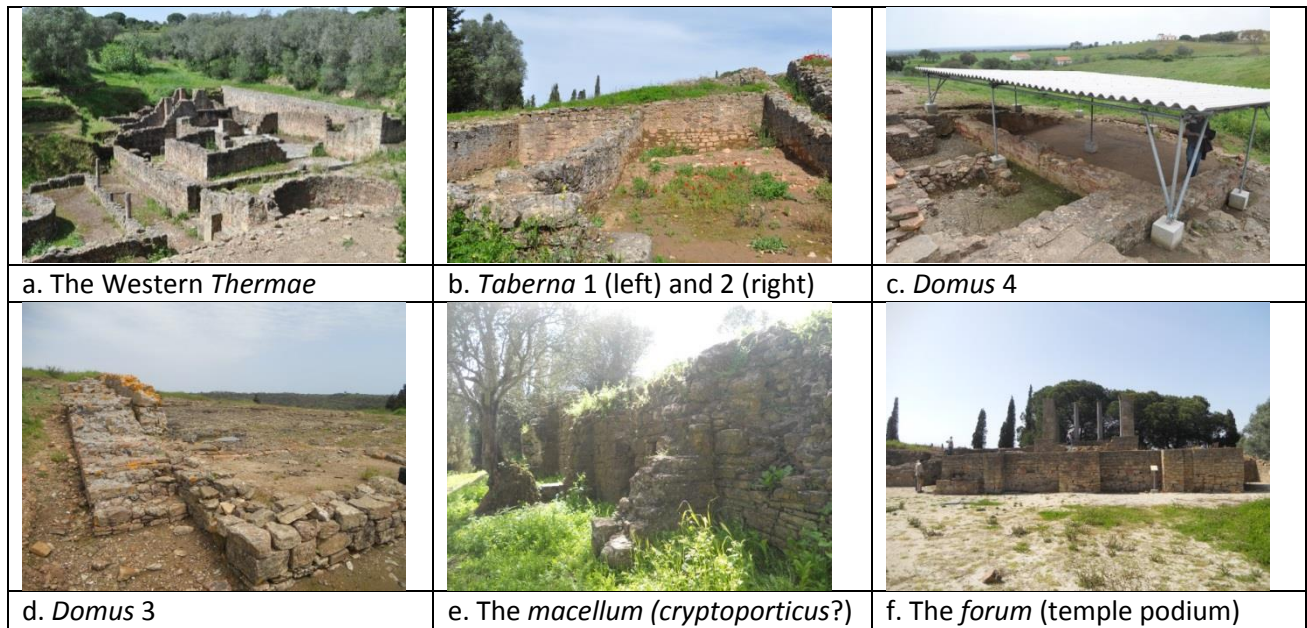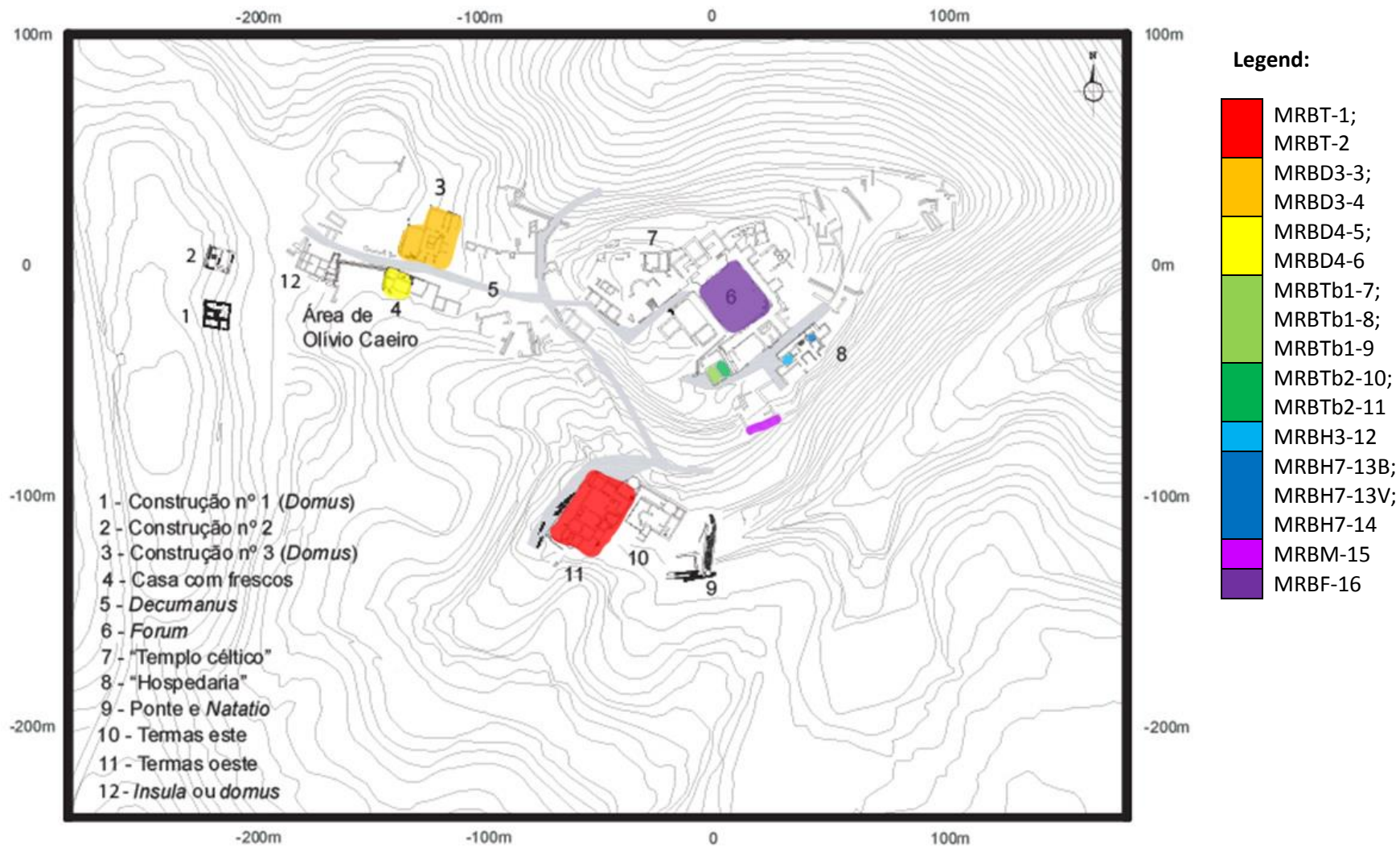
Roman mortar was lime-based, and the ancient Greeks have been widely credited with the initiation of its large-scale use in Europe during the Classical period (Davey, 1961, cited in Hughes & Válek, 2003, p. 5). This technology was later adopted by the Romans, who greatly improved it through the invention of concrete. The importance of this new material is evident, as it was used extensively for

concrete constructions across much of the Roman world from the 1ˢᵗ century BC onwards (Wright, 2005, p. 176).

Like all mortars, Roman lime-based mortar consisted of an aggregate, a binder (in this case lime), and water. One of the most important sources of information for the aggregate and binder used for the production of Roman mortar is Vitruvius' *On Architecture*. This information may be found in Book II of his multi-volume work. It may be added that some information on this subject can also be found in Pliny's *Natural History*, specifically in Book XXXVI.

Sand was commonly used as an aggregate by the Romans. In both Vitruvius' *On Architecture* (Book II, Chapter IV) and Pliny's *Natural History* (Book XXXVI, Chapter LIV), three different types of sand are distinguished – pit sand, river sand, and sea sand. Vitruvius goes on to discuss the advantages and disadvantages of each variety of sand, and provides simple instructions to determine whether a sand is suitable for use as an aggregate.

With the regards to the binder, both Vitruvius (*On Architecture*, Book II, Chapter V, 1) and Pliny (*Natural History*, Book XXXVI, Chapter LIII) agree that the best lime is obtained from the burning of white limestone. Both authors also distinguish two types of stone – hard and soft, for the production of lime. The former is better suited for structural parts, whilst the latter for plasters. Additionally, the burning of lime is mentioned in both works, and a detailed explanation of the 'science' behind this process is provided by Vitruvius (*On Architecture*, Book II, Chapter V, 2):

"The reason why lime makes a solid structure on being combined with water and sand seems to be this: that rocks, like all other bodies, are composed of the four elements. Those which contain a larger proportion of air, are soft; of water, are tough from the moisture; of earth, hard; and of fire, more brittle. Therefore, if limestone, without being burned, is merely pounded up small and then mixed with sand and so put into the work, the mass does not solidify nor can it hold together. But if the stone is first thrown into the kiln, it loses its former property of solidity by exposure to the great heat of the fire, and so with its strength burnt out and exhausted it is left with its pores open and empty. Hence, the moisture and air in the body of the stone being burned out and set free, and only a residuum of heat being left lying in it, if the stone is then immersed in water, the moisture, before the water can feel the influence of the fire, makes its way into the open pores; then the stone begins to get hot, and finally, after it cools off, the heat is rejected from the body of the lime."

This process is known today as the lime cycle, and is explained through chemistry as follows:

1. When calcium carbonate ($CaCO_3$), *e.g.* limestone, is burnt in a kiln at high temperatures. i.e. between 900 and 1000 °C, calcium oxide (CaO), known as quicklime or burnt lime, is produced, and carbon dioxide (CO_2) is released. This process is known as calcination.

$$CaCO_3 \text{ (s)} \xrightarrow{\Delta} CaO \text{ (s)} + CO_2 \text{ (g)} \qquad \text{(Eq. 1)}$$

2. Water (H_2O) is added to hydrate the quicklime in a process known as slaking, thus forming calcium hydroxide [$Ca(OH)_2$], which is referred to as slaked or hydrated lime. As an exothermic reaction, heat is released. If just enough water is added during the slaking process, the resultant slaked lime will be a in a dry powder form. If excess water in added, however, the final product will be in a paste form known as lime putty.

$$CaO \text{ (s)} + H_2O \text{ (l)} \longrightarrow Ca(OH)_2 \text{ (s)} + \text{heat} \qquad \text{(Eq. 2)}$$

3. As slaked lime is turned into mortar (by adding the aggregate, and additional water if necessary), applied onto a structure, and left to dry, it loses water, and absorbs carbon dioxide from the surrounding atmosphere. As a result of this, the slaked lime returns to its original form, i.e. calcium carbonate, causing the mortar to harden.

$$Ca(OH)_2 \text{ (aq)} + CO_2 \text{ (g)} \longrightarrow CaCO_3 \text{ (s)} + H_2O \text{ (l)} \qquad \text{(Eq. 3)}$$
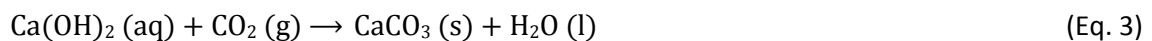
Another piece of important information provided by the ancient authors about Roman mortar is the ratio between the binder and the aggregate. In *On Architecture*, Book II, Chapter V, 1, Vitruvius states that the ratio of binder depends on the type of sand. For pit sand, the ratio of binder to aggregate is given as 1:3, whilst for river and sea sand, 1:2. Pliny (*Natural History*, Book XXXVI, Chapter LIV), on the other hand, provides a different recipe. For pit sand, a 1:4 binder to aggregate ratio is provided, whilst for river and sea sand, 1:3. Both writers agree, however, that the quality of mortar made with river or sea sand may be improved by adding powdered baked bricks or ceramics to the mixture.

The **Lime** Cycle

Water-born Carbon Dioxide (CO_2) is absorbed over time to form Calcium Carbonate ($CaCO_3$)

Burning limestone in a kiln drives off Carbon Dioxide (CO_2) and water (H_2O)

Limestone from the quarry

CARBONATION

BURNING

Limestone
Calcium Carbonate
($CaCO_3$)

Slaked lime (putty) is mixed with selected sands to produce mortars and plasters, or with water to produce limewash

Burnt lime is also known as quicklime or lumplime

Slaking Lime
Calcium Hydroxide
($Ca(OH)_2$)

Burnt Lime
Calcium Oxide
(CaO)

SLAKING

Heat

Slaking burnt lime in either:

or iii) in damp sand to produce a hot mix

i) an excess of water to produce a putty

or ii) a shortfall of water to produce a powder (hydrate)

Figure 1.4. The lime cycle, taken and adapted from Tŷ-Mawr Lime Ltd (https://www.lime.org.uk/community/the-lime-cycle/lime-and-its-production.html).

1.3. Aims and Objectives

The aims of this thesis were three-fold:

1. To identify and characterise the raw materials (the aggregate, binder, and additives) that were used for the production of the mortars.

2. To determine the provenance of the raw materials.

3. To study the technology employed for the production of the mortars.

A number of complementary techniques were used to analyse the samples. With these techniques, the chemical, mineralogical, and microstructural characterisation of the mortar could be achieved.

Additionally, by combining the results of these analyses with the geological survey of the region around *Mirobriga*, and with the writings of ancient Roman authors, the provenance of the raw materials, as well as the production technique of the mortars could be determined.

Moreover, comparisons between the mortars were made according to their function, and the type of structures they were taken from.

2. Methodology

The methodology for the analysis of the mortars in this study is as follows:

2.1. Sampling

A total of 17 mortar samples were collected from the site. Some samples (MRBT-1, MRBT-2, MRBH3-12, MRBH7-13B, MRBH7-13V, and MRBF-16) have stratigraphic layers, and hence divided into external and internal layers (marked by an 'E' and an 'I' respectively at the end of the sample's name). The samples were taken from eight different buildings (see Annex 2.1. and 2.2.), which may be divided according to their function, *i.e.* domestic, commercial, or public. Archaeologists were present to aid the sample collection process.

As a general rule, mortars that could be easily dislodged were preferred, as this minimised the damage inflicted on the aesthetics of the structure. When necessary, however, a hammer and chisel was used to procure the mortar sample. In addition, several samples were obtained from the depot, where they were collected and stored during previous excavations. In certain areas, namely the *thermae*, where restoration work had been carried out in the past, precaution was taken not to collect the restoration material, *i.e.* cement. After being photographed, the samples were placed in individual transparent plastic bags, and labelled.

2.2. General Sample Preparation

The samples were photographed with a *Nikon COOLPIX S2500* digital camera (see Annex 2.3.), and a preliminary visual assessment was made. The samples were dried by leaving them in an oven overnight at 50 °C. After the samples cooled down, they were cleaned using brushes and a chisel. Traces of dirt, soil, and biological colonisation were removed. The samples were observed under a *Leica M205 C* stereo microscope (Leica Camera AG, Wetzlar, Germany), and the images were acquired with a *Leica DFC290 HD* digital camera (Leica Camera AG, Wetzlar, Germany) (see Annex 2.3.).

The specific sample preparation for each technique will be discussed in the sections that follow.

2.3. Stereo Microscopy

Stereo microscopy was used to provide a preliminary assessment of the samples in terms of consistency, morphology and dimension of the aggregates, inclusions (*eg.* ceramic fragments), and the presence of stratigraphic layers.

The samples prepared for SEM-EDS (see 2.8.) were used for this technique.

A *Leica M205 C* stereo microscope (Leica Camera AG, Wetzlar, Germany) was used to observe the samples, and the images were acquired with a *Leica DFC290 HD* digital camera (Leica Camera AG, Wetzlar, Germany).

2.4. Polarised Light Microscopy

Polarised light microscopy was used for the visual identification of the aggregates within the samples, as well as their grain size and texture.

In the samples where stratigraphy was present (MRBT-1, MRBT-2, MRBH3-12, MRBH7-13B, MRBH7-13V, and MRBF-16), the pieces were removed by cutting them with the *Discoplan-TS* (Struers, Cleveland, Ohio, USA), so as to preserve the stratigraphic layers. The rest of the samples were removed with the aid of a rubber mallet and a chisel. The samples were then embedded in epoxy resin (*EpoFix Resin* and *EpoFix Hardener*, Struers, Cleveland, Ohio, USA), in accordance with the manufacturer's instructions. The embedding was done at room temperature and pressure. After the resin hardened, the surface of each sample was polished by hand with P # 280 SiC paper, and then with P # 1000 SiC paste. The glass slides were also mechanically polished with the P # 400 SiC paste on a millstone. Once the polishing of the samples and the slides were completed, resin (EpoThin resin and EpoThin hardener, 2.0 : 0.9) was used to mount the samples onto the slides, after which they were left overnight under pressure. The samples were cut using the diamond blade of a *Discoplan-TS* (Struers, Cleveland, Ohio, USA), and grinded with the same machine. The samples were then polished by hand using P # 1000 SiC paste until a thinness of 0.03 mm was reached. The final polishing was done with P # 4000 SiC paper, and the samples were coated with a layer of lacquer for protection.

The finished thin sections were observed with a *Leica DM2500 P* polarising microscope (Leica Camera AG, Wetzlar, Germany), under both plane polarised light (PPL) and cross polarised light (XPL), and the images were acquired with a *Leica MC170 HD* digital camera (Leica Camera AG, Wetzlar, Germany).

2.5. Chemical and Granulometric Analysis

Chemical analysis was used to determine the ratio between the soluble fraction and the insoluble residue of the samples, whilst granulometric analysis was used mainly to quantify the size distribution of the grains in the insoluble residue. The latter also allowed the composition and morphology of the insoluble residue to be identified.

Approximately 20 g of material was removed from the main samples. MRBTb1-9 and MRBH3-12 were not analysed, as there was not enough material. Additionally, for MRBT-2, MRBH7-13B, and MRBH7-13V, each stratigraphic layer was prepared and analysed separately. On the other hand, the analysis was only performed on the internal layers of MRBT-1 and MRBF-16.

The samples were subjected to acid attack (10 g) with hydrochloric acid (HCl, concentration of 1:3 v/v %, 120 mL), heated to boiling temperature for 10 minutes, filtered in vacuum, and washed with distilled water. By this means, the soluble fraction and insoluble residue were separated. The insoluble residues were left to dry overnight (in an oven at around 50 °C), and weighed the following day. The procedure was performed in duplicate, and the average values of the results from each sample were recorded.

Granulometric analysis was performed by sieving the insoluble residue with a stainless steel sieve (ASTM E11, diameter of 100 mm x 40 mm, with the following mesh sizes: 4, 2, 1, 0.500, 0.250, 0.125, and 0.063 mm). The different fractions of the insoluble residue were weighed, and observed under a *Leica M205 C* stereo microscope (Leica Camera AG, Wetzlar, Germany), after which images were acquired with a *Leica DFC290 HD* digital camera (Leica Camera AG, Wetzlar, Germany). The average values of the results obtained from each sample were recorded.

2.6. Thermogravimetric Analysis

Thermogravimetric Analysis (TGA) was used primarily to quantify the amount of binder with a carbonate composition. The first derivative of the TG curve (the DTG curve) shows the rate of change of the sample's mass during the analysis, and allowed the decomposition temperature of certain compounds in the samples to be determined more accurately. By combining the results of this analysis with those obtained from the chemical analysis, the aggregate: carbonate: solubles ratio of the samples could be calculated. The global fraction was used for this analysis.

The samples were first grounded into a fine powder. With the exception of MRBH3-12 (both external and internal layers), which was grounded manually with an agate mortar and pestle, the rest of the samples were grounded with a ball mill, *Planetary Ball Mill PM 100* (Retsch GmbH, Haan, Germany), at 500 rpm for a duration of 10 minutes. It may be added that for MRBT-2, MRBH3-12, MRBH7-13B, MRBH7-13V, and MRBF-16, each stratigraphic layer was prepared and analysed separately, whilst the analysis was only performed on the internal layer of MRBT-1.

The powdered samples were analysed in a simultaneous thermal analyser, *STA 449 F3 Jupiter* (NETZSCH-Gerätebau GmbH, Selb, Germany), under inert atmosphere (nitrogen – 70 ml/min.), with a uniform heating velocity of 10°C/min. from 40 to 1000 °C.

2.7. Powder X-Ray Diffraction

Powder X-Ray Diffraction (XRD) was used to determine the mineralogical composition of the samples by identifying their crystalline phases. The global and the fine fractions (which contains a higher concentration of the binder, *i.e.* particles **<** 0.063 mm in size) of the samples were used for this analysis.

For both analyses, it was necessary for the samples to be grounded into a fine powder. For the global fraction, this was done with a ball mill, *Planetary Ball Mill PM 100* (Retsch GmbH, Haan, Germany), at 500 rpm for a duration of 10 minutes. MRBH3-12 (both external and internal layers) was the exception, as it was grounded manually with an agate mortar and pestle. For MRBT-2, MRBH3-12, MRBH7-13B, MRBH-13V, and MRBF-16, each stratigraphic layer was prepared and analysed separately, whilst for MRBT-1, only the internal layer was analysed. As for the fine fraction, the samples were first disaggregated using a rubber mallet, and then passed through a stainless steel sieve with a mesh size of 0.063 mm (ASTM E11, diameter of 100 mm x 40 mm). XRD analysis of the fine fraction was not performed on MRBD4-5, MRBTb1-9, and MRBH3-12, as well as MRBT-1E, MRBH7-13BE, MRBH7-13VE, and MRBF-16E.

The diffractograms were produced using an X-ray diffractometer, *Bruker AXS-D8 Advance* (Bruker Corp, Billerica, Mass. USA), with Cu-Kα radiation (λ = 0.1540598 nm), under the following conditions: scanning between 3° and 75° (2θ), scanning velocity of 0.05° 2θ/s, accelerating voltage of 40 kV, and current intensity of 30 mA.

2.8. Variable Pressure Scanning Electron Microscopy-Energy Dispersive Spectrometry

Scanning Electron Microscopy (SEM) was utilised for imaging purposes, which allowed the morphology of the aggregates to be assessed. To a lesser extent, a preliminary elemental analysis (based on brightness) was undertaken. The process made use of the back-scattered electrons (BSE) produced by the samples. Energy Dispersive Spectroscopy (EDS), on the other hand, utilised the X-ray emissions from the samples for elemental analysis, elemental mapping, and punctual analyses.

A small piece of each sample was selected for this technique. A rubber mallet and a chisel were used to remove these pieces. In the samples where stratigraphy was present (MRBT-1, MRBT-2, MRBH3-12, MRBH7-13B, MRBH7-13V, and MRBF-16), the pieces were removed by cutting them with the

Discoplan-TS (Struers, Cleveland, Ohio, USA), so as to preserve the stratigraphic layers. Next, the samples were observed under a *Leica M205 C* stereo microscope (Leica Camera AG, Wetzlar, Germany), and images were acquired with a *Leica DFC290 HD* digital camera (Leica Camera AG, Wetzlar, Germany). Epoxy resin (*EpoFix Resin* and *EpoFix Hardener*), prepared in accordance with the manufacturer's instructions, was used to embed the samples. The embedding was done at room temperature and pressure. After the resin hardened, the surface of each sample was polished by hand. Silicon carbide (SiC) paste of different grit sizes, *i.e.* P # 400, P # 800, and P # 1000 (from coarse to fine) was used. The final polishing of the samples was done on SiC paper (P # 2400 and P # 4000).

A *Hitachi S-3700N* SEM (Hitachi High Technologies, Berlin, Germany) coupled with a *Bruker XFlash 5010 SDD* detector (Bruker Corp, Billerica, Mass. USA) was used for the sample analysis. The analysis samples were performed under low vacuum, *i.e.* 40 Pa, with a current of 20 kV. The spectra were plotted on an energy scale of 0-20 keV, with a spectral resolution of 129 eV at Mn Kα.

3. Results

3.1. Sampling and Preliminary Observations

A general description of each sample is presented in Table 3.1, which includes the following aspects: the structure and location where each sample was collected from, the historical period, the function of the mortar, their colour, and inclusions seen in them.

The samples were collected from public, commercial, and domestic buildings. From the public buildings, two samples (MRBT-1 and MRBT-2) (Annex 3.1., Figure 1) were collected from the *thermae*, whilst a sample was collected from the *forum* (MRBF-16) (Annex 3.1., Figure 5). From the commercials buildings, five samples were taken from two *tabernae*, *Taberna* 1 (MRBTb1-7, MRBTb1-8, and MRBTb1-9) (Annex 3.1., Figure 4), and *Taberna* 2 (MRBTb2-10, and MRBTb2-11) (Annex 3.1., Figure 4), whereas from the *macellum*, a sample (MRBM-15) (Annex 3.1., Figure 4) was collected. The rest of the samples were collected from domestic buildings, *i.e.* the *domus*, and the 'Hospedaria'. For the former, two samples each were collected from *Domus* 3 (MRBD3-3 and MRBD3-4) (Annex 3.1., Figure 2), and *Domus* 4 (MRBD4-5 and MRBD4-6) (Annex 3.1., Figure 3). As for the latter, a sample was collected from Room 3 of the 'hospedaria' (MRBH3-12) (Annex 3.1., Figure 4), whilst three samples were taken from Room 7 of the same structure (MRBH7-13B, MRBH7-13V, and MRBH-14) (Annex 3.1., Figure 4). Most of the samples were collected from walls, though several of them were taken from other parts of the buildings. MRBD3-4, and MRBD4-5 were taken from stairs, the former being attached to *Domus* 3, whilst the latter coming from the street outside *Domus* 4. MRBTb2-11 was collected at the entrance of *Taberna* 2, whereas MRBM-15 was taken from what is believed to be the *cryptoporticus* of the *macellum*.

All the structures have been dated to the Roman period, specifically between the 1st and 2nd centuries AD. As the samples may be said to be contemporaneous, it would neither be possible nor necessary to divide the samples according to historical periods.

The samples may be classified according to their function. The majority of them have been identified as filling mortars, though several of them, namely MRBT-1, MRBTb1-9, and MRBH7-14, have been designated as rendering mortars. In certain samples (MRBT-1, MRBT-2, MRBH3-12, MRBH7-13B, and MRBH7-13V, and MRBF-16), stratigraphic layers were identified, and these layers served different functions. MRBT-2I served as a filling mortar, MRBT-2E functioned as a render. MRBH3-12, MRBH7-13B, and MRBH7-13V were taken from frescoes, and, in addition to the chromatic layer, contain two stratigraphic layers that may be considered to be mortars. The internal layer of these three samples may either be the "very rough rendering coat" or the "layers of sand mortar", as described by Vitruvius in his

16

treatment of stucco work (*On Architecture*, Book VII, Chapter III, 5). As for the outer layer of these samples, these are likely to be Vitruvius' "layers of marble powder" (*On Architecture*, Book VII, Chapter III, 6). Although the rendering coat / sand mortar, and marble powder layer were also visible in MRBT-1 and MRBF-16, it may be noted that it is unclear whether these samples once had chromatic layers on them.

In terms of colour, the samples are quite uniform, as most of them are beige in colour. The exceptions are MRBT-1E, MRBT-2E, MRBH3-12E, MRBH7-13BE, and MRBH7-13VE, MRBF-16E. These samples are white in colour, with the exception of MRBT-2E, which has a red colour.

As for inclusions, lime lumps were visible in almost all of the samples, whilst numerous samples contained ceramic fragments. The latter is especially evident in MRBT-2E, and the red colour of this layer is due to the addition of powdered bricks / ceramics. In addition, relatively large lithic fragments (as aggregates) were observed in certain samples, for instance, MRBT-2I and MRBD3-3.

Table 3.1. General description of the samples.

Sample	Structure	Location	Period	Function	Colour	Inclusions	Notes
MRBT-1	Western *Thermae*	Frigidarium; south wall; internal; from the upper part of the wall	Roman	E: Layer of 'powdered marble'	E: White	-	Two layers of mortar
				I: Rendering / 'sand mortar' for stucco	I: Beige	Lime lumps	
MRBT-2	Western *Thermae*	Frigidarium; north wall; internal; between marble skirting and wall	Roman	E: Rendering	E: Red	E: Lime lumps, ceramic fragments	Heterogeneous stratigraphy; external layer very fragile
				I: Filling	I: Beige	I: Lime lumps, stones	
MRBD3-3	*Domus* 3	North wall; external	Roman	Filling	Beige	Lime lumps, stones	
MRBD3-4	*Domus* 3	Stairs; external	Roman	Filling	Beige	Lime lumps	
MRBD4-5	*Domus* 4	Stairs from the street	Roman	Filling	Beige	Lime lumps	
MRBD4-6	*Domus* 4	North wall; internal	Roman	Filling	Beige	Lime lumps	
MRBTb1-7	*Taberna* 1	South wall; external; from the top of the wall	Roman	Filling (?)	Beige	Lime lumps, ceramic fragments	
MRBTb1-8	*Taberna* 1	East wall; internal, between Tb1 and Tb2; from the top of the wall	Roman	Filling (?)	Beige	Lime lumps, ceramic fragments	
MRBTb1-9	*Taberna* 1	North wall; internal, from the vertical face of the wall	Roman	Render (?)	Beige	Lime lumps	
MRBTb2-10	*Taberna* 2	East wall; external; adjacent to the street	Roman	Filling	Beige	Lime lumps	
MRBTb2-11	*Taberna* 2	Entrance	Roman	Filling	Beige	Lime lumps, ceramic fragments	
MRBH3-12	'Hospedaria', Room 3	North wall; internal; wall with paintings	Roman	E: Layer of 'powdered marble'	E: Orange, white	-	Heterogeneous stratigraphy; internal layer fragile; chromatic layer and two layers of mortar
				I: Rendering / 'sand mortar' for stucco	I: Beige	I: Lime lumps	

Table 3.1. General description of the samples (cont.).

MRBH7-13B	'Hospedaria', Room 7	Northeast wall; internal	Roman	E: Layer of 'powdered marble'	E: White	-	From the depot; homogenous stratigraphy, chromatic layer, two layers of mortar
				I: Rendering / 'sand mortar' for stucco	I: Beige	I: Lime lumps	
MRBH7-13V	'Hospedaria', Room 7	Northeast wall; internal	Roman	E: Layer of 'powdered marble'	E: Red, white	-	From the depot; homogenous stratigraphy, chromatic layer, two layers of mortar
				I: Rendering / 'sand mortar' for stucco	I: Beige	I: Lime lumps, stones	
MRBH7-14	'Hospedaria', Room 7	South wall; internal	Roman	Rendering	Beige	Lime lumps	
MRBM-15	*Macellum*	Back of structure, *cryptoporticus* (?); internal (?)	Roman	Filling	Beige	Lime lumps	*Macellum* yet to be excavated
MRBF-16	*Forum*	Podium of the temple	Roman	E: Layer of 'powdered marble'	E: White	-	Two layers of mortar
				I: Rendering / 'sand mortar' for stucco	I: Beige	I: Lime lumps	

3.2. Stereo Microscopy

The results of stereo microscopy suggest that, as a whole, there is little difference, in terms of composition, between the samples. Within each individual sample, however, the composition may be said to be heterogeneous. The use of stereo microscopy also allowed the stratigraphic layers of MRBT-1 and MRBF-16 to be verified.

For the majority of the samples, the aggregate consists mainly of hyaline and milky quartz (some of the latter possibly being feldspars). The quartz grains may be described as uniform, and its roundness ranging from 'subangular' to 'well-rounded' (Figure 3.1.a.). Black minerals (later identified as ilmenite), and lime lumps (associated with the binder) (Figure 3.1.b.) were also visible in the samples.

Both layers of MRBT-2 are noticeably different from the rest of the samples. MRBT-2E is distinct due to the red colour of its binder, and the presence of ceramic fragments (Figure 3.1.e.) of various colours, *i.e.* red, grey, and black, as aggregates, whilst the use of a higher quantity of relatively large lithic fragments (as aggregates) (Figure 3.1.d.) were observed in MRBT-2I. Additionally, a transitional layer (Figure 3.1.f.) was observed between the two layers of this sample. MRBT-1E, MRBH3-12E, MRBH7-13BE, MRBH7-13VE, and MRBF-16E are also clearly different, due to the presence of 'angular' / euhedric calcite grains (Figure 3.1.c., see yellow arrow) in them.

a. Hyaline quartz and milky quartz / feldspar (MRBD3-4)	b. A lime lump (MRBTb1-9)	c. Chromatic layer and calcite crystals (MRBH3-12)
d. A lithic (dolomite) fragment (MRBT-2I)	e. A ceramic fragment (MRBT-2E)	f. The transition layer in MRBT-2
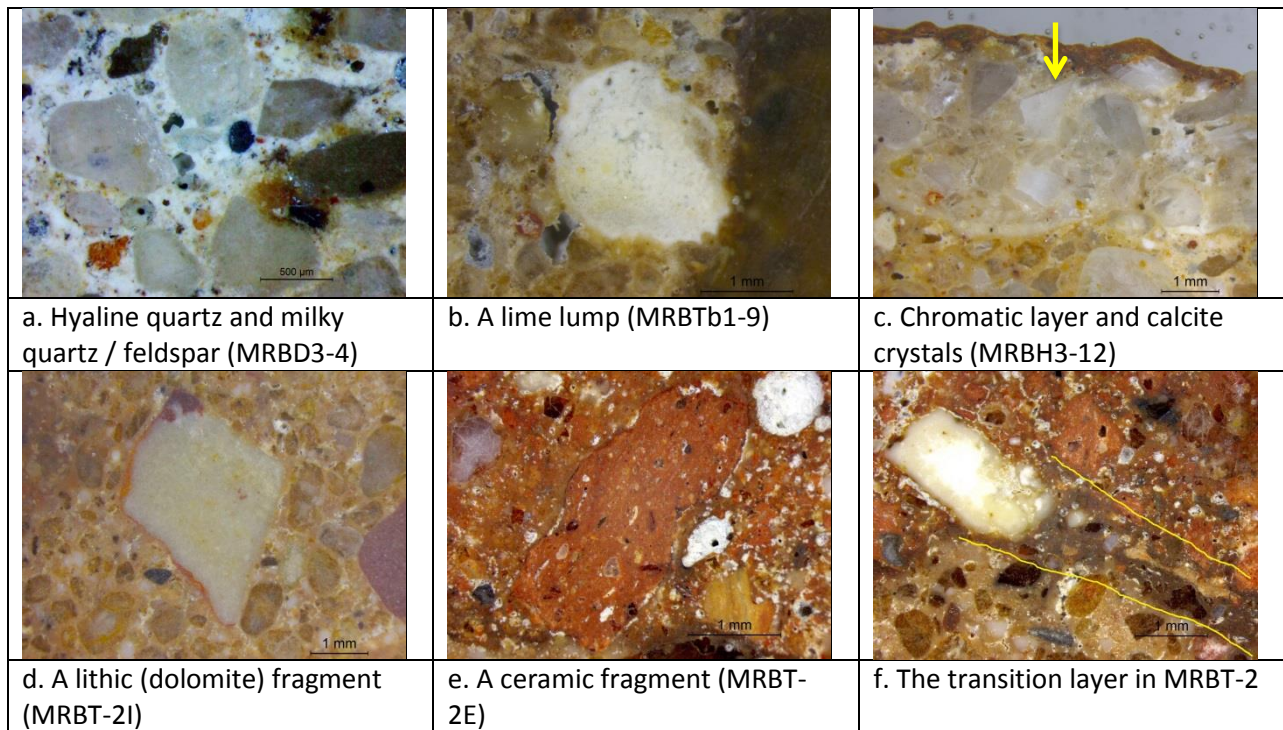
Figure 3.1. General aspects of the samples observed under the stereo microscope.

3.3. Polarised Light Microscopy

With this technique, it may be remarked that for the majority of the samples, quartz (Figure 3.2.a.) is the principal constituent of the aggregate. This mineral is present either as single grains, or as lithic fragments, *i.e.* quartzite, and the roundness of the grains range from 'subangular' to 'well-rounded'. Feldspars (both K-feldspar and plagioclase) (Figure 3.2.b.) were also commonly found in the samples. Ilmenite was viewed under PPL, whilst tourmaline (Figure 3.2.c.) is present in many of the samples, albeit in small quantities, *i.e.* one or two grains.

| a. Quartz grains (MRBT-1I) | b. K-feldspar (MRBTb1-8) | c. Tourmaline (MRBTb2-10). |
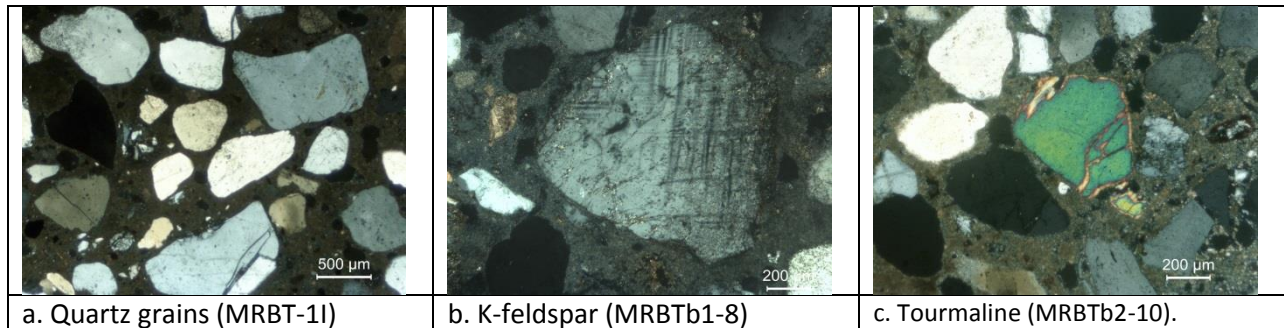
Figure 3.2. Observations under the polarising microscope in XPL.

In MRBT-1E, MRBH3-12E, MRBH7-13BE, MRBH7-13VE, and MRBF-16E, large calcite grains (Figure 3.3.a.) were observed. It may be added that these grains have an 'angular' / euhedral form. In MRBF-16E, two different types of carbonates were observed, one being the aforementioned calcite grains, whilst the other having a more rounded form, as well as a sparitic texture (Figure 3.3.b.). These are probably fragments of slightly metamorphosed limestone.

A relatively high amount of carbonates, which are possibly fragments of dolomite limestone, was also observed in MRBT-2I (Figure 3.3.c.). Due to its sparitic texture, these carbonates have been identified as lithic fragments, as opposed to crystal grains. This type of carbonate is also visible in trace amounts in some of the other samples, for example, MRBD3-3 and MRBTb2-10.

a. Calcite grains (MRBH7-13VE)	b. Slightly metamorphosed lithic fragments (MRBF-16E)	c. Lithic (dolomite) fragments (MRBT-2I)
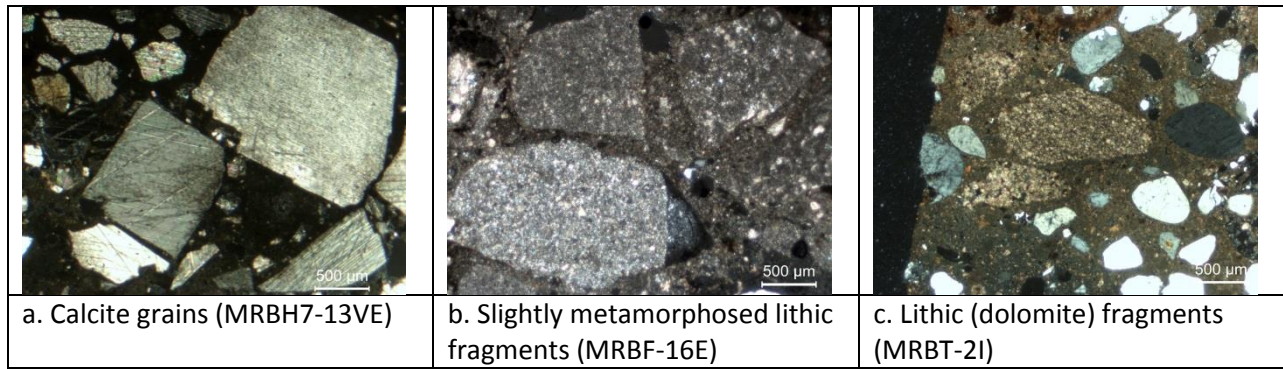
Figure 3.3. Observations under the polarising microscope in XPL.

Several 'oddities' were also noticed in the samples. The quantity of these features may be described as 'extremely minute', *i.e.* one or two crystals / fragments in one specific sample. Of most interest are the ones seen in MRBD3-4 and in MRBD4-5. In the former, a fragment of charcoal (Figure 3.4.) was visible, whilst in the latter, a fragment of oolitic limestone (Figure 3.5.) was identified. In a study conducted by Pavía & Caro (2008), a mortar sample was found to contain "abundant, evenly distributed charcoal", and the authors suggested that this charcoal could have been deliberately added as a pozzolan. Considering that there was only one fragment of charcoal in MRBD3-4, as opposed to being spread out evenly throughout the sample, it is unlikely that this were the case.

a. The charcoal fragment (XPL)	b. The charcoal fragment (PPL)
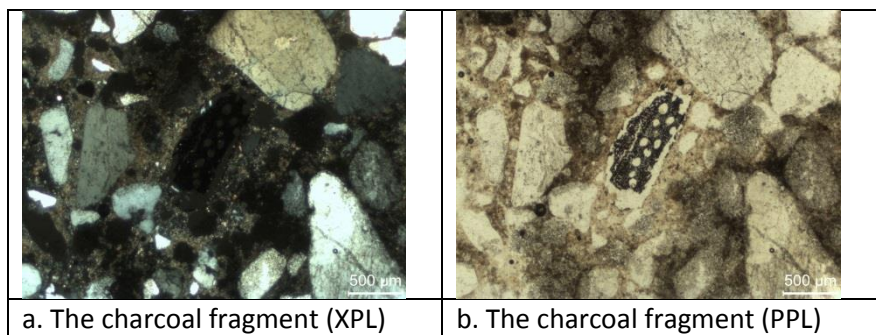
Figure 3.4. Observations under the polarising microscope (MRBD3-4).

a. The oolitic limestone (XPL)	b. The oolitic limestone (PPL)
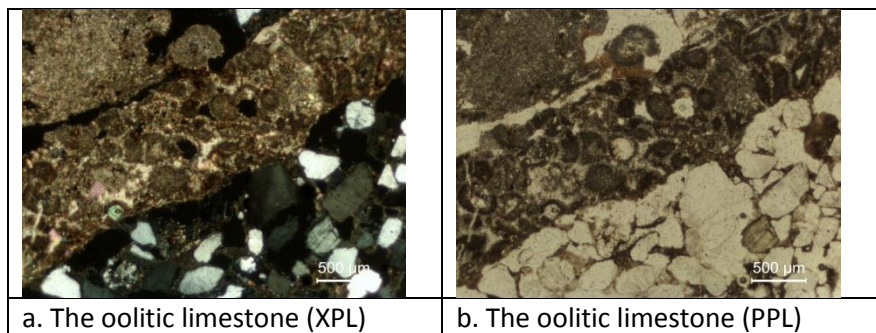
Figure 3.5. Observations under the polarising microscope (MRBD4-5).

3.4. Chemical and Granulometric Analysis

The results of these two analytical techniques are divided into four parts – the amount of insoluble residue to soluble fraction, the granulometric fractions, the stereo microscopic observation of the insoluble residue, and the classification of the aggregate.
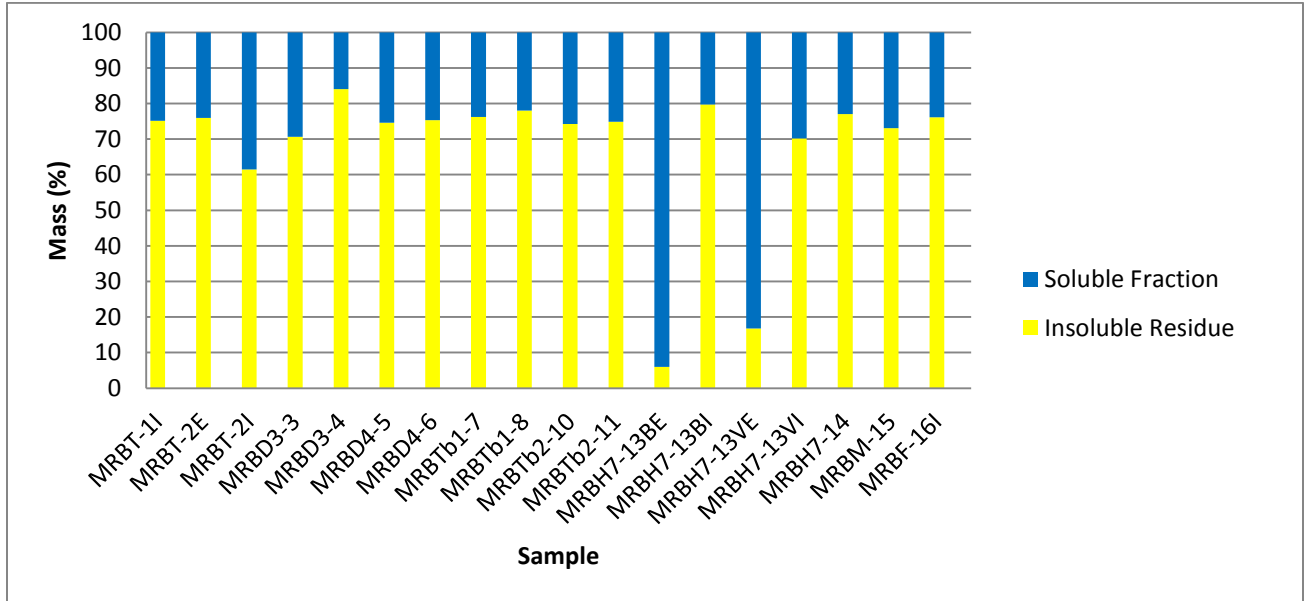
Figure 3.6. The insoluble residue and soluble fraction of the samples.

Figure 3.6. shows the amount of insoluble residue and soluble fraction (in percentage) of each sample, whilst the exact values of these components are provided in Annex 3.1. In MRBH7-13BE and MRBH7-13VE, the amount of insoluble residue is 5.98% and 16.76% respectively. These are the only two samples in which the amount of insoluble residue is lower than that of the soluble fraction. As carbonates were used as aggregates in these samples, they would have been dissolved during the acid attack. Therefore, the soluble fraction of these samples consists of both the aggregate and the binder. For the rest of the samples, the amount of soluble residue is higher than that of the insoluble fraction, and ranges from 61.47% in MRBT-2I to 84.08% in MRBD3-4. The insoluble residue and the soluble fraction may be equated with the aggregate and binder respectively, and hence has been used for the calculation of the binder to aggregate ratio (*eg.* Cardoso, 2011; Velosa et al., 2007). It may be mentioned that this calculation would not be possible for MRBH7-13BE and MRBH7-13VE, considering that the soluble fraction of these samples contain both the aggregate and the binder.

Table 3.2. Grain size distribution of the insoluble residue.

Sample	Mass of fractions (%)								
	< 0.063 (mm)	0.063 - 0.125 (mm)	0.125 - 0.250 (mm)	0.25 - 0.50 (mm)	0.5 - 1.0 (mm)	1.0 - 2.0 (mm)	2.0 - 4.0 (mm)	> 4.0 (mm)	TOTAL
MRBT-1I	0.75	0.79	2.11	20.69	56.62	16.45	0.79	1.32	99.50
MRBT-2E	2.63	4.33	6.42	26.11	16.00	16.44	20.10	6.67	98.68
MRBT-2I	0.61	1.85	9.83	25.78	29.45	21.22	10.37	0.00	99.10
MRBD3-3	1.18	3.21	12.03	47.67	27.84	6.55	0.59	0.00	99.05
MRBD3-4	0.84	3.26	6.02	12.68	57.06	17.12	2.83	0.00	99.78
MRBD4-5	0.91	4.23	14.21	68.94	8.97	1.33	0.61	0.00	99.19
MRBD4-6	0.92	3.16	15.90	70.22	8.56	0.45	0.00	0.00	99.19
MRBTb1-7	1.26	4.66	9.41	77.89	3.71	0.25	0.30	2.04	99.50
MRBTb1-8	0.51	2.04	6.09	38.90	38.23	11.98	1.77	0.00	99.50
MRBTb2-10	0.76	2.47	8.30	82.05	5.19	0.38	0.20	0.00	99.33
MRBTb2-11	2.63	2.88	10.91	75.17	3.50	0.31	0.47	3.63	99.47
MRBH7-13BE	1.37	8.58	20.76	31.31	23.30	9.70	4.34	0.00	99.34
MRBH7-13BI	0.86	3.70	6.59	30.82	43.83	12.31	0.92	0.00	99.02
MRBH7-13VE	1.43	4.73	7.62	13.20	37.04	33.07	1.66	0.00	98.73
MRBH7-13VI	0.79	3.06	4.90	14.52	46.23	24.22	5.53	0.00	99.24
MRBH7-14	1.88	4.33	12.36	71.55	7.02	0.87	0.75	0.00	98.73
MRBM-15	0.48	5.32	21.27	62.60	9.50	0.46	0.22	0.00	99.84
MRBF-16I	0.33	2.33	5.40	13.39	60.94	16.47	0.64	0.00	99.49

Table 3.2. shows the grain size distribution of the insoluble residue for each sample. The graphic presentation of the data may be found in Annex 3.2. In terms of modality, all but one sample may be classified as unimodal. The predominant fraction for these samples is either 0.25 – 0.50 mm or 0.5 – 1.0 mm, the former being a 'fine fraction', whilst the latter a 'medium fraction', according to the designation provided by Coutinho (1999, p. 31). MRBTb1-8 is the only sample that may be described as bimodal, as it has both 0.25 – 0.50 mm and 0.5 – 1.0 mm as its predominant fraction. These factors, *i.e.* size and volume of the granulometric fractions, have an effect on the physical-mechanical properties of the mortars produced. Experiments conducted by Grassl et al. (2010), for instance, found that the shrinkage-induced micro-cracking of mortars was influenced by the size and fractional volume of the aggregates in them.

Table 3.3. Description of the insoluble residue.

Sample	Modality	Sorting**	Predominant Fraction (mm)	Predominant Mineral	Other Minerals / Lithics, and Additives	Roundness of Aggregates	Textural Group*	Aggregate Classification*
MRBT-1I	Unimodal	Moderately Sorted	0.5 - 1.0 (56.62%)	Quartz (hyaline, milky)	Quartzite, feldspar, ilmenite, tourmaline (?), clays / micas	Subangular - Well-rounded	Slightly Gravelly Sand	Slightly Fine Gravelly Coarse Sand
MRBT-2E	Unimodal	Poorly Sorted	0.25 - 0.50 (26.11%)	Quartz (hyaline, milky)	Quartzite, feldspar, clays / micas, ceramic fragments (red, yellow, grey)	Subangular - Well-rounded	Gravelly Sand	Very Fine Gravelly Medium Sand
MRBT-2I	Unimodal	Poorly Sorted	0.5 - 1.0 (29.45%)	Quartz (hyaline, milky)	Quartzite, feldspar, ilmenite, tourmaline (?), clays / micas	Subangular - Well-rounded	Gravelly Sand	Very Fine Gravelly Coarse Sand
MRBD3-3	Unimodal	Moderately Sorted	0.25 - 0.50 (47.67%)	Quartz (hyaline, milky)	Quartzite, feldspar, ilmenite, tourmaline (?), clays / micas	Subangular - Well-rounded	Slightly Gravelly Sand	Slightly Very Fine Gravelly Medium Sand
MRBD3-4	Unimodal	Moderately Sorted	0.5 - 1.0 (57.06%)	Quartz (hyaline, milky)	Quartzite, feldspar, clays / micas	Subangular - Well-rounded	Slightly Gravelly Sand	Slightly Very Fine Gravelly Coarse Sand
MRBD4-5	Unimodal	Moderately Well Sorted	0.25 - 0.50 (68.94%)	Quartz (hyaline, milky)	Quartzite, feldspar, clays / micas	Subangular - Well-rounded	Slightly Gravelly Sand	Slightly Very Fine Gravelly Medium Sand
MRBD4-6	Unimodal	Moderately Well Sorted	0.25 - 0.50 (70.22%)	Quartz (hyaline, milky)	Quartzite, feldspar, ilmenite, tourmaline (?), clays / micas	Subangular - Well-rounded	Sand	Moderately Well Sorted Medium Sand
MRBTb1-7	Unimodal	Moderately Well Sorted	0.25 - 0.50 (77.89%)	Quartz (hyaline, milky)	Quartzite, feldspar, ilmenite, tourmaline (?), clays / micas	Subangular - Well-rounded	Slightly Gravelly Sand	Slightly Fine Gravelly Medium Sand

Table 3.3. Description of the insoluble residue (cont.).

MRBTb1-8	Bimodal	Moderately Sorted	0.25 - 0.50 (38.90%); 0.5 - 1.0 (38.23%)	Quartz (hyaline, milky)	Quartzite, feldspar, ilmenite, tourmaline (?), clays / micas	Subangular - Well-rounded	Slightly Gravelly Sand	Slightly Very Fine Gravelly Medium Sand
MRBTb2-10	Unimodal	Well Sorted	0.25 - 0.50 (82.05%)	Quartz (hyaline, milky)	Quartzite, feldspar, ilmenite, tourmaline (?), clays / micas	Subangular - Well-rounded	Slightly Gravelly Sand	Slightly Very Fine Gravelly Medium Sand
MRBTb2-11	Unimodal	Moderately Well Sorted	0.25 - 0.50 (75.17%)	Quartz (hyaline, milky)	Quartzite, feldspar, ilmenite, tourmaline (?), clays / micas	Subangular - Well-rounded	Slightly Gravelly Sand	Slightly Fine Gravelly Medium Sand
MRBH7-13BE	Unimodal	Poorly Sorted	0.25 - 0.50 (31..31%)	Quartz (hyaline, milky)	Quartzite, feldspar, clays / micas	Subangular - Well-rounded	Slightly Gravelly Sand	Slightly Very Fine Gravelly Medium Sand
MRBH7-13BI	Unimodal	Moderately Sorted	0.5 - 1.0 (43.83%)	Quartz (hyaline, milky)	Quartzite, feldspar, ilmenite, tourmaline (?), clays / micas	Subangular - Well-rounded	Slightly Gravelly Sand	Slightly Very Fine Gravelly Coarse Sand
MRBH7-13VE	Unimodal	Poorly Sorted	0.5 - 1.0 (37.04%)	Quartz (hyaline, milky)	Quartzite, feldspar, clays / micas, red-coloured powder (from chromatic layer)	Subangular - Well-rounded	Slightly Gravelly Sand	Slightly Very Fine Gravelly Coarse Sand
MRBH7-13VI	Unimodal	Poorly Sorted	0.5 - 1.0 (46.23%)	Quartz (hyaline, milky)	Quartzite, feldspar, ilmenite, tourmaline (?), clays / micas	Subangular - Well-rounded	Gravelly Sand	Very Fine Gravelly Coarse Sand
MRBH7-14	Unimodal	Moderately Well Sorted	0.25 - 0.50 (71.55%)	Quartz (hyaline, milky)	Quartzite, feldspar, ilmenite, tourmaline (?), clays / micas	Subangular - Well-rounded	Slightly Gravelly Sand	Slightly Very Fine Gravelly Medium Sand
MRBM-15	Unimodal	Moderately Sorted	0.25 - 0.50 (62.60%)	Quartz (hyaline, milky)	Quartzite, feldspar, clays / micas	Subangular - Well-rounded	Slightly Gravelly Sand	Slightly Very Fine Gravelly Medium Sand

Table 3.3. Description of the insoluble residue (cont.).

MRBF-16I	Unimodal	Moderately Sorted	0.5 - 1.0 (60.94%)	Quartz (hyaline, milky)	Quartzite, feldspar, ilmenite, tourmaline (?), clays / micas	Subangular - Well-rounded	Slightly Gravelly Sand	Slightly Very Fine Gravelly Coarse Sand

* According to the Folk and Ward Method, as used by GRADISTAT
** According to GRADISTAT.

Table 3.3. provides a description of the insoluble residue. A summary of the observations made with the stereo microscope forms part of this table. As expected, the bulk of the insoluble residue is made up of quartz (both hyaline and milky) (Figure 3.8.a.). The roundness of these grains range from 'subangular' to 'well-rounded'. It may also be noted that in certain samples, lumps of clay minerals were visible in the 0.25-0.50 mm, 0.125-0.250 mm, and 0.063-0.125 mm fractions, due to a lack of disaggregation during the sieving of the insoluble residue. A sample, MRBT-1I was re-sieved (see Annex 3.4.), and the results suggest that the values of the 0.063 – 0.125 mm and/or < 0.063 mm fractions may be higher, whilst those of the 0.25-0.50 mm and/or 0.125-0.250 mm and/or 0.063-0.125 mm fractions lower, than the values plotted on the graphs. These differences, however, are minor, and do not affect the granulometric results drastically. Nevertheless, the re-sieving shows that the clay content of the samples, as represented by the 0.063 – 0.125 mm and < 0.063 mm fractions, is higher than originally shown.

a. > 4.0 mm	b. 2.0 - 4.0 mm	c. 1.0 - 2.0 mm
d. 0.5 - 1.0 mm	e. 0.25 - 0.50 mm	f. 0.125 - 0.250 mm
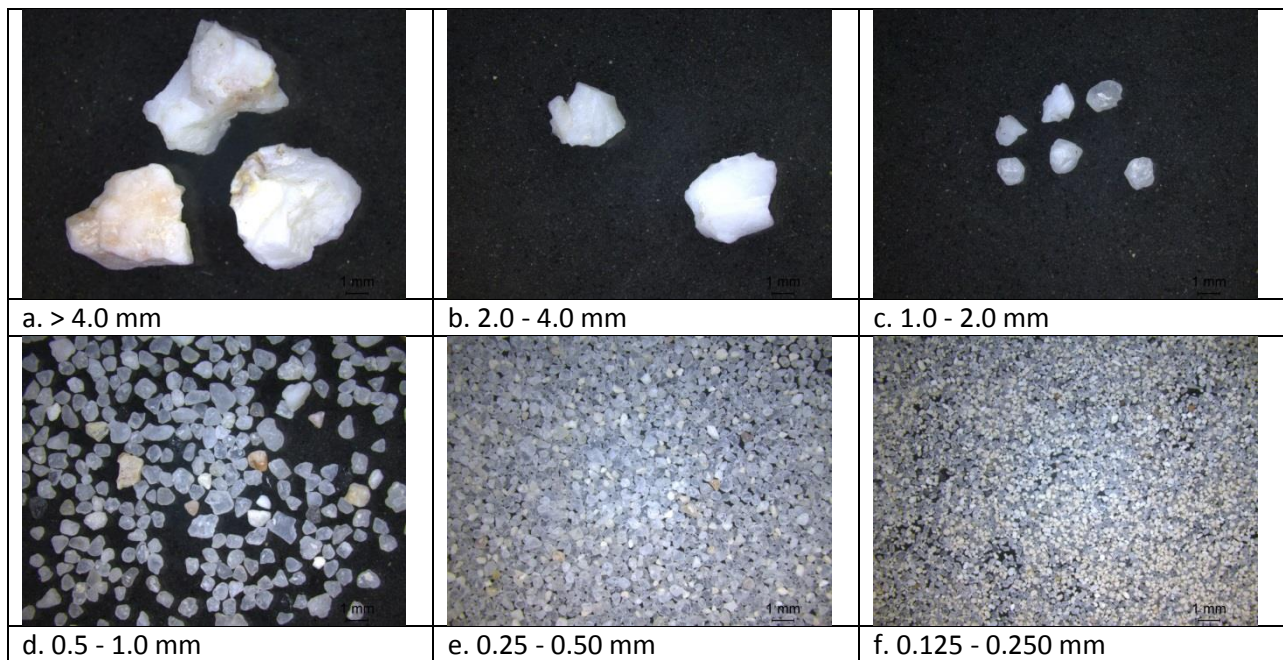
Figure 3.7. The grain size distribution of the insoluble residue, observed under the stereo microscope (MRBTb1-7).

| a. Quartz grains (MRBF-16I) | b. Ceramic fragments (MRBT-2E) |
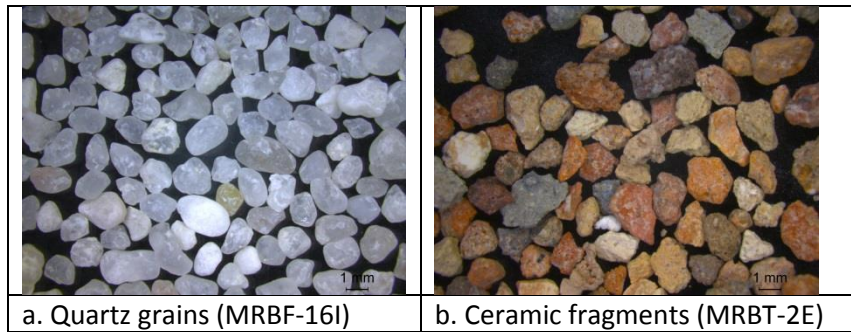
Figure 3.8. Examples of the insoluble residue observed under the stereo microscope.

In addition, Table 3.3. displays some of the results, *i.e.* the sorting, textural group, and classification of the insoluble residue from the analysis performed using GRADISTAT, a particle size analysis software written by Simon Blott (downloaded from http://www.kpal.co.uk/gradistat.html) (Kenneth Pye Associates Ltd, 2018). It may be added that although a European standard for aggregates (*European Standard EN 13139:2002 Aggregates for mortar*) is available, this was not used, as it did not contain a classification of the aggregate fractions according to their size.

The results suggest that the aggregate in all the samples consists of sand, as opposed to mud or gravel, though of different textures, *i.e.* either 'Sand', 'Slightly Gravelly Sand' or 'Gravelly Sand'. Moreover, the sorting of the aggregate ranges from 'poorly sorted' to 'well sorted'. This sorting has an effect on the workability of the mortar (Schnabel, 2008, p. 1), and has been shown to affect the final quality of the mortar (see, for example, Arizzi and Cultrone, 2013).
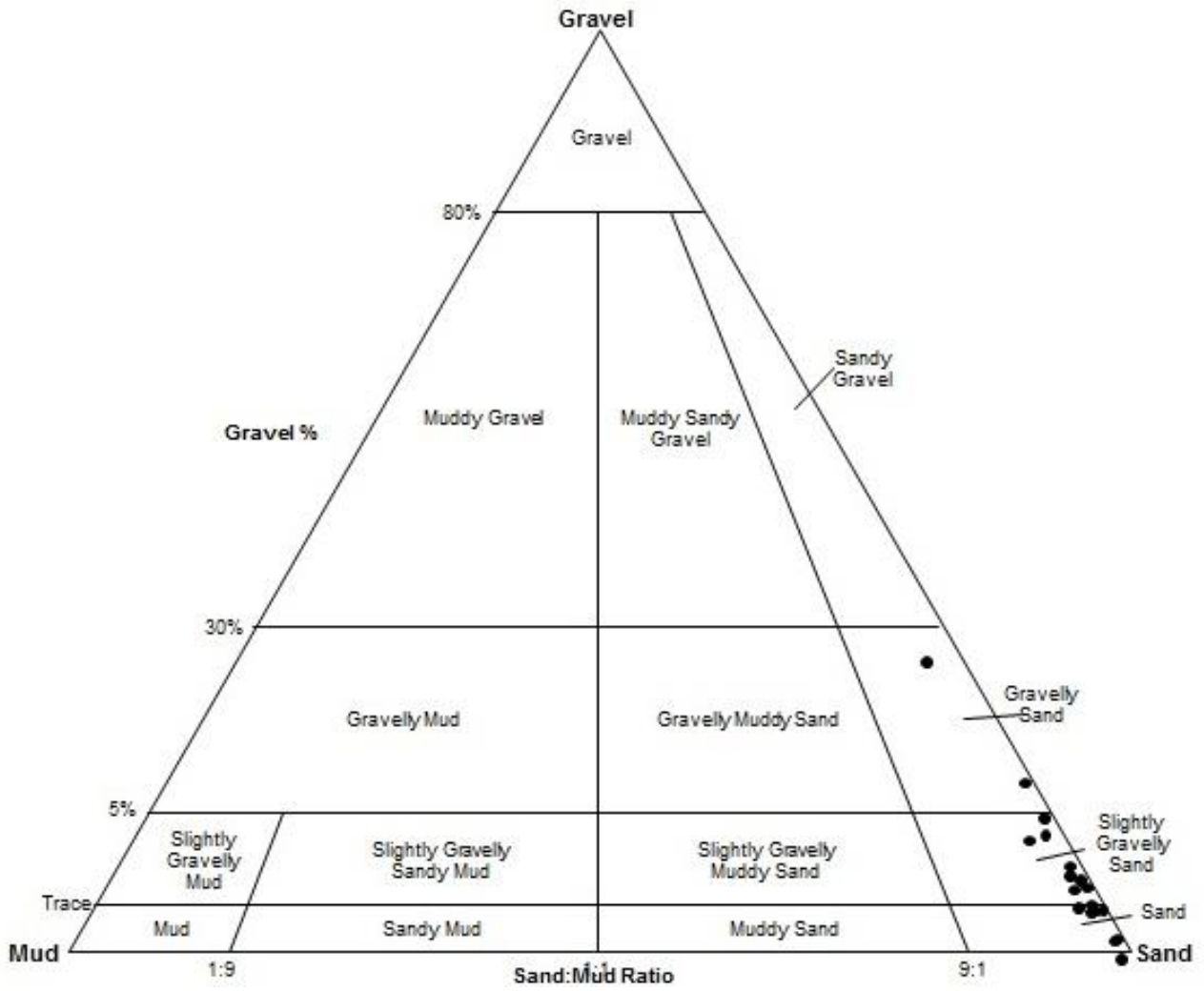
Figure 3.9. The Gravel Sand Mud Diagram.

3.5. Thermogravimetric Analysis

The thermograms presented in Annex 3.5. show the results of the Thermogravimetric Analysis (TGA). The thermogravimetric (TG), as well as the derivative thermogravimetric (DTG) curves of each sample are displayed in these figures, whereas Table 3.4. shows the mass change (in percentage) of the samples. Additionally, the carbon dioxide / structurally bound water ratio is also presented in the table. The 40-120 °C, 200-600 °C, and 600-950 °C ranges corresponds to the change in mass attributed to the physically bound / absorbed water (also referred to as hygroscopic water), the structurally bound water (also referred to as chemically bound water or hydraulic water), and the decomposition of carbonates (more specifically the calcites) (resulting in the release of carbon dioxide) respectively (Bakolas et al., 1998; Moropoulou et al., 1995).
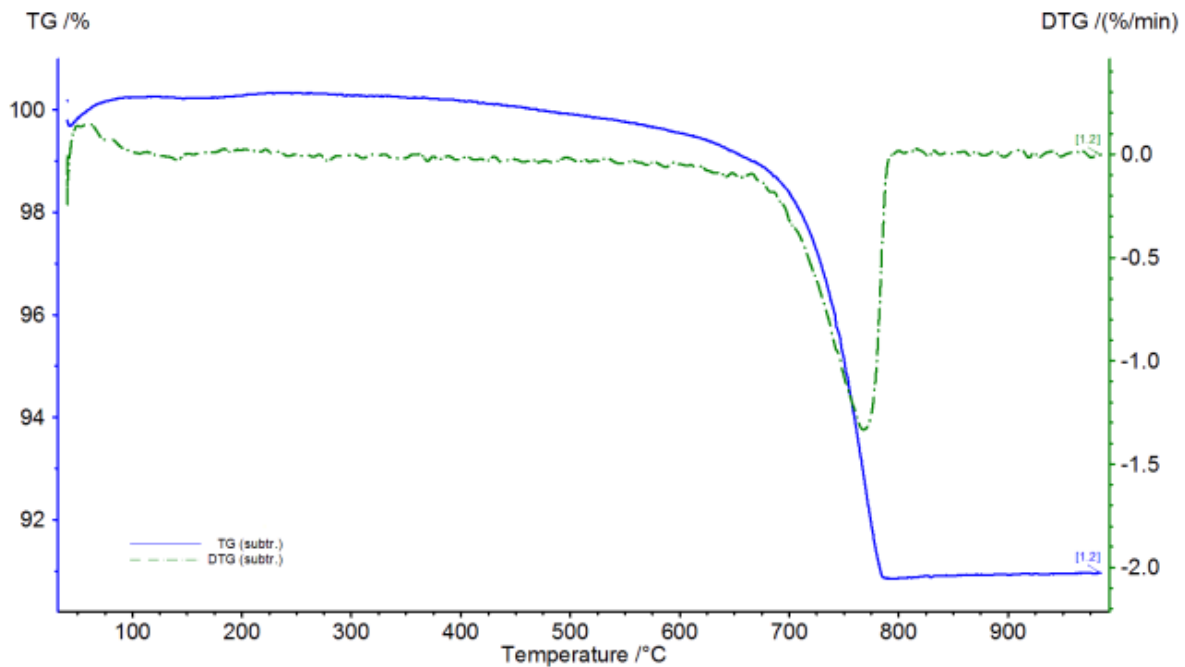
Figure 3.10. The TGA results of MRBT-1I, showing the thermogravimetric (TG), and the derivative thermogravimetric (DTG) curves.

Table 3.4. TGA mass change, and the carbon dioxide / structurally bound water ratio.

Sample	Mass Change (%)					Carbon Dioxide / Structurally Bound Water
	40-120 °C	120-200 °C	200-600 °C	600-950 °C	Total	
MRBT-1I	0.49	0.03	-0.74	-8.59	-8.81	11.61
MRBT-2E	-0.58	-0.99	-2.06	-4.33	-7.96	2.10
MRBT-2I	0.21	-0.03	-0.78	-15.16	-15.76	19.44
MRBD3-3	0.20	-0.02	-0.89	-9.52	-10.23	10.70
MRBD3-4	-0.16	-0.15	-0.76	-3.52	-4.59	4.63
MRBD4-5	-0.06	-0.28	-1.41	-7.76	-9.51	6.81
MRBD4-6	-0.36	-0.24	-2.01	-13.48	-16.09	6.71
MRBTb1-7	-0.11	-0.12	-0.82	-7.57	-8.62	9.23
MRBTb1-8	-0.19	-0.27	-1.36	-7.94	-9.76	5.84
MRBTb1-9	-0.17	-0.23	-2.07	-11.73	-14.20	5.67
MRBTb2-10	-0.11	-0.08	-1.14	-7.78	-9.11	6.82
MRBTb2-11	-0.24	-0.26	-1.27	-7.88	-9.65	6.20
MRBH3-12E	-0.03	-0.08	-1.69	-29.84	-31.64	17.66
MRBH3-12I	-0.41	-0.31	-2.53	-8.38	-11.63	3.31
MRBH7-13BE	-0.07	-0.12	-1.15	-37.99	-39.33	33.03
MRBH7-13BI	-0.27	-0.20	-1.41	-6.44	-8.32	4.57
MRBH7-13VE	-0.09	-0.12	-1.41	-32.32	-33.94	22.92
MRBH7-13VI	0.39	-0.12	-1.08	-9.99	-10.80	9.25
MRBH7-14	0.00	-0.07	-1.09	-7.89	-9.05	7.24
MRBM-15	-0.47	-0.37	-1.18	-4.43	-6.45	3.75
MRBF-16E	-0.41	-0.38	-1.80	-26.18	-28.77	14.54
MRBF-16I	-0.06	-0.15	-0.66	-7.96	-8.83	12.06

In Table 3.4., it may be remarked that mass change in the 200-600 °C range (attributed to the structurally bound water) is low in the samples, the lowest being -0.66% (MRBF-16), and the highest being -2.53% (MRBH3-12I). On the contrary, the change in mass in the 600-950 °C (attributed to the calcite decomposition, during which carbon dioxide is released) varies between the samples, ranging from -3.52% in MRBD3-4 to -37.99% in MRBH7-13BE. In most of the samples, the carbon dioxide content may be described as 'low', *i.e.* < 10.00%. The rest of the samples may either be described as having a 'medium' (10–20 %) or 'high' (> 20%) proportion of calcite. MRBT-2I, MRBD4-6, and MRBTb1-9 belong to the former, whilst MRBH3-12E, MRBH13-BE, MRBH7-13VE, and MRBF-16E belong to the latter. The

'high' amount of calcite in the latter four samples was expected, as their aggregate consist mainly of this mineral.

With the values in the 200-600 °C and 600-950 °C ranges, *i.e.* the amount of structurally bound water and the carbonates, the carbon dioxide / structurally bound water ratio could be calculated. This ratio has been used as an indicator of a mortar's level of hydraulicity (Bakolas et al., 1998; Moropoulou et al., 1995; Moropoulou et al., 2005), and will be discussed further in the following chapter.

3.6. Powder X-Ray Diffraction

Table 3.5. shows the semi-quantitative results of the Powder X-Ray Diffraction (XRD) analysis on the global fractions, whereas those of the fine fractions are presented in Table 3.6. The diffractograms of the global and fine fractions are presented in Annexes 3.6. and 3.7. respectively. The results of the XRD analyses provide an overview mineralogical composition of the samples, as well as a semi-quantitative analysis of these minerals.

Figure 3.11. The diffractogram of MRBD3-3 (global fraction).
Legend: Q – quartz; C – calcite; F – K-feldspar.

Commander Sample ID (Coupled TwoTheta/Theta)
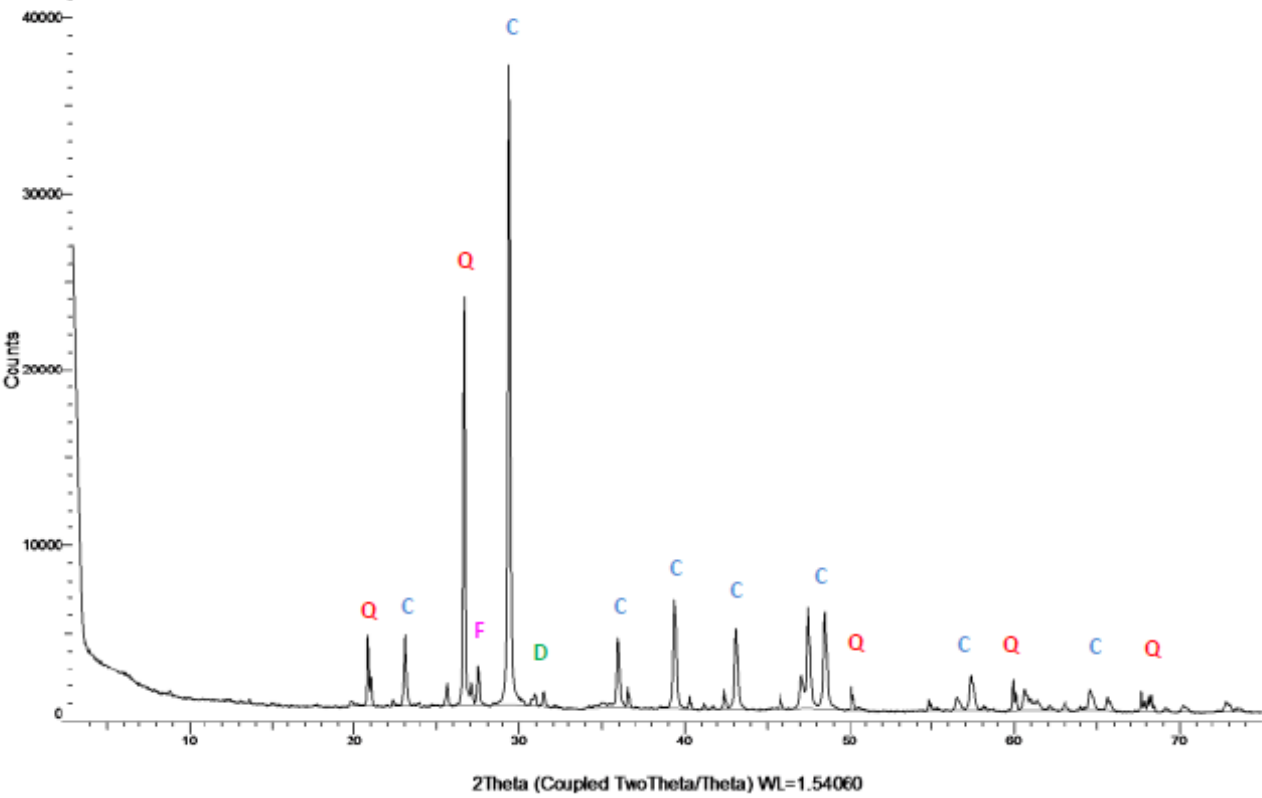
Figure 3.12. The diffractogram of MRBD3-3 (fine fraction).
Legend: Q – quartz; C – calcite; F – K-feldspar; M – Muscovite; D – Dolomite.

Table 3.5. The semi-quantitative results of the XRD analysis (global fraction).

Sample	Mineral						
	Quartz	Calcite	K-Feldspar	Plagioclase	Micas	Dolomite	Aragonite
MRBT-1I	++++	+	++	+	++	-	-
MRBT-2E	+++	+	++	+	++	-	-
MRBT-2I	++++	+	++	-	++	+	-
MRBD3-3	++++	++	++	-	-	-	-
MRBD3-4	++++	+	++	-	-	-	+
MRBD4-5	+++	+	++	-	+++	-	-
MRBD4-6	++++	+	++	-	-	-	-
MRBTb1-7	++++	+	++	-	++	-	-
MRBTb1-8	++++	+	++	-	++	-	-
MRBTb1-9	++++	+	++	-	+	-	-
MRBTb2-10	++++	+	+	-	+	-	-
MRBTb2-11	++++	+	++	-	+	-	-
MRBH3-12E	++	++++	+	-	-	-	-
MRBH3-12I	++++	++	+	+	++	-	-
MRBH7-13BE	+	++++	++	+	-	++	-
MRBH7-13BI	++++	+	++	-	+	-	-
MRBH7-13VE	++	++++	+	-	-	-	-
MRBH7-13VI	++++	+	++	+	-	-	-
MRBH7-14	++++	+	+	-	-	-	-
MRBM-15	++++	+	++	-	+	-	-
MRBF-16E	++++	+++	+	-	-	-	-
MRBF-16I	++++	+	+	-	-	-	-
++++ (very high proportion / predominant mineral); +++ (high proportion); ++ (medium proportion); + (low proportion); - (undetected)							

In Table 3.5, it is clear that quartz is the predominant mineral in almost all of the samples. By contrast, calcite exists either in small or medium quantities in these samples. The inverse is true for MRBH3-12E, MRBH7-13BE, and MRBH7-13VE, where calcite is the predominant mineral, as expected, whereas quartz is present either in low or medium quantities. It may be added that in the case of MRBF-16E, whilst quartz is the predominant mineral, a high amount of calcite was detected as well. Feldspars were also detected in the samples. K-feldspar was detected in all of the samples (either in small or medium proportions), whilst plagioclase was found only in several of the samples. In addition, the presence of micas was detected in several samples, whilst dolomite was observed in two samples (MRBT-2I and MRBH7-13BE). Finally, aragonite was detected in MRBD3-4.

Table 3.6. The semi-quantitative results of the XRD analysis (fine fraction).

Sample	Mineral											
	Quartz	Calcite	Mg Calcite	K-Feldspar	Plagioclase	Micas	Clays	Dolomite	Ilmenite	Tourmaline	Aragonite	Gypsum
MRBT-1I	++	++++	++	++	+	-	-	tr.	-	+	-	?
MRBT-2E	+++	++	++	+	+	++	+	+	tr.	+	-	-
MRBT-2I	+	++++	++	+	-	-	++	+	tr.	+	-	-
MRBD3-3	++	+++	++	++	-	++	++	tr.	tr.	+	-	-
MRBD3-4	++	+++	++	++	+	-	++	tr.	+	+	++	-
MRBD4-6	++	++++	++	++	-	++	+	tr.	tr.	+	-	-
MRBTb1-7	++	+++	++	+	-	++	++	tr.	-	+	-	-
MRBTb1-8	++	++++	++	++	+	++	+	+	-	+	-	-
MRBTb2-10	++	+++	++	+	+	++	+++	tr.	-	-	-	-
MRBTb2-11	+++	+++	++	++	+	+	+	+	tr.	+	-	-
MRBH7-13BI	++	+++	++	++	-	++	++	+	tr.	+	-	-
MRBH7-13VI	++	++++	+++	++	+	-	++	tr.	+	+	-	-
MRBH7-14	+++	+++	++	++	+	++	+	tr.	-	+	-	-
MRBM-15	+++	+++	+	++	+	++	+	+	tr.	+	-	-
MRBF-16I	+	+++	++	++	tr.	++	+	+++	tr.	+	-	-

++++ (very high proportion / predominant mineral); +++ (high proportion); ++ (medium proportion); + (low proportion); tr. (traces); ? (uncertain); - (undetected)

As the extremely intense peaks of quartz masked those of the other minerals in the samples, the fine fractions were also analysed. In Table 3.6., it is evident that the proportion of quartz was significantly reduced, thus allowing other minerals within the samples to be identified. The higher amount of binder present in the fine fractions is reflected in the increased proportion of calcite. Moreover, magnesium calcite was also detected in the samples, though this mineral is present only in low or medium quantities (the exception being MRBH7-13VI, where a high proportion of magnesium calcite was observed). Micas and clay minerals were also present in most samples, either in low or medium proportions. Dolomite was detected in all samples, either in low amounts, or as traces. In MRBF-16I, however, a high amount of dolomite was identified in the diffractogram. Ilmenite was found in most samples, though as traces, whilst tourmaline was detected in low quantities in all but one sample. Finally, it may be pointed out that aragonite was detected in MRBD3-4, whilst gypsum might be present in MRBT-1I.

3.7. Variable Pressure Scanning Electron Microscopy-Energy Dispersive Spectrometry

The results of the Scanning Electron Microscopy-Energy Dispersive Spectrometry (SEM-EDS) analysis may be divided into two main parts – the aggregate and the binder.

From the SEM-EDS analysis, it was found that in all the samples (apart from MRBT-IE, MRBH3-12E, MRBH7-13BE, MRBH7-13VE, and MRBF-16E), the aggregate is of a siliceous nature (Figure 3.13.a.). In other words, the aggregate used for the production of these mortars was quartz (SiO_2) sand, as opposed to carbonate sand, the other main type of sand. It may also be remarked that the morphology of the quartz grains range from being 'subangular' to 'well-rounded'. In many of the samples, grains containing aluminium (Al) and potassium (K), in conjunction with silicon (Si), were also seen. These were identified as K-feldspars (Figure 3.13.b.). Additionally, grains containing both titanium (Ti) and iron (Fe) were common, and were identified as ilmenites (Figure 3.14.b.). On the other hand, calcium (Ca) was found to be the main element of the aggregates in MRBT-IE, MRBH3-12E, MRBH7-13BE, MRBH7-13VE, and MRBF-16E (Figure 3.15.b.). Apart from calcium (Ca), the aggregates in these samples were found to contain little impurities. Additionally, these grains may be described as 'angular' / euhedric in shape. These aggregates were identified as calcite. Carbonates containing higher amounts of magnesium (Mg) were also present as aggregates in certain samples, *eg.* MRBT-2I. These grains were identified as dolomite limestone fragments.

| a. Quartz grains (yellow) | b. Quartz grains (yellow) and K-feldspars (pink) |
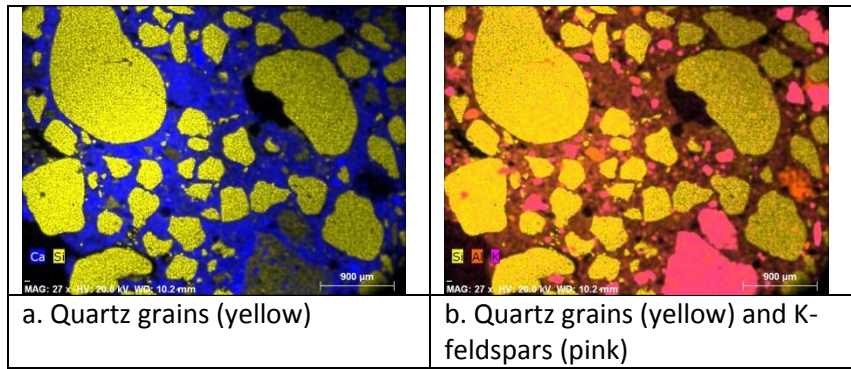
Figure 3.13. Elemental maps of MRBTb1-8.

| a. BSE image (bright spots) | b. Elemental map (Fe, Ti)(orange spots) |
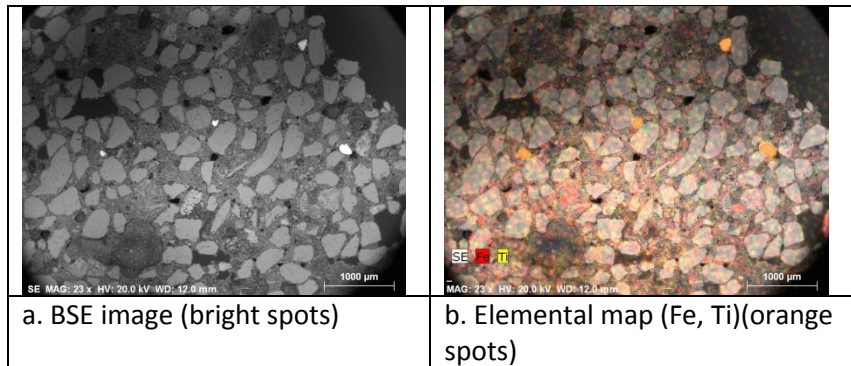
Figure 3.14. Ilmenites in MRBTb2-10.

| a. BSE image | b. Elemental map (Ca, Si) |
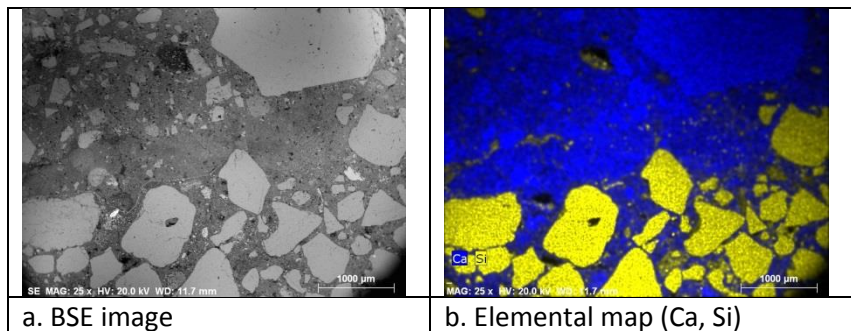
Figure 3.15. External and internal layers of MRBH7-13B.

The analysis of the binder with SEM-EDS was carried out using both point analysis and elemental mapping. The results obtained from the point analysis suggest that, as a whole, the binder is of a heterogeneous nature. In some of the analysed points, it was found that the binder consisted of calcium (Ca) with little magnesium (Mg), though with a noticeable amount of silicon (Si) (Figures 3.16., 3.17.). The presence of silicon (Si) in conjunction with aluminium (Al) suggests the presence of clay minerals in the binder. Point analyses were also performed on the lime lumps, as these are the remains of the burnt limestone that had not been thoroughly slaked, and therefore represent the original limestone that had

been used for the production of the binder. The point analysis of the lime lumps shows that the limestone used contained little impurities (Figures 3.18., 3.19.). The elemental mapping of In MRBT-1, MRBH3-12, MRBH7-13B, and MRBH7-13V suggest that there is a difference in the chemical composition of the binder in the different stratigraphic layers (Figure 3.20.). The elemental maps of these samples show that the binder in the external layers contains a lower amount of magnesium (Mg) than that in the internal layers, which suggest that limestone with fewer impurities may have been deliberately selected for the production of the former.
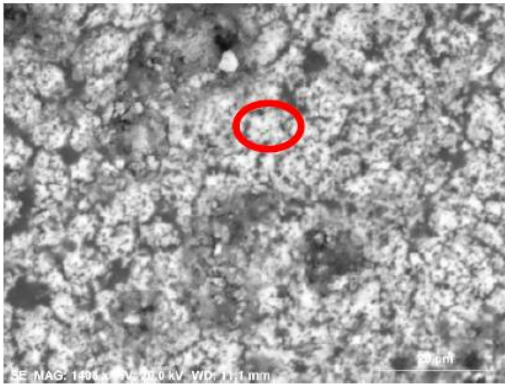
Figure 3.16. The BSE image for the point analysis performed on the binder in MRBH7-14.
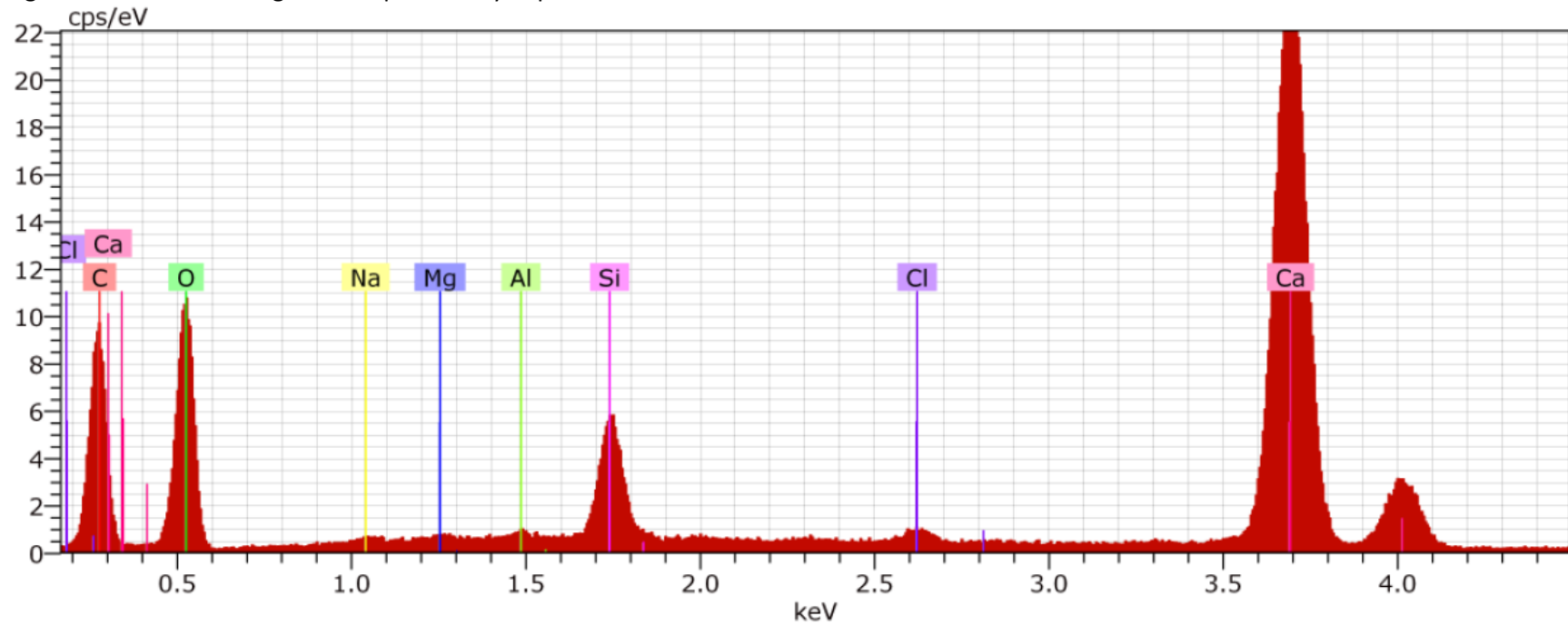
Figure 3.17. EDS spectrum of a point analysis performed on the binder in MRBH7-14.

Figure 3.18. The BSE image for the point analysis performed on a lime lump in MRBTb1-8.
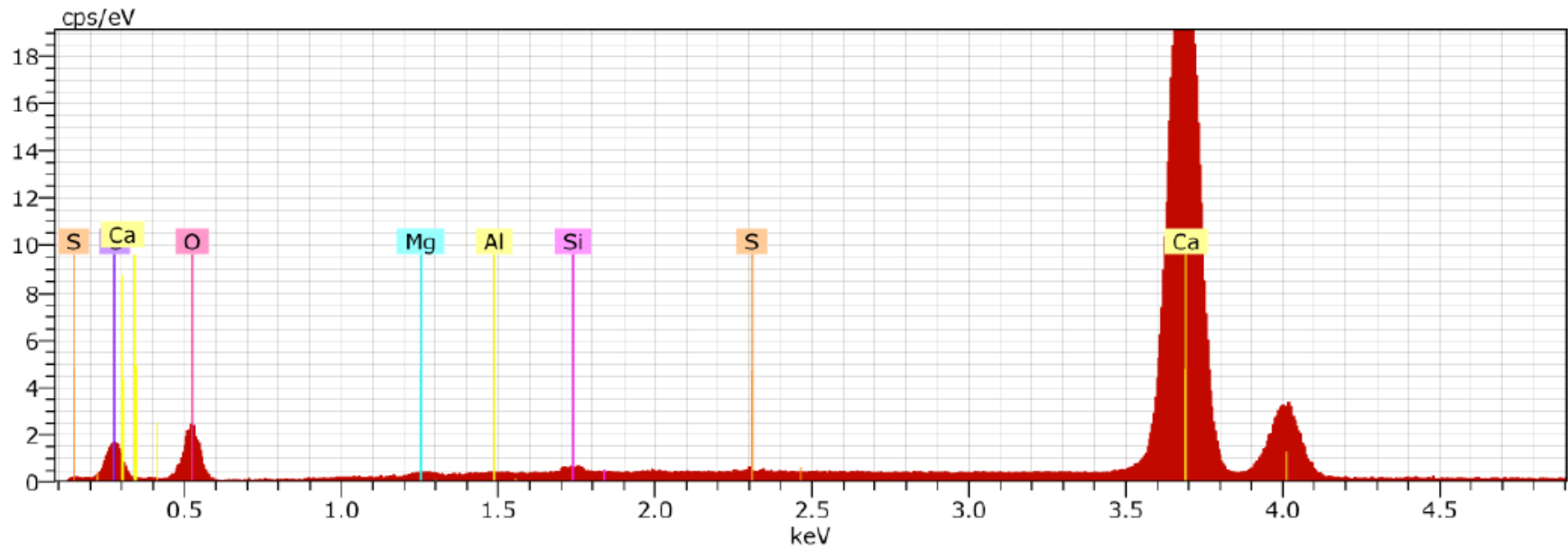
Figure 3.19. EDS spectrum of a point analysis performed on a lime lump in MRBTb1-8.

| a. Elemental map of MRBH7-13B (Mg, Ca) | b. Elemental map of MRBH7-13V (Mg, Ca) | c. Elemental map of MRBH7-13B (K, Al) |
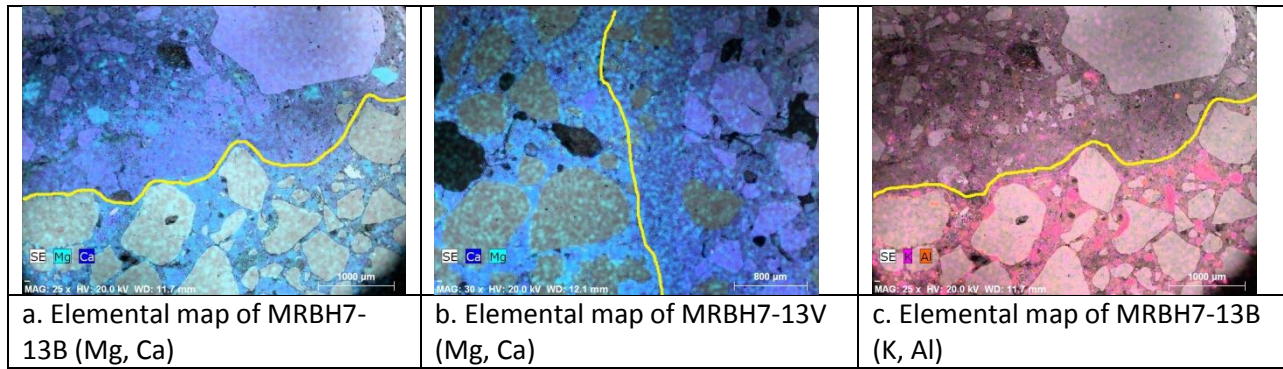
Figure 3.20. Differences between the external and internal layers.

Apart from the aggregate and the binder, SEM was also used to analyse the ceramic fragments in MRBT-2E. It is known that ceramic fragments were used by the Romans as an additive, more precisely as an artificial pozzolan. Signs of pozzolanic reaction may be seen in reaction rims around the fragments (Borsoi et al., 2010; Kramar et al., 2011). In the ceramic fragments of MRBT-2E, it was unclear if such reaction rims were present. Nevertheless, a transition layer was seen between MRBT-2E and MRBT-2I. The elemental mapping of this layer shows that it contains a higher than normal concentration of aluminium (Al), silicon (Si) and iron (Fe), and a low concentration of calcium (Ca) (Figure 3.21.), which was confirmed by point analysis. The aluminium (Al), silicon (Si) and iron (Fe) are probably from the aluminosilicates in the brick powder (in MRBT-2E). These aluminosilicates could react with the lime from the binder in MRBT-2I in the presence of water or humidity to produce a pozzolanic reaction (Böke et al., 2006, pp. 1115-1116; Maravelaki-Kalaitzaki et al., 2003, p. 656).

| a. Al and Fe | b. Ca and Mg | c. Ca and Si |
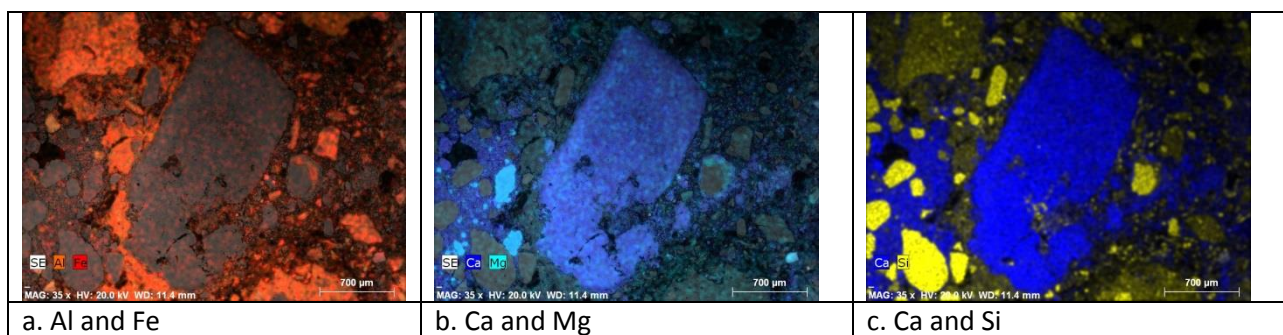
Figure 3.21. Elemental maps of the transition layer in MRBT-2.

4. Discussion

4.1. Raw Materials

The raw materials of the samples may be divided into its two main components, the aggregate and the binder.

Based on the results of the various techniques (stereo microscopy, polarised light microscopy, SEM-EDS, and XRD), it is clear that in the majority of samples, quartz sand (both hyaline and milky) is the main component of the aggregate. This is evident in all the techniques with which the aggregate was analysed. From the microscopic (stereo microscopy, polarised light microscopy, and SEM-EDS) observation of the quartz, it may also be remarked that the morphology of these grains range from 'subangular' to 'well-rounded', as already mentioned in the previous chapter. Whilst these techniques also provide a rough idea about the size of the grains, a more precise evaluation of this aspect was obtained with the use of granulometry. The results of this technique have also been dealt with already in the preceding chapter.

Other constituents of the aggregate that were observed during the analyses include feldspars (both K-feldspars and plagioclases), ilmenite, and tourmaline. It may be remarked that feldspars and ilmenites are more common than tourmaline. The presence of feldspars and ilmenites in the samples was visible in polarised light microscopy. Additionally, ilmenites were observed with stereo microscopy. SEM-EDS and XRD also allowed both feldspars and ilmenites to be identified. Tourmaline was identified with XRD, and was probably observed under the stereo microscope in the insoluble fraction that remained after the dissolution of the samples in hydrochloric acid. Additionally, tourmaline was observed as well under the polarising microscope. It was, however, difficult to differentiate this mineral from another similar one, amphibole, based merely on microscopic observations. As the optic signs of these minerals are different, uniaxial for tourmaline, and biaxial for amphibole, it was possible to identify the grains correctly as tourmaline. It may also be mentioned that whilst several point analyses were performed on these grains with SEM-EDS[1], the results were not sufficient to distinguish them from amphiboles, as the major elements in both minerals are similar. In some samples, *e.g.* MRBT-1I, fragments of dolomite limestone were detected, and may have been an aggregate. It may be remarked, however, that these lithic fragments could have been an additive as well, though if so, its function is unclear.

---

[1] The protective lacquer layer for these thin sections had to be first removed before the analysis could be done.

In MRBT-1E, MRBH3-12E, MRBH7-13BE, MRBH7-13VE, and MRBF-16E, the aggregate consist mainly of carbonates, specifically grains of calcite. The results of the analyses performed on these samples using XRD, polarised light microscopy, SEM-EDS, and TGA support each other. Whilst XRD allowed the samples to be characterised mineralogically, polarised light microscopy and SEM-EDS provided information about the morphology of the grains, ('angular' / euhedric), and a rough estimation of their size (large). Moreover, polarised light microscopy allowed the texture of these grains to be observed, thus allowing it to be differentiated from fragments of limestone. These aspects have been touched upon in Chapter 3. Furthermore, the DTG curves obtained from the TGA curves of these samples (with the exception of MRBT-1E) show that the thermal reaction peaked at 800°C or higher. As a comparison, in the other samples, the peaks occur at a lower temperature, *i.e.* between 700°C and 800°C. The thermal decomposition temperature of carbonates may vary due to a number of factors, one of which is the crystallinity of the material (Földvári, 2011, p. 108; Duran et al., 2010, p. 807), and another being the grain size. The thermal decomposition of minerals with higher crystallinity and larger grains occurs at a higher temperature than those with lower crystallinity and smaller grains. Therefore, the combined results of these analyses suggest that the calcite came from a metamorphic rock, *i.e.* marble, rather than from a sedimentary one, *e.g.* limestone. Additionally, Vitruvius (*On Architecture*, Book VII, Chapter III, 6) mentions the application of three layers of marble powder over three layers of sand mortar for stuccos. The marble in these samples show that the Romans at *Mirobriga* followed Vitruvius' recipe to some extent, *i.e.* applying a layer of marble powder, instead of the recommended three.

Three techniques – SEM-EDS, TGA, and XRD, allowed the binder to be characterised. The results of the point analyses conducted using SEM-EDS (both on the binder and on the lime lumps) showed that the binder is composed mainly of calcium carbonate ($CaCO_3$) with little impurities. Although magnesium (Mg) was detected in the binder, this element occurred only in trace amounts, thus making it unlikely that the raw material of the binder was dolomite. As for TGA, the peak of the DTG curves in the majority of the samples was registered between 700°C and 800°C, which lies within the temperature range in which calcite decomposes (Chiari et al., 1992, p. 113). Additionally, the use of XRD allowed the identification of the calcium carbonate ($CaCO_3$) is calcite, as opposed to one of its other polymorphs, *i.e.* aragonite and vaterite. Hence, the most probable raw material used for the production of the binder is limestone.

Materials that do not fall conveniently under the category of either aggregate or binder were also detected during the analyses, some of which will be dealt with presently. In certain samples, additives were observed. This is most notable in MRBT-2E, where ceramic / brick fragments were visible both with the naked eye, and on a microscopic level. These may have served as a substitution for the famous pozzolana [the volcanic earth found "in the neighbourhood of Baiae and in the country belonging to the towns round about Mt. Vesuvius" (*On Architecture*, Book II, Chapter VI, 1)] (Wright, 2005, p. 198). The addition of ceramic / brick fragments is commonly found in Roman mortars, and was meant to improve the mortar's impermeability and hydraulicity (Borsoi et al., 2010, p. 50; Silva et al., 2006, pp. 86-87). The pozzolanic quality of this sample would have also been provided by the addition of crushed brick / ceramic powder to the mortar itself.

The presence of clay minerals and / or micas in the samples was detected with XRD. It has been noted, however, that the identification of these minerals with this technique is complicated due to two factors – firstly, these minerals usually occur in small quantities in the samples, meaning that they might either not stand out adequately, or be masked by the major components (this problem was mitigated by analysing the fine fraction of the samples); secondly, the peaks of these minerals occur within a narrow range, and may overlap one another, making it difficult to separate one from the other (Alvarez et al., 2000, p. 1414). Apart from XRD, these minerals were observed as well under the stereo microscope in the insoluble residue left behind by the acid attack. The presence of clay minerals and / or micas in the mortar is important as they have generally been considered to be a possible substitute for the famed pozzolana (Coutelas, 2003, p. 86). These minerals may have been part of the limestone, hence associated with the binder (see, for example, Pavía & Caro, 2008. p. 1810), or collected along with the sand, thus being part of the aggregate, or perhaps even coming from both sources. SEM-EDS analysis of the lime lumps suggests that they contain little impurities (silicon, aluminium, and magnesium). Due to this reason, it may be said that these minerals were unlikely to have come from the limestone, but may be associated with the sand. This may also explain the lack of impurities in MRBT-IE, MRBH3-12E, MRBH7-13BE, MRBH7-13VE, and MRBF-16E, as the aggregates in these samples consist mainly of calcite grains, rather than sand. Additionally, it has been suggested that the presence of such fine particles may be an indication that the aggregate had been selected with less care, or insufficiently sieved before being used (Ontiveros-Ortega et al., 2016, p. 221).

4.2. Provenance

The provenance of the mortar's raw materials was determined by combining the results of the analyses with the information provided by ancient authors, and the geological map of the area surrounding *Mirobriga*. This section may be divided two parts – the aggregate and the binder.
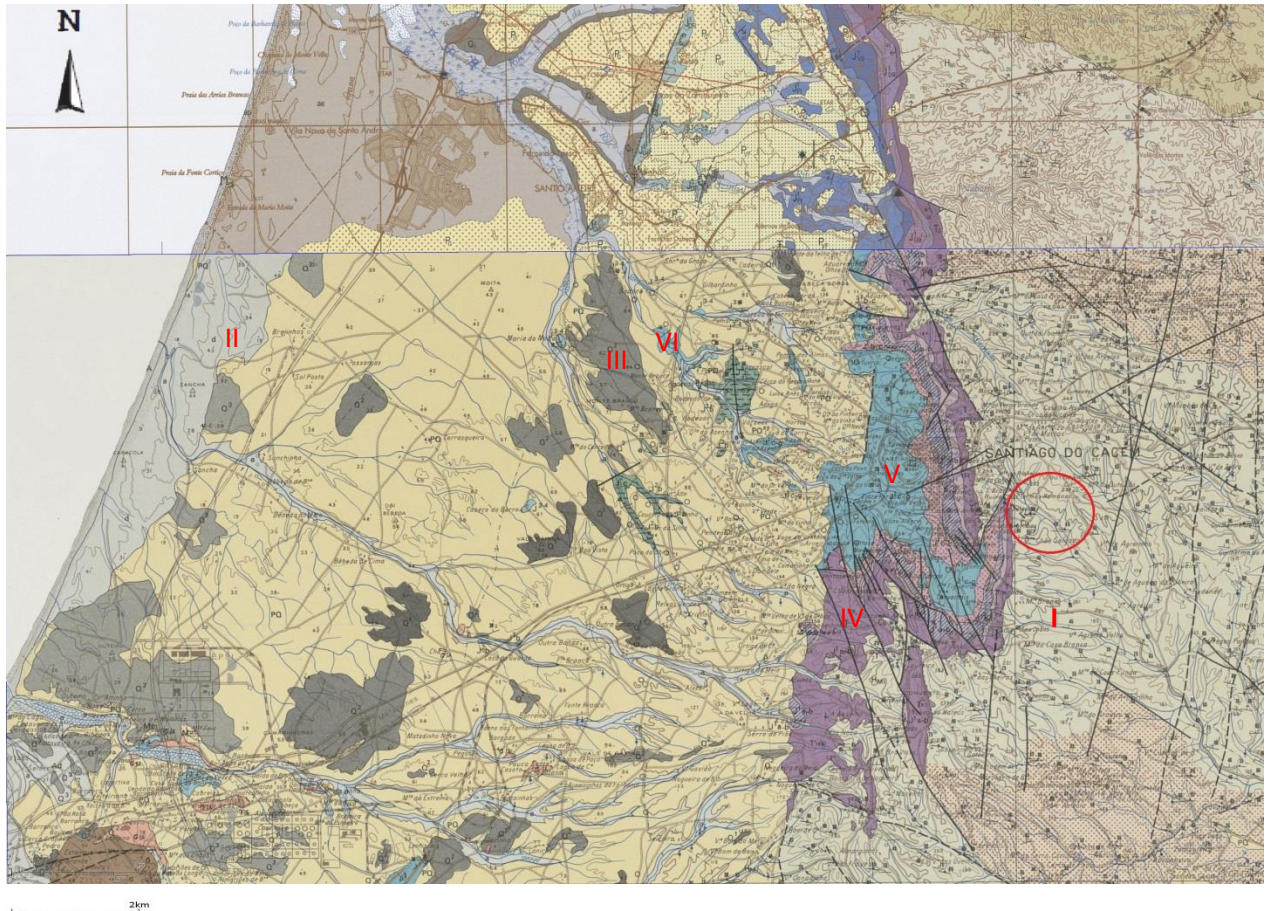
Figure 4.1. Geological map of the area around *Mirobriga* (in the red circle) (the Roman numerals identify areas and will be referenced in the text) (see Annex 4.1. for the legend) [taken and adapted from *Laboratório Nacional de Energia e Geologia* (LNEG), http://geoportal.lneg.pt/geoportal/mapas/index.html].

According to Vitruvius (*On Architecture*, Book II, Chapter IV) and Pliny (*Natural History* ,Book XXXVI, Chapter LIV), three types of sand may be used as the aggregate of a mortar – river sand, sea sand, and pit sand. Due to the high cost of transporting sand over long distances (because of its weight and bulk), the sand used for the production of mortars would have normally been acquired from local sources (Schnabel, 2008, p. 2). The geological map of the land around *Mirobriga* (Map 4.1.) shows that

all three types of sand mentioned by Vitruvius and Pliny may be found locally, and therefore each would be considered in turn.

The geological map shows that there are numerous streams within the vicinity of *Mirobriga*, and these would have been the closest source of sand (I) available to the builders of the site. The morphology of the sand grains (which range from 'subangular' to 'well-rounded'), however, suggest that they have been transported over a great distance. There are no major river systems within the vicinity of the site, and the closest one, the Sado River, lies further to the north. Moreover, if sand from these streams was used to produce the mortars, the presence of minerals / lithic fragments from the surrounding area would be expected to be found in the samples. The geological map shows that the streams flow through the Mira Formation (H_{Mi}), which was formed during the Namurian A. This formation has been identified as a flysch (a type of sedimentary rock formation) consisting predominantly of greywacke, siltstone, and carbonaceous schist ("*A Formação de Mira,… uma formação turbidítica do tipo «flysch», constituída predominantemente por grauvaques finos e siltitos,… e xistos carbonosos.*") (Inverno et al., 1993, p. 15). Neither fragments of such local rocks nor minerals definitively associated with them were detected in the samples.

As the site is situated not too far (about 20km) from the Alentejo coast, sea sand (II) would have been another option available to the Roman builders of *Mirobriga*. In *On Architecture*, Book II, Chapter IV, 2, Vitruvius mentions the possibility of using sea sand as the aggregate of a mortar. He adds, however, that this type of sand has certain defects, for instance, that it dries slowly, and that it gives out a salty efflorescence. Moreover, Vitruvius recommends that crushed bricks be added to a mortar with sea sand, so as to improve its quality (*On Architecture*, Book II, Chapter V, 1). In the samples from *Mirobriga*, salts were not detected by the analyses. As an illustration, Silva et al. (2011, p. 1645-1647) was able to determine the presence of halides with XRD, and attributed the TGA weight loss at 120-200 °C to hydrated salts. Such indicators were not present in the samples studied. Additionally, fragments of seashells, which are expected to be present in sea sand (see, for example, Silva et al., 2011), were not seen in the samples.

Although river and sea sand may be used as aggregates, Vitruvius recommends their use only if pit sand is not available. Much of the area to the west of *Mirobriga* is covered by sand dunes and deposits of ancient beaches (III) formed either during the Plio-Pleistocene (marked as PQ) or the Pleistocene (marked as Q^{1-4}) (Inverno et al., 1993, pp. 30-33). The general composition of the former is as follows – orange and red sands with small quartz pebbles, schist chips, and fragments of reddish

sandstones from the Triassic ("*Os depósitos são constituídos, em regra, por areias alaranjadas e avermelhadas com pequenos seixos de quartzo, lascas de xisto e fragmentos de arenitos avermelhados do Triásico.*") (Inverno et al., 1993, p. 31). As the mortar samples consist of colourless or white-coloured quartz grains, rather than those of the red or orange variety, it is unlikely that the sand was sourced from this area. The latter is divided according to the height of the ancient beaches, with areas of Q^1 (90-100 m) and Q^2 (60-70 m) being closest to the site. Q^1 is composed of gravel with poorly rolled pebbles ("*São constituídos por cascalheiras com seixos mal rolados*"), whilst general composition of Q^2 has been given as well-rounded sand with pebbles ("*São constituídos por areias com seixos, em regra bem rolados*") (Inverno et al., 1993, p. 32). It is most probable that the aggregate used for the manufacture of the mortars came from Q^2.

The main aggregate in MRBT-1E, MRBH3-12E, MRBH7-13BE, MRBH7-13VE, and MRBF-16E, is not quartz, but calcitic crystal grains, most likely marble chips. Neither the results of the analyses nor the archaeological data is sufficient to determine the provenance of the marble with a reasonable amount of certainty. In 1988, Keay (p. 112) wrote that "to date only a few of the major ancient marble quarries have been located in Iberia", and this gap in knowledge persists till this day (J. C. Quaresma, pers. comm., 26 July 2018). Nevertheless, the geological map of the area shows that there are no sources of marble in the vicinity of the site. As a consequence, the marble would have needed to be obtained from further afield. The best-known source of marble in Portugal is located in Estremoz, and it is known that white marble from the quarries there was not only used locally, but also exported across central and southern Spain during the Roman Imperial period (Russell, 2013, p. 23). Closer to *Mirobriga* is the site of Trigaches (located to the northwest of Beja), where grey marble was extracted and used locally during the Roman period (Russell, 2013, p. 57). It has been suggested during the 1990s that the marble from the *thermae* was obtained from this site (J. C. Quaresma, pers. comm., 26 July 2018). Moreover, under the stereo microscope, the marble aggregates seem to have a greyish hue. Therefore, it is plausible that the marble chips were obtained from the quarry of Trigaches. It may be noted that in MRBF-16E, the carbonate aggregates consist not only of calcitic grains, but contains carbonates of a sedimentary (though slightly metamorphosed) origin as well. As these two types of rocks are not expected to occur together naturally, it may be speculated that they were intentionally mixed together.

From the geological map, two potential sources for the limestone used to produce the binder were identified – J^1c-g (V), and J^{3-4} (VI).

Before discussing these potential limestone sources, some attention may be drawn to the area marked as J^1a-b (IV), which lies just to the west of *Mirobriga*. This area contains dolomites, and is the closest source of calcium carbonate ($CaCO_3$) available to the Romans. These rocks, however, also contain a high amount of magnesium oxide (MgO) (between 20-21%) (Inverno et al., 1993, p. 20). The use of dolomites as the raw material for a binder may be determined through XRD [in the form of the mineral magnesite, ($MgCO_3$) or as lithic fragments] and TGA [where two peaks, one representing the thermal decomposition of magnesium carbonate ($MgCO_3$), and the other that of calcium carbonate ($CaCO_3$), may be seen] (Montoya et al., 2003). In most of the samples, only a small amount of dolomite was detected by XRD (in the fine fraction), whilst the DTG curves show only a single peak, which corresponds to the decomposition of the calcium carbonate ($CaCO_3$). Moreover, the SEM-EDS analysis of the binder and the lime lumps shows that they contain little magnesium (Mg) in them. Therefore, in spite of the fact that there was a source of calcium carbonate ($CaCO_3$) close to the site, it was not used for making the mortar's binder. This may show an adherence to the advice given by both Vitruvius (*On Architecture*, Book II, Chapter V, 1) and Pliny (*Natural History*, Book XXXVI, Chapter LIII) that lime be produced from white limestone. It may be noted, however, that this could be the source of the dolomite fragments seen in some samples, for instance, MRBT-2I.

The limestone used to make the binder could have been obtained from an area further away from the site, though still close enough to be considered as local. J^1c-g lies to the west of J^1a-b, and contains dolomite, dolomite marl, and Fateota limestone (Inverno et al., 1993, p. 23). Two types of limestone were identified by the geological surveys conducted in this area – oolitic limestone and dolomitised calcite clastic limestone ("*calcários oolíticos e calciclásticos dolomitizados*") (Inverno et al., 1993, pp. 23-24). In MRBD4-5, a fragment of oolitic limestone was observed under the polarising microscope. This fragment, however, does not show signs of dolomitisation, which would cause the individual ooids to lose their features. Moreover, as the limestone from this area is undergoing a process of dolomitisation, a higher level of magnesium (Mg) ought to be detected during the analyses.

Further to the west and the north of the site is J^{3-4}, which is composed of limestone, marl, and Deixa-o-Resto conglomerate (Inverno et al., 1993, p. 26). The types of limestone identified by the geological surveys are bioclastic limestone, clayey limestone, and oolitic limestone (Inverno et al., 1993, pp. 26-27). As mentioned earlier, a fragment of oolitic limestone was observed in MRBD4-5 under the

polarising microscope, which may indicate that the limestone came from this area. Nevertheless, SEM-EDS analysis of the lime lumps showed that they contained little impurities (silicon and aluminium), making it less likely that the limestone came from here, due to the presence of clayey limestone.

The possibility that the limestones came from further afield may also be considered. Vitruvius (*On Architecture*, Book II, Chapter V, 3) reports that when limestone is burnt, about a third of its original weight is lost. By performing the calcination of the limestone at the quarry, the raw material could be more easily transported to a worksite (Malacrino, 2010, p. 62). One possible source of the raw limestone is the site of São Brissos (close to Trigaches). During the Roman period, limestone from the site was not only used locally, but also exported regionally (Russell, 2013, p. 51).

4.3. Production Technology

Two types of technologies will be discussed in this section – the binder to aggregate ratio, and the hydraulicity of the mortars.

The binder to aggregate ratio of the samples was calculated with the following formula, and the results may be found in Annex 3.1.:

Binder : Aggregate = Soluble Fraction (%) / Insoluble Residue (%)   (Eq. 4)

With the exception of a few samples, the proportion of aggregates was found to have been 75±5%. Vitruvius' formula for mortar made with pit sand (*On Architecture*, Book II, Chapter V, 1) is 1 : 3, and the results of the chemical analysis shows that most of the samples respect this recipe.

One of the exceptions is MRBT-2I, where the amount of aggregate is lower than the norm (61.47%). This may be explained by the fact that there was a significant amount of dolomitic limestone as aggregates / additives in the sample, which would have been dissolved by the heated HCl. Another exception is MRBD3-4, where the aggregate was found to have been 84.08%. This sample came from a flight of stairs outside *Domus* 3, and therefore may have been made using a different recipe, so as to suit its function. It seems that MRBH7-13BE and MRBH7-13VE have a high binder-to-aggregate ratio. The aggregates in these samples consist mainly of calcitic grains, hence the higher proportion of insoluble residue compared to the soluble fraction. As the insoluble residue of these samples contain both the binder and the carbonate aggregates, their binder-to-aggregate ratio was not calculated.

The hydraulicity of historical mortars may be determined using a range of analyses, each of which has its own strengths and weaknesses (Elsen et al., 2010, pp. 136-140). For this study, the hydraulic property of the samples was determined using two techniques – chemical analysis and TGA.

Chemical analysis allows the insoluble residue and the soluble fraction of the mortars to be separated. The latter may be divided further between carbonates and solubles (defined as "substances soluble in acid without the evolution of carbon dioxide,") (Jedrzejewska, 1960, p. 132). These substances may include salts and soluble silica, the latter being an indicator of a mortar's hydraulicity (Böke et al., 2006, p. 1116; Jedrzejewska, 1960, p. 132; Maravelaki-Kalaitzaki et al., 2003, p. 657; Stewart & Moore, 1982, p. 11). The method proposed by Jedrzejewska (1960, pp. 132-133) allows the proportion of these three components to be calculated, thus allowing a "very simplified image of the basic composition of the analysed sample,"

Jedrzejewska's experimental setup allowed the values of the insoluble residue and the carbonate to be determined with a single experiment. In this study, however, the proportion of the former was determined using chemical analysis, whilst the latter with TGA. The amount of calcium carbonate ($CaCO_3$) and solubles in each sample was calculated using Equation 5 and Equation 6 respectively:

$$CaCO_3 \ (\%) \ = \ \Delta W \ (\%) \times \frac{M \ CaCO_3}{M \ CO_2} \hspace{3cm} \text{(Eq. 5)}$$

ΔW (%) = TG weight change at 600-950 °C range
$M \ CaCO_3$ = Molar mass of $CaCO_3$ = 100.0868 g/mol
$M \ CO_2$ = Molar mass of CO_2 = 44.01 g/mol

$$\text{Solubles (\%) = 100\% - Insoluble Residue (\%)} – CaCO_3 \ (\%) \hspace{2cm} \text{(Eq. 6)}$$

Whilst the amount of calcium carbonate ($CaCO_3$) was calculated with Equation 5, the amount of lime before the carbonation process, *i.e.* the calcium hydroxide [$Ca(OH)_2$], was calculated with the following equation:

$$Ca(OH)_2 \ (\%) \ = \ \frac{CaCO_3 \ (\%) \ \text{x} \ M \ Ca(OH)_2}{M \ CaCO_3} \hspace{3cm} \text{(Eq. 7)}$$

$M \ Ca(OH)_2$ = Molar mass of $Ca(OH)_2$ = 74.093 g/mol
$M \ CaCO_3$ = Molar mass of $CaCO_3$ = 100.0868 g/mol

Table 4.1. The insoluble residue, the calcium carbonate, $CaCO_3$, the solubles, and the calcium hydroxide, $Ca(OH)_2$[2].

Sample	Insoluble Residue (%)	Calcium Carbonate, $CaCO_3$ (%)	Solubles (%)	Calcium Hydroxide, $Ca(OH)_2$ (%)
MRBT-1I	75.17	19.54	5.29	14.47
MRBT-2E	75.95	9.85	14.20	7.29
MRBT-2I	61.47	34.48	4.05	25.53
MRBD3-3	70.64	21.65	7.71	16.03
MRBD3-4	84.08	8.01	7.91	5.93
MRBD4-5	74.61	17.65	7.74	13.07
MRBD4-6	75.29	30.66	-5.95	22.70
MRBTb1-7	76.26	17.21	6.53	12.74
MRBTb1-8	78.05	18.06	3.89	13.37
MRBTb1-9	-	26.68	-	19.75
MRBTb2-10	74.26	17.69	8.05	13.10
MRBTb2-11	74.89	17.92	7.19	13.27
MRBH3-12E	-	67.86	-	50.24
MRBH3-12I	-	19.06	-	14.11
MRBH7-13BE	5.98	86.40	7.62	63.96
MRBH7-13BI	79.69	14.65	5.66	10.86
MRBH7-13VE	16.76	73.50	9.74	54.41
MRBH7-13VI	70.18	22.72	7.10	16.82
MRBH7-14	77.06	17.94	5.00	13.28
MRBM-15	73.06	10.07	16.87	7.45
MRBF-16E	-	59.54	-	44.08
MRBF-16I	76.13	18.10	5.77	13.40

The accuracy and applicability of Jedrzejewska's method for the analysis of historical mortars was tested by Steward and Moore (1982). In this study, a correlation between the solubles and a mortar's hydraulicity was proposed, "a high content of complex silicates would indicate an hydraulic component and a low content would indicate a non-hydraulic lime mortar." (Stewart & Moore, 1982, p. 11). Although absolute values are provided by experiments conducted by the researchers, these would not be used for the present study, as these values were obtained from standards created specifically for their study, as opposed to mortars from an archaeological site.

---

[2] The negative value of the solubles in MRBD4-6 may be due to the heterogeneity of the sample, *i.e.* that an area with less calcium carbonate was acquired for the chemical analysis, or one with more for the TGA.

Studies concerning the hydraulicity of mortars have also been made based on the results of TGA. It has been found that the carbon dioxide / structurally bound water ratio has an inverse relationship with the hydraulic property of a mortar, *i.e.* the higher the ratio, the lower the hydraulicity, and *vice versa* (Bakolas et al., 1998; Moropoulou et al., 1995; Moropoulou et al., 2005). This follows that as the amount of carbon dioxide increases, the carbon dioxide / structurally bound water ratio increases too. An exponential correlation between the two has been reported (Moropoulou et al., 2005, p. 299). Although the chemical characteristics of the most common types of historical mortars as derived from TGA were identified, and presented in a table by Moropoulou et al. (2005, p. 297) (see Annex 4.2.), its application as a classification guide would not be viable for this study. As an example, for "artificial pozzolanic mortars", the values (in percentage) for the physically bound water, structurally bound water, carbon dioxide, and carbon dioxide / structurally bound water are 1-4, 3.5-8.5, 22-29, and 3-6 respectively. As a comparison, MRBT-2E, which may be classified as an "artificial pozzolanic mortar" based on visual observation, has the following values (in percentage): 0.58, 2.06, 4.33, and 2.10.

Considering that both the solubles and the structurally bound water ratio are indicators of hydraulicity, it may be possible to establish a relationship between these two factors. For instance, Cardoso (2011, pp. 21-22) found that there was an acceptable linear correlation between the solubles and the structurally bound water.

In this study, several correlations were done, resulting in three graphs – Carbon Dioxide vs Carbon Dioxide / Structurally Bound Water (Figure 4.2.I), Solubles vs Structurally Bound Water (Figure 4.2.II), and Solubles vs Carbon Dioxide / Structurally Bound Water (Figure 4.2.III).
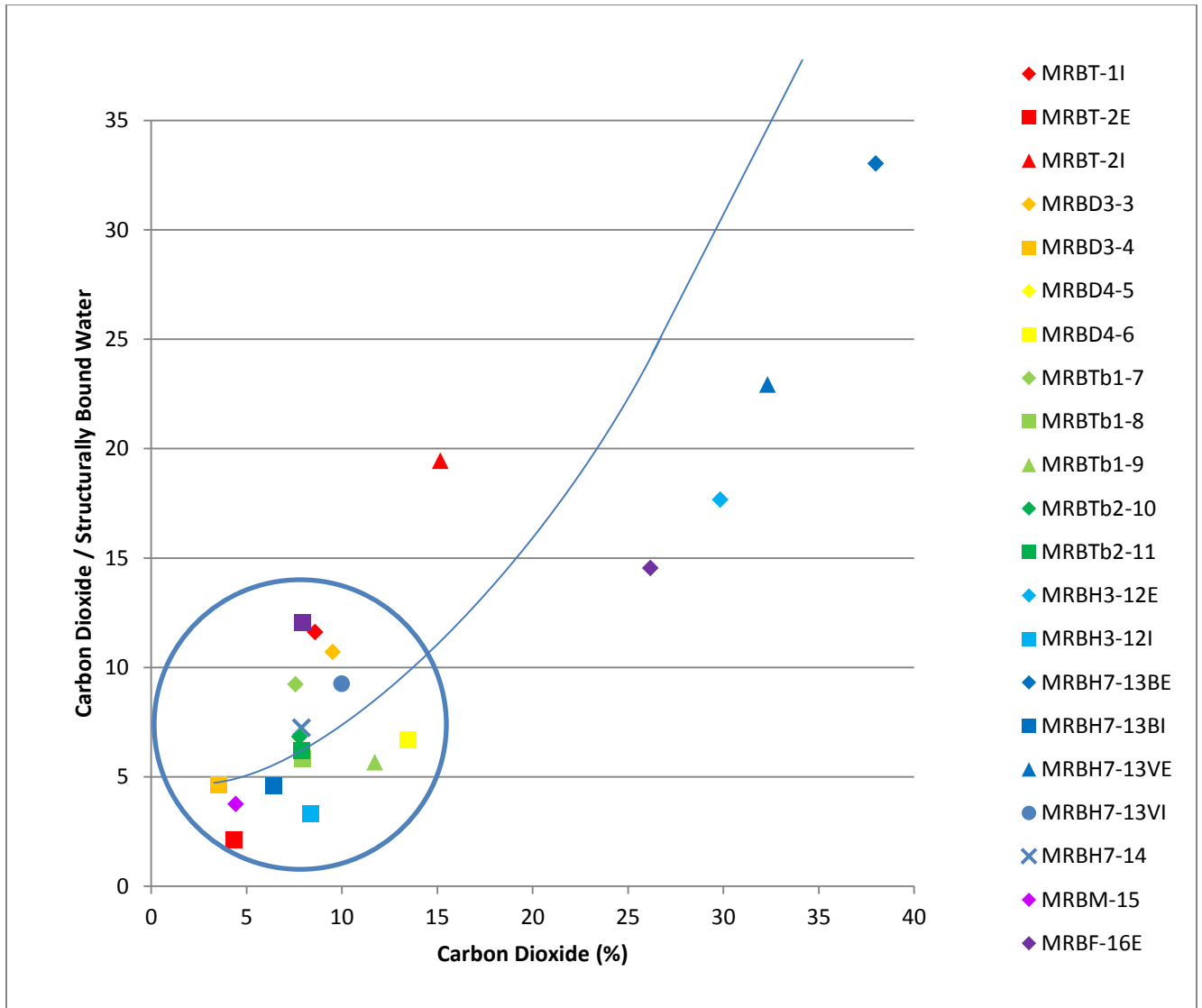
Figure 4.2.I. Carbon Dioxide vs Carbon Dioxide / Structurally Bound Water.
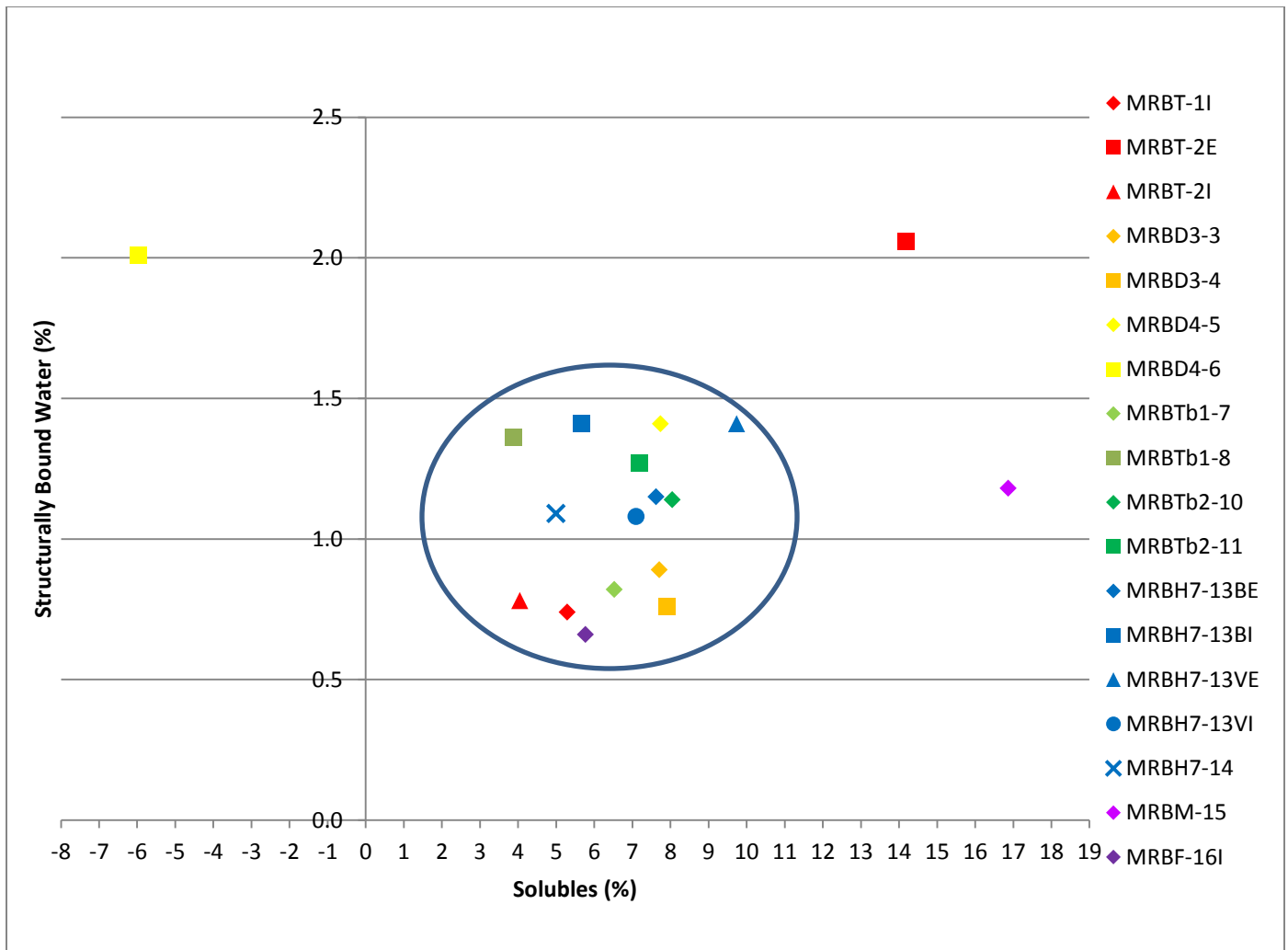
Figure 4.2.II. Solubles vs Structurally Bound Water.
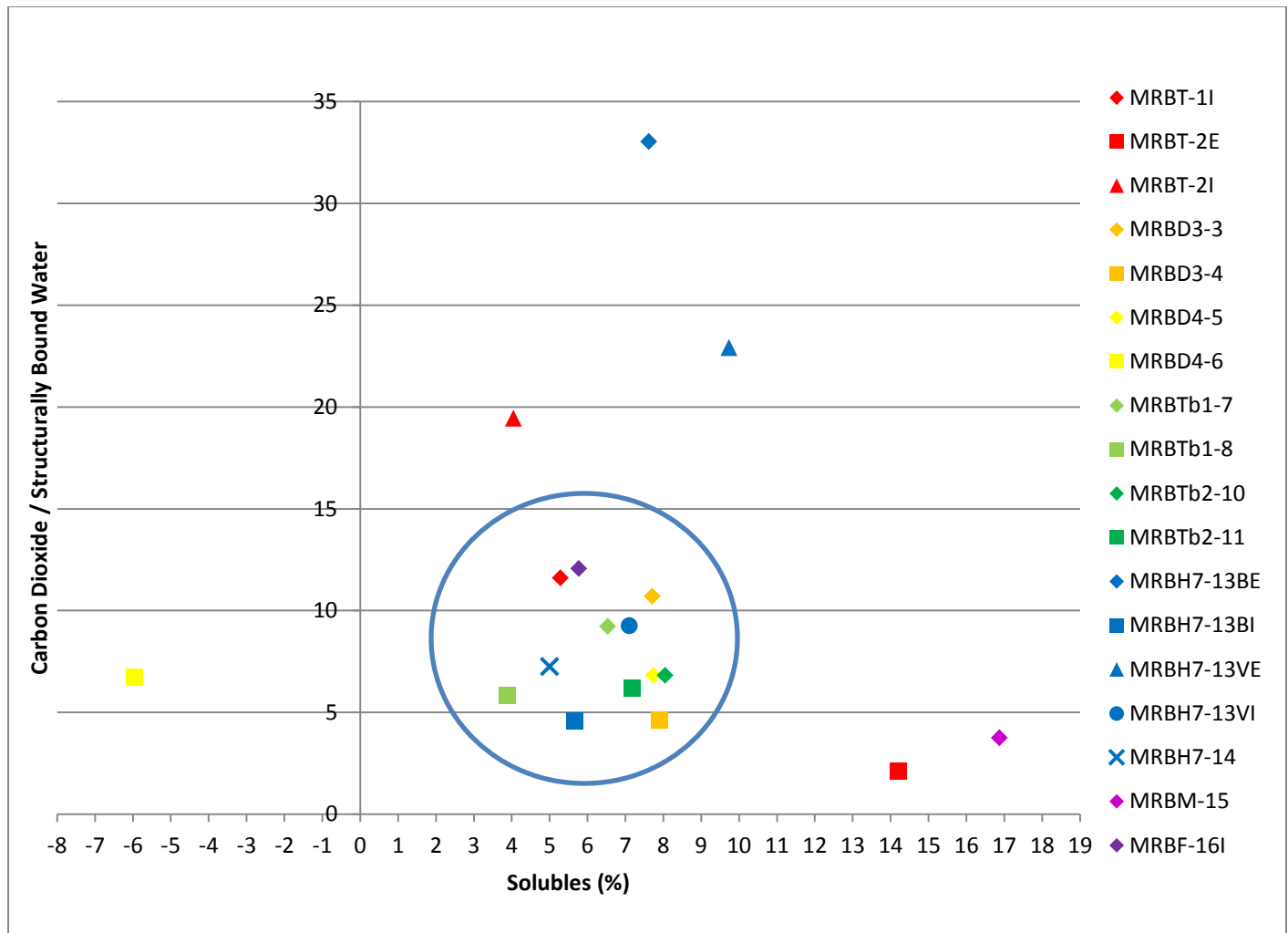
Figure 4.2.III Solubles vs Carbon Dioxide / Structurally Bound Water.

In Figure 4.2.I, there may be an exponential correlation between the carbon dioxide and the carbon dioxide / structurally bound water. It may be added that the exponential correlation between these two factors was also reported by Moropoulou et al. (2005, p. 299), Genestar et al. (2006, p. 337), and Maravelaki-Kalaitzaki et al. (2003, p. 655). Although Cardoso (2011, p. 22) established a linear correlation between the solubles and the structurally bound water, this might not be the case in Figure 4.2.II.

Nevertheless, there is a significant difference between these two sets of graphs. In both Figures 4.2.I. and 4.2.II., it may be observed that the points are concentrated in a small area, as opposed to

being spread out over the graph. This is an indication that in terms of hydraulicity, most of the samples are quite similar to each other.

In Figure 4.2.I., MRBH3-12E, MRBH7-13BE, MRBH-13VE, and MRBDF-16E are located away from the majority of samples. As the aggregates in these layers consist mainly of calcite, a higher amount of carbon dioxide would be expected to be released during the TGA, hence explaining their positions in the graph. Additionally, the position of MRBT-2I away from the cluster of samples in the same graph suggests that it is less hydraulic than the other samples. This sample has a higher mass change in the 600-950 °C range than most samples due to the presence of dolomite fragments as aggregates. Additionally, its position higher up on the y-axis shows that it has a low amount of structurally bound water.

In the Figure 4.2.II., it may be observed that MRBT-2E has a high amount of both solubles and structurally bound water. It has been reported that thermally decomposed clay minerals from the ceramic fragments are soluble in acid (Kramar et al., 2011, p. 1052). As MRBT-2E is rich in ceramic fragments, a high proportion of solubles was expected to be obtained from the chemical analysis. The high quantity of structurally bound water supports this finding. On the other hand, although MRBM-15 shows a high proportion of solubles, it has a lower than expected amount of structurally bound water. It may be suggested that the solubles in the sample contain other acid-soluble compounds apart from complex silicates.

In Figure 4.2.III., it may be observed that the majority of the samples are concentrated in one area of the graph, which further demonstrates their uniformity. The powdered marble layers, *i.e.* MRBH7-13BE and MRBH7-13VE are located outside this cluster due to their high proportion of carbon dioxide / structurally bound water. The position of MRBT-2I shows that it is less hydraulic than most of the other samples, whereas those of MRBT-2E and MRBM-15 show that these samples have a higher hydraulicity than the norm. This graph may also be used to describe the relative hydraulicity of the samples. The majority of the samples may be said to display 'some level of hydraulicty', whilst those outside the norm may either be less hydraulic (to the left of the norm) or more hydraulic (to the right of the norm).

5. Conclusion

5.1. General Considerations

The most striking aspect about the samples studied is their uniformity. It may be said that no clear difference was observed between the filling and rendering mortars, in terms of chemical and mineralogical composition, as well as their microstructure. In addition, this uniformity would lend support to the archaeological results regarding the period of the buildings' construction, *i.e.* that they are contemporaneous, and were built between the 1st and 2nd centuries AD.

In terms of the composition of the mortars, it was found that in most of the samples, the aggregate consists mainly of quartz, and that these grains have a consistent morphology and size. The same may be said of the binder, in that they are chemically and mineralogically consistent in the majority of the samples.

Be that as it may, there are several samples that are different, due to their function. The aggregates in MRBT-IE, MRBH3-12E, MRBH7-13BE, MRBH7-13VE, and MRBF-16E were found to consist mainly of calcitic crystal grains, probably marble. Additionally, it may be said that the binder for these layers contain less impurities. These samples served as stucco layers on which paint was applied. MRBT-2E is also noticeably different due to the addition of ceramic fragments. Additionally, powdered bricks / ceramics were also mixed into the binder, causing it to have a reddish colour. These additives function as an artificial pozzolan in the mortar.

In terms of provenance, it is most probably that the quartz sand came from local sand pits. The marble in MRBT-IE, MRBH3-12E, MRBH7-13BE, MRBH7-13VE, and MRBF-16E, on the other hand, would have been imported from further afield, either from Estremoz or from Trigaches. As for the limestone used to produce the binder, it is quite certain that they were not obtained from the nearby dolomite outcrops. It is possible that the limestone was acquired from local quarries, or that they came from outside the area, for instance, from Trigaches.

In terms of technology, the aggregate to binder ratio for most of the samples may be said to be similar. The majority of the samples have a 1 : 3 binder to aggregate ratio, which adheres to the recipe provided by Vitruvius. In MRBT-IE, MRBH3-12E, MRBH7-13BE, MRBH7-13VE, and MRBF-16E, a higher binder-to-aggregate ratio was seen. In fact, the soluble fraction of these samples consists of both the binder and the calcitic aggregates that dissolved in the hydrochloric acid, resulting in a higher binder-to-aggregate ratio. MRBT-1I was another exception, due to the lower amount of aggregates that was

recorded. This is due to the fact that fragments of dolomitic limestone were present in it, either as an aggregate or as an additive. In any case, these lithic fragments dissolved in the acid along with the lime binder.

In addition, most of the samples display a comparable level of hydraulicity. The correlation between the carbon dioxide and the carbon dioxide / structurally bound water (Figure 4.2) agrees with the findings of previous research. This does not seem to be the case, however, with the Solubles vs Structurally Bound Water graph (Figure 4.3.). The majority of samples in this study were found to be clustered in a specific area, indicating that they are quite similar to one another. Be that as it may, there are, once again, several exceptions, notably MRBH3-12E, MRBH7-13BE, MRBH-13VE, MRBDF-16E, and MRBT-1I in Figure 4.2.., and MRBT-2E and MRBF-16I in Figure 4.3. Lastly, a graph showing the relationship between the solubles and carbon dioxide / structurally bound water (Figure 4.4.) was plotted. Like the other two graphs, this graph shows that most of the samples belong in a cluster, which signifies their uniformity. This graph may also be used to describe the sample's relative hydraulicity, those within the cluster having 'some level of hydraulicity', whilst those outside the norm having either a higher or lower level of hydraulicity than the norm.

5.2. Suggestions for the Future

1. Although geoarchaeological studies have yet to be conducted at *Mirobriga*, it is hope that they will begin next year (J. C. Quaresma, pers. comm., 26 July 2018). This may be a good opportunity to collect and analyse rocks from the site and from the surrounding area. This would be useful to ascertain the provenance of the limestone used for the binder. Sand form the potential sources in the area may also be sampled in order to confirm its provenance.

2. Point counting could be carried out as a means to determine the binder to aggregate ratio of the samples. This would be useful for samples in which the aggregates would dissolve along with the binder in the acid, for example, the calcitic grains in MRBT-IE, MRBH3-12E, MRBH7-13BE, MRBH7-13VE, and MRBF-16E.

3. More samples from the *thermae* and structures built to be in contact with water, for example, cisterns, could be collected and analysed. This would allow more studies to be carried out on the pozzolanic reaction and its products. Additionally, the hydraulicity of this type of mortar may be further studied. Such studies would lead to a better understanding of this Roman technology. Moreover, the ceramic fragments in these samples may be analysed as well using XRD.

4. Mortar samples (if available) from structures built before the Roman period could be collected in order to understand the technological evolution of this material.

5. A more comprehensive study of the soluble fraction through chemical analysis (see, for instance, Maravelaki-Kalaitzaki *et al.*, 2003) could be carried out.

6. The physical-mechanical properties of the mortars could be studied, so as to characterise them more thoroughly. Moreover, the relationship between the composition of the mortars and their physical-mechanical properties could be established (see, for instance, Moropoulou *et al.*, 2005). This would be useful future conservation and restroation purposes.

7. Collaboration with archaeologists from *Mirobriga* should continue. Considering that the site is still being excavated, new samples may be obtained, and their characterisation may be required.

8. The results of this study could be compared with those obtained from other Roman sites in Portugal, or even from other parts of the former Roman Empire. In this way, this study could be fitted into a bigger picture.

Bibliography

Alarcão, J. de, 1967. On the Westernmost Road Of the Roman Empire. *Archaeology,* 20(3), pp. 174-177.

Alarcão, J. de, 1976. MIROBRIGA (Santiago do Cacém) Alentejo, Portugal.. In: R. Stillwell, W. L. MacDonald & M. H. McAllister, eds. *The Princeton Encyclopedia of Classical Sites.* Princeton, New Jersey: Princeton University Press, p. 584.

Alvarez, J., Navarro, I., Martín, A. & Casado, P. G., 2000. A study of the ancient mortars in the north tower of Pamplona's San Cernin church. *Cement and Concrete Research,* Volume 30, pp. 1413-1419.

Arizzi, A. & Cultrone, G., 2013. The influence of aggregate texture, morphology and grading on the carbonation of non-hydraulic (aerial) lime-based mortars. *Quarterly Journal of Engineering Geology and Hydrogeology,* Volume 46, pp. 507-520.

Bakolas, A., Biscontin, G., Moropoulou, A. & Zendri, E., 1998. Characterization of structural byzantine mortars by thermogravimetric analysis. *Thermochimica Acta,* Volume 321, pp. 151-160.

Biers, W. R., Biers, J. C. & Soren, D., 1983. Excavations At Mirobriga, The 1982 Season. *MUSE,* Volume 20, pp. 29-43.

Böke, H., Akkurt, S., İpekoğlu, B. & Uğurlu, E., 2006. Characteristics of brick used as aggregate in historic brick-lime mortars and plasters. *Cement and Concrete Research,* Volume 36, p. 1115–1122.

Borelli, E., 1999. *ARC Laboratory Handbook, Volume 4/99.* Rome: ICCROM.

Borsoi, G. et al., 2010. 'Chemical, mineralogical and microstructural characterization of historical mortars from the Roman villa of Pisões, Beja, Portugal', in J. Válek, C. Groot & J. J. Hughes (eds.), *2nd Conference on Historic Mortars - HMC 2010 and RILEM TC 203-RHM final workshop, 22-24 September 2010, Prague, Czech Republic*, RILEM Publications, Paris, pp. 43-54.

Cardoso, I., 2011, 'Cidade Romana de Ammaia: estudo das argamassas', Mestrado em Conservação e Restauro, Universidade Nova de Lisboa, Lisbon.

Chiari, G., Santarelli, M. & Torraca, G., 1992. Caratterizzazione delle malte antiche mediante l'analisi di campioni non frazionati. *Materiali e Strutture. Problemi di Conservazioni,* Volume 3, pp. 111-137.

Claude Ptolémée, *Traité de géographie de Claude Ptolémée d'Alexandrie*. Fac-similé, Paris: Jean Peyroux, 1989.
[Halma, N. B. (trad.), 1828. *Traité de géographie de Claude Ptolémée d'Alexandrie.* Paris: Eberhart, Imprimeur du collège royal de France]

Coutelas, A., 2003, 'Pétroarcheologie du mortier de chaux gallo-romain. Essai de reconstitution et d'interprétation des chaînes opératoires : du matériau au métier antique', Thèse de doctorat, Université Panthéon-Sorbonne (Paris 1), Paris.

Coutinho, J. de S., 1999. *Materiais de construção I : agregados para argamassas e betões*. Porto: FEUP.

Direção-Geral do Património Cultural, Ministério da Cultura, 2011. *Cidade romana de Miróbriga / Ruínas de Miróbriga / Castelo Velho.* [Online] Available at: http://www.monumentos.gov.pt/Site/APP_PagesUser/SIPA.aspx?id=4076 [Accessed 21 May 2018].

Duran, A., Pérez-Maqueda, L. A., Poyato, J. & Pérez-Rodríguez, J. L., 2010. A thermal study approach to Roman age wall painting mortars. *Journal of Thermal Analysis and Calorimetry,* Volume 99, pp. 803-809.

Elsen, J., Van Balen, K., Mertens, G., 2010. 'Hydraulicity in historic lime mortars: a review', in J. Válek, C. Groot & J. J. Hughes (eds.), *2nd Conference on Historic Mortars - HMC 2010 and RILEM TC 203-RHM final workshop, 22-24 September 2010, Prague, Czech Republic*, RILEM Publications, Paris, pp. 129-145.

European Committee for Standardization, 2002, *European Standard EN 13139:2002 Aggregates for mortar*, European Committee for Standardization, Brussels.

Földvári, M., 2011. *Handbook of thermogravimetric system of minerals and its use in geological practice.* Budapest: Geological Institute of Hungary.

Genestar, C., Pons, C. & Más, A., 2006. Analytical characterisation of ancient mortars from the archaeological Roman city of Pollentia (Balearic Islands, Spain). *Analytica Chimica Acta,* Volume 557, pp. 373-379.

Grassl, P., Wong, H. S. & Buenfeld, N. R., 2010. Influence of aggregate size and volume fraction on shrinkage induced micro-cracking of concrete and mortar. *Cement and Concrete Research,* Volume 40, pp. 85-93.

Hughes, J. J. & Válek, ., 2003. *Literature Review - Mortars in Historic Buildings. A Review of the Conservation, Technical, and Scientific Literature.* Edinburgh: Historic Scotland.

Inverno, C. M. C. et al., 1993. *Notícia Explicativa da Folha 42-C, Santiago do Cacém.* Lisbon: Serviços Geológicos de Portugal.

Jedrzejewska, H., 1960. Old Mortars in Poland: A New Method of Investigation. *Studies in Conservation,* 5(4), pp. 132-138.

Keay, S. J., 1988. *Roman Spain.* Berkeley, Calif.: University of California Press.

Kenneth Pye Associates Ltd, 2018. *GRADISTAT.* [Online] Available at: http://www.kpal.co.uk/gradistat.html [Accessed 27 July 2018].

Kramar, S. et al., 2011. Mineralogical and microstructural studies of mortars from the bath complex of the Roman villa rustica near Mošnje (Slovenia). *Materials Characterization,* Volume 62, pp. 1042-1057.

Malacrino, C. G., 2010. *Constructing the Ancient World: Architectural Techniques of the Greeks and Romans.* Translated by J. Hyams. Los Angeles, Calif.: The J. Paul Getty Museum.

Maravelaki-Kalaitzaki, P., Bakolas, A. & Moropoulou, A., 2003. Physico-chemical study of Cretan ancient mortars. *Cement and Concrete Research,* Volume 33, p. 651–661.

Montoya, C. et al., 2003. Study of ancient dolomitic mortars of the church of Santa Maŕia de Zamarce in Navarra (Spain): Comparison with simulated standards. *Thermochimica Acta,* 398(1), pp. 107-122.

Moropoulou, A., Bakolas, A. & Anagnostopoulou, S., 2005. Composite materials in ancient structures. *Cement & Concrete Composites,* Volume 27, pp. 295-300.

Moropoulou, A., Bakolas, A. & Bisbikou, K., 1995. Characterization of ancient, byzantine and later historic mortars by thermal and X-ray diffraction techniques. *Thermochimica Acta,* Volume 269/270, pp. 779-795.

Ontiveros-Ortega, E., Rodríguez-Gutiérrez, O. & Navarro, A. D., 2016. Mineralogical and physical–chemical characterisation of Roman mortars used for monumental substructures on the Hill of San Antonio, in the Roman city of Italica (prov. Baetica, Santiponce, Seville, Spain). *Journal of Archaeological Science: Reports,* Volume 7, pp. 205-223.

Pavía, S. & Caro, S., 2008. An investigation of Roman mortar technology through the petrographic analysis of archaeological material. *Construction and Building Materials,* Volume 22, pp. 1807-1811.

Pliny the Elder, *Natural History*
[Rackham, H. (trans.), 1938. *Pliny the Elder's Natural History, Vol. II: Books 3-7.* London: William Heinemann Ltd.]

Pliny the Elder, *Natural History*
[Eichholz, D.E. (trans.), 1938. *Pliny the Elder's Natural History, Vol. X: Books 36*. London: William Heinemann Ltd.]

Quaresma, J. C., 2010, Changement et continuité: la romanisation à Chãos Salgados, Santiago do Cacém – *Mirobriga*? – (Portugal). In Corsi C. & Vermeulen, F., eds. *Changing Landscapes: The Impact of Roman Towns in the Western Mediterranean: Proceedings of the International Colloquium, Castelo de Vide, Marvão, 15th-17th May, 2008*. Bologna: Ante Quem, pp. 347-356

Quaresma, J. C., 2012. *Economia antiga a partir de um centro de consumo lusitano. Terra sigillata cozinha em Chãos Salgados (Mirobriga?).* Lisbon: Centro de Arqueologia da Universidade de Lisboa.

Revell, L., 2014. Romanization. In: R. B. Ulrich & C. K. Quenemoen, eds. *A Companion to Roman Architecture.* Chichester, West Sussex: Blackwell Publishing Ltd, pp. 381-398.

Russell, B. J. (2013). *Gazetteer of Stone Quarries in the Roman World*. Version 1.0. Accessed (12 September 2018): www.romaneconomy.ox.ac.uk/databases/stone_quarries_database/

Schnabel, L., 2008. Mortar Analysis Part 1: Mortar-Making Materials. *APT Bulletin: The Journal of Preservation Technology,* 39(1), pp. 1-4.

Silva, A. S. et al., 2006. Characterization of Roman mortars from the historical town of Mertola. In: R. Fort, M. A. de Buergo, M. Gomez-Heras & C. Vazques-Calvo, eds. *Heritage, Weathering and Conservation, Volume 2: Proceedings of the International Conference on Heritage, Weathering and Conservation, HWC-2006, 21-24 June 2006, Madrid, Spain.* London: Taylor & Francis, pp. 85-90.

Silva, A. S. et al., 2011. Mineralogical and chemical characterization of historical mortars from military fortifications in Lisbon harbour (Portugal). *Environmental Earth Sciences,* Volume 63, pp. 1641-1650.

Slane, K. W., Biers, W. R., Biers, J. C. & Soren, D., 1984. Mirobriga: The 1983 Season. *Muse,* Volume 17, pp. 38-63.

Slane, K. W. et al., 1985. Mirobriga: A Portuguese-American Project in Southern Portugal. *Muse,* Volume 18, pp. 35-54.
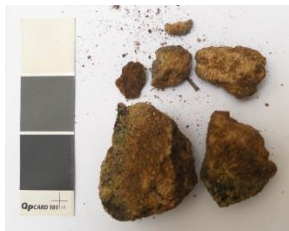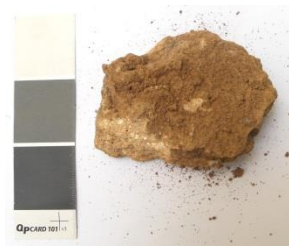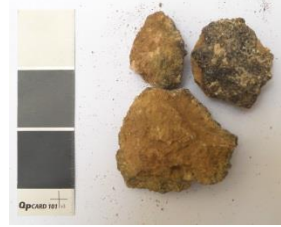
Soren, D. & Soren, N., 1996. Surrogate Stone. *Archaeology,* 49(3), p. 76.

Stewart, J. & Moore, J., 1982. Chemical Techniques of Historic Mortar Analysis. *Bulletin of the Association for Preservation Technology,* 14(1), pp. 11-16.

Velosa, A. L., Coroado, J., Veiga, M. R. & Rocha, F., 2007. Characterisation of roman mortars from Conímbriga. *Materials Characterization,* Volume 58, pp. 1208-1216.

Wright, G. R. H., 2005. *Ancient Building Technology, Vol. 2: Materials, Part 1: Text.* Leiden: Brill.

Annex 2.1. Photographic Register and Observation of the Mortar Samples under the Stereo Microscope

Photographic Register	Stereo microscope (7.8 x magnification)	Photographic Register	Stereo microscope (7.8 x magnification)
MRBT-1		**MRBT-2**	
MRBD3-3		**MRBD3-4**	
MRBD4-5		**MRBD4-6**	
MRBTb1-7		**MRBTb1-8**	

MRBTb1-9	MRBTb2-10
MRBTb2-11	MRBH3-12
MRBH7-13B	MRBH7-13V
MRBH7-14	MRBM-15
MRBHF-16	

Figure 1. Photographic register and observation of the mortar samples under the stereo microscope.

Annex 3.1. Location of the Mortar Samples in Each Structure
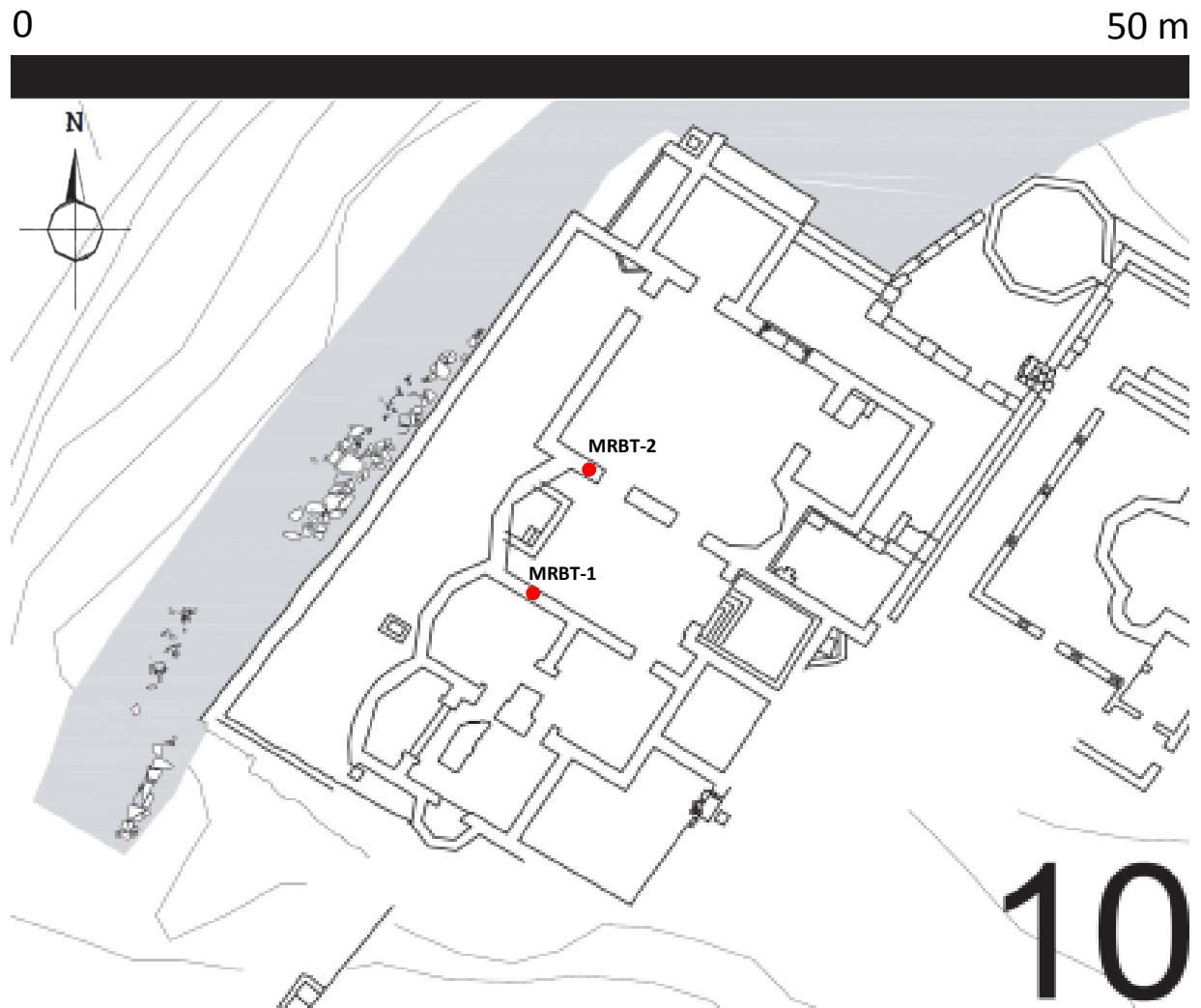
Figure 1. The Western *Thermae* (No. 11 in the general plan) (adapted from Quaresma, 2012, p. 29, Fig. 4).
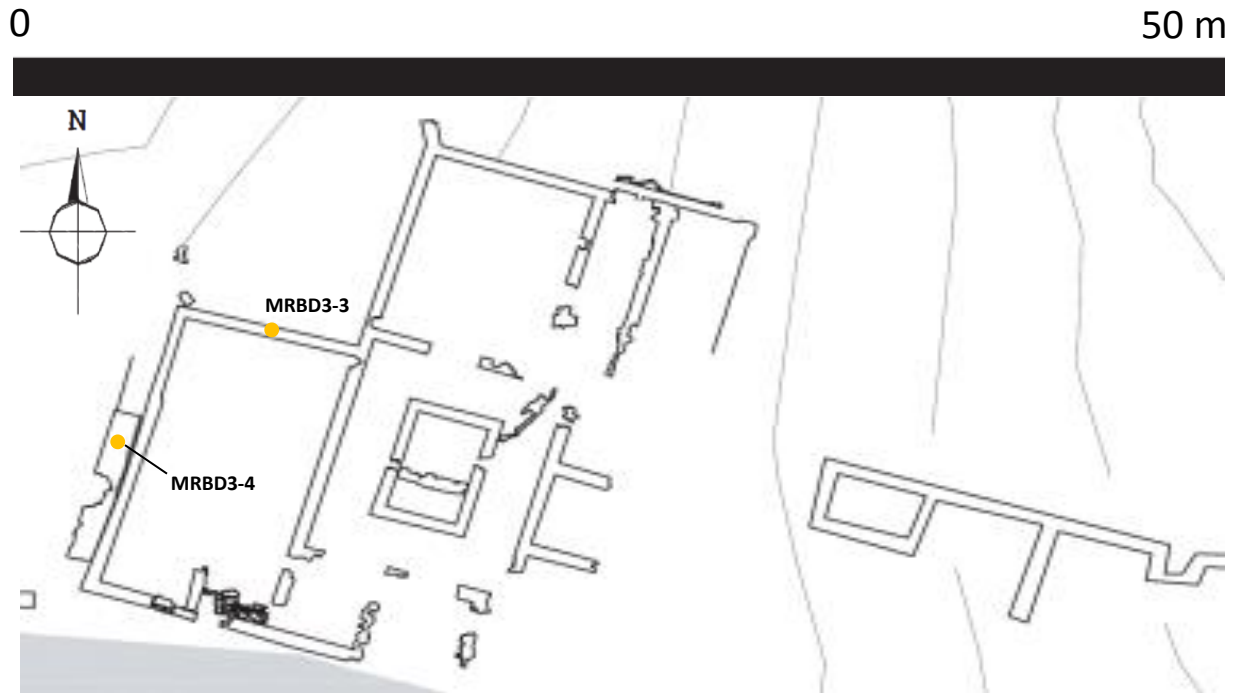
Figure 2. *Domus* 3 (No. 3 in the general plan) (adapted from Quaresma, 2012, p. 29, Fig. 4).
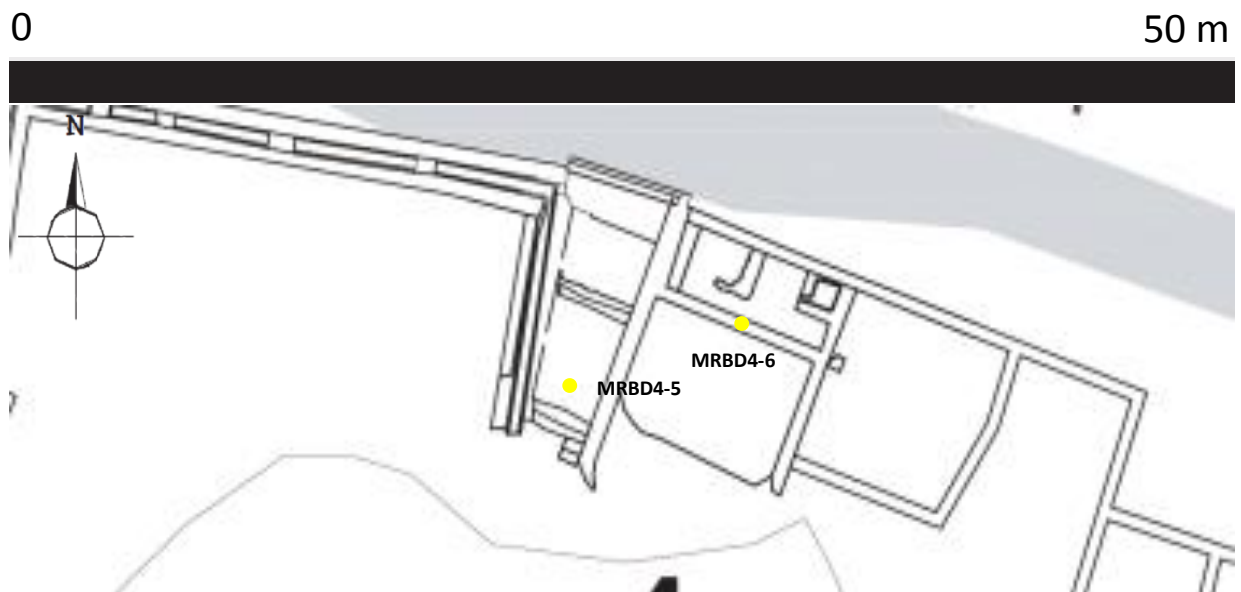
Figure 3. *Domus* 4 (No. 4 in the general plan) (adapted from Quaresma, 2012, p. 29, Fig. 4).
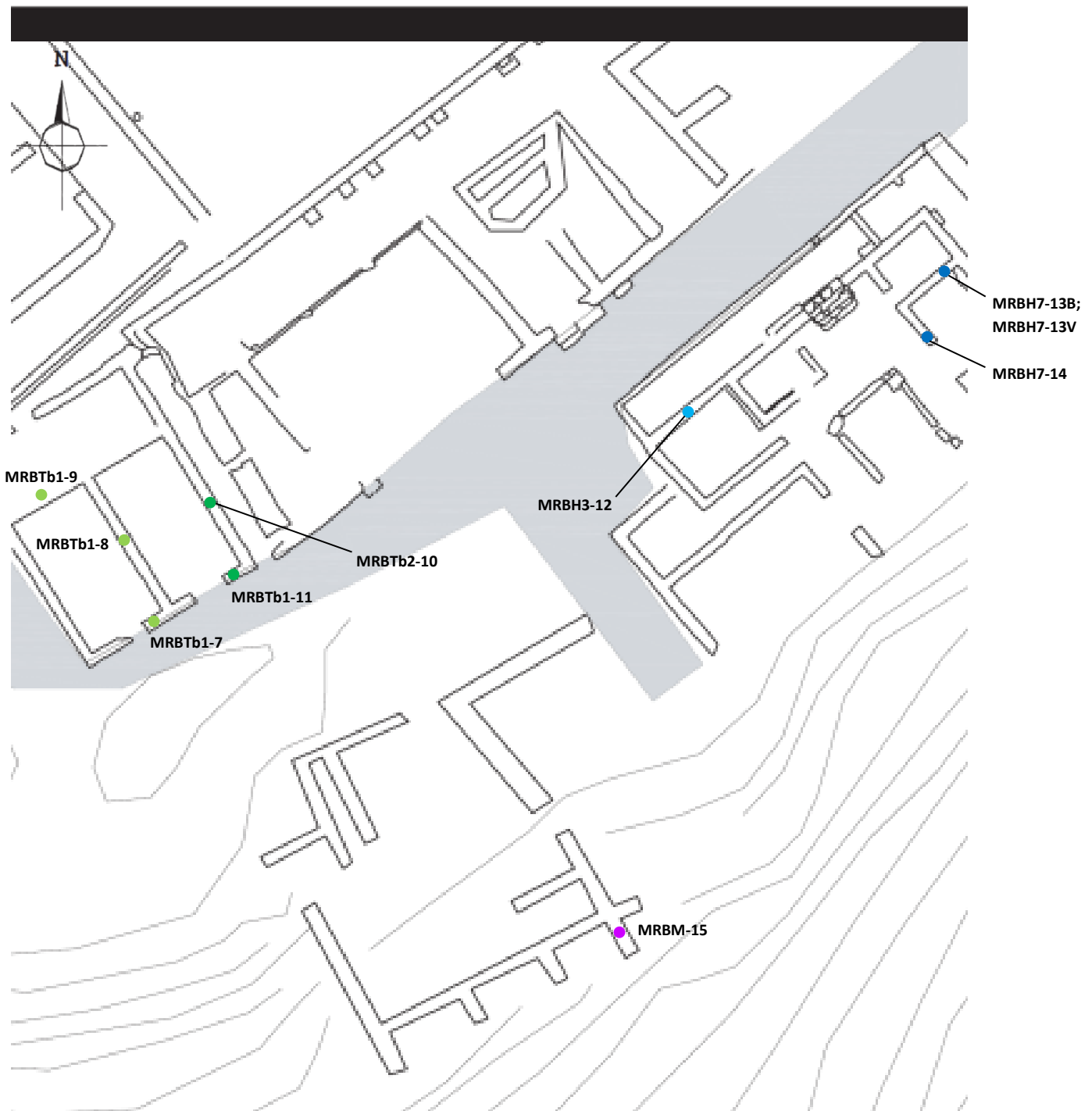
Figure 4. *Taberna* 1 (unmarked in the general plan), *Taberna* 2 (unmarked in the general plan), the 'Hospedaria' (No. 8 in the general plan), and the *macellum* (unmarked in the general plan) (adapted from Quaresma, 2012, p. 29, Fig. 4).

N

MRBF-16

6

Figure 5. The f*orum* (No. 6 in the general plan) (adapted from Quaresma, 2012, p. 29, Fig. 4).

Annex 3.2. The Insoluble Residue, Soluble Fraction, and Binder to Aggregate Ratio of the Mortar Samples

Table 1. The insoluble residue, soluble fraction, and binder to aggregate ratio of the mortar samples.

Sample	Insoluble Residue (%)	Soluble Fraction (%)	Binder : Aggregate
MRBT-1I	75.17	24.83	1 : 3
MRBT-2E	75.95	24.05	1 : 3
MRBT-2I	61.47	38.53	1 : 2
MRBD3-3	70.64	29.36	1 : 2
MRBD3-4	84.08	15.92	1 : 5
MRBD4-5	74.61	25.39	1 : 3
MRBD4-6	75.29	24.71	1 : 3
MRBTb1-7	76.26	23.74	1 : 3
MRBTb1-8	78.05	21.95	1 : 4
MRBTb2-10	74.26	25.74	1 : 3
MRBTb2-11	74.89	25.11	1 : 3
MRBH7-13BE	5.98	94.02	-
MRBH7-13BI	79.69	20.31	1 : 4
MRBH7-13VE	16.76	83.24	-
MRBH7-13VI	70.18	29.82	1 : 2
MRBH7-14	77.06	22.94	1 : 3
MRBM-15	73.06	26.94	1 : 3
MRBF-16I	76.13	23.87	1 : 3

Annex 3.3. The Grain Size Distribution of the Insoluble Residue
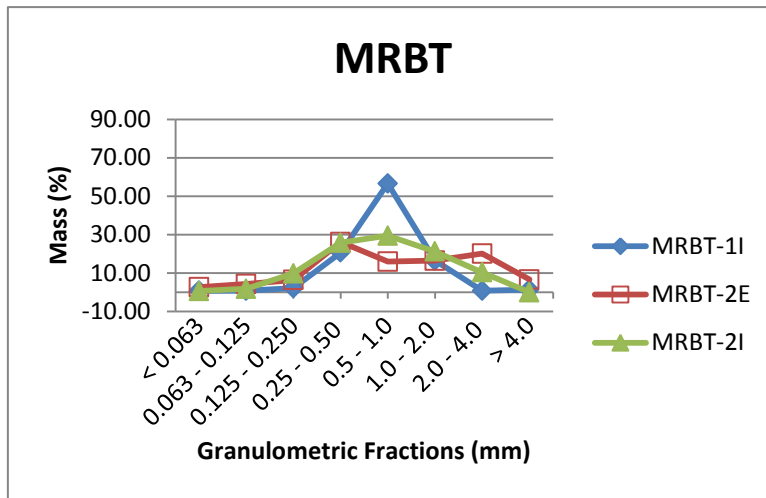
Figure 1. MRBT-1I, MRBT-2E, MRBT-2I.
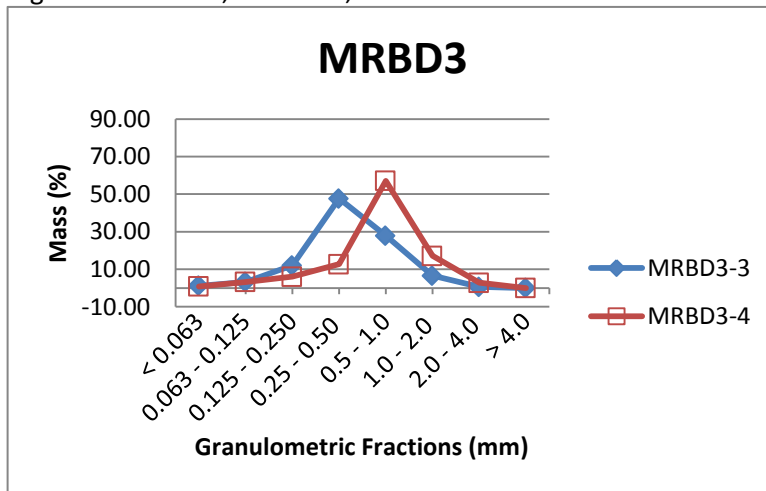
Figure 2. MRBD3-3, MRBD3-4.
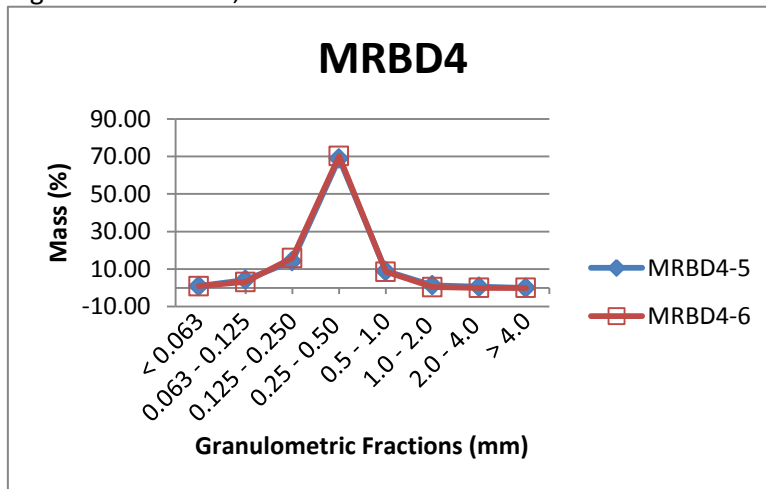
Figure 3. MRBD4-5, MRBD4-6.
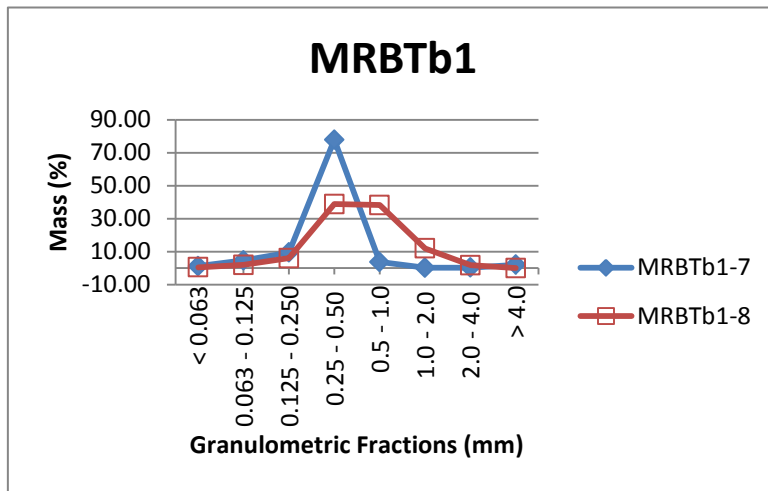
Figure 4. MRBTb1-7, MRBTb1-8.
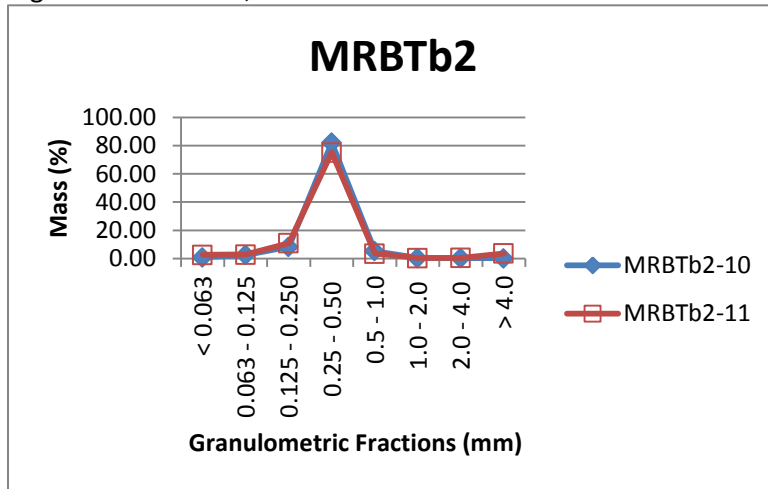
Figure 5. MRBTb2-10, MRBTb2-11.
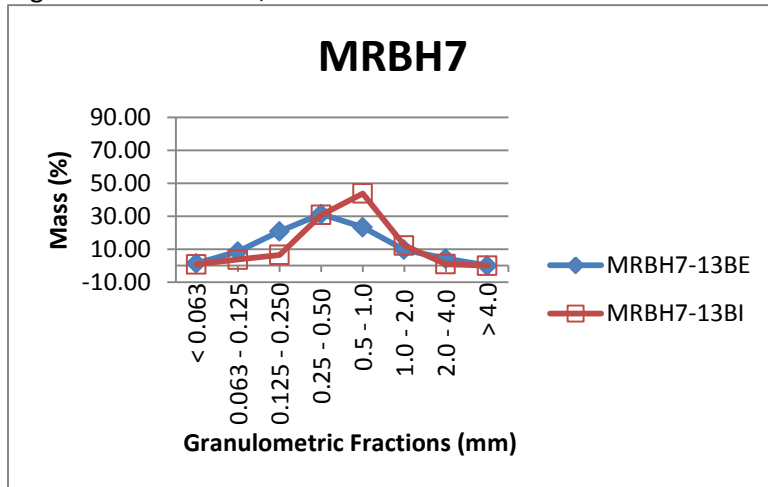
Figure 6. MRBH7-13BE, MRBH7-13BI.
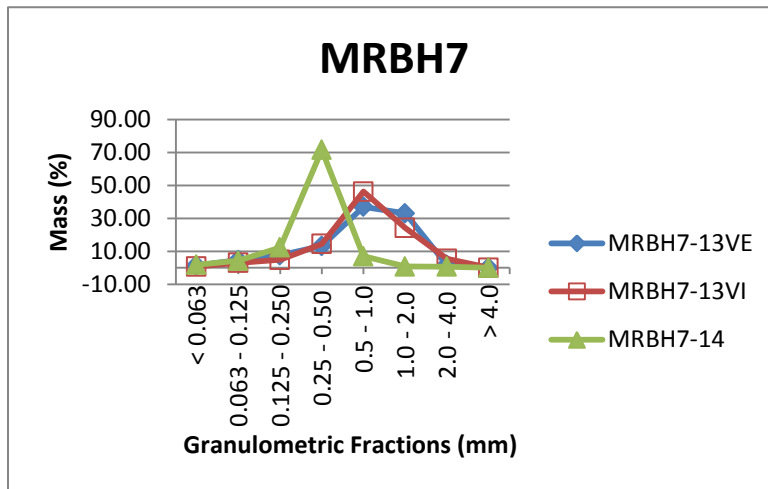
Figure 7. MRBH7-13VE, MRBH7-13VI, MRBH7-14.
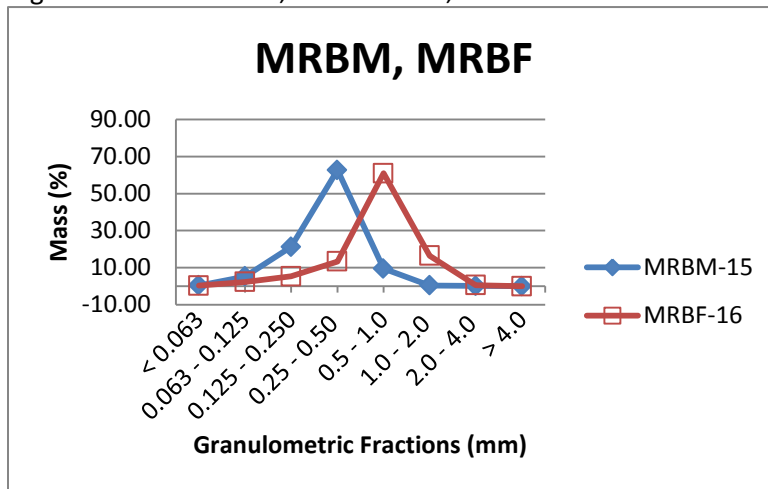
Figure 8. MRBM-15, MRBF-16.

Annex 3.4. Re-sieving of MRBT-1I (SIMAX)

Four fractions of this sample (0.25-0.50 mm, 0.125-0.250 mm, 0.063-0.125 mm and < 0.063 mm) were re-sieved, as lumps of straw-coloured material were observed under the stereo microscope (Figures 1 and 3). To ascertain that these were not remnants of binder due to an incomplete acid attack, a drop of HCL (10 % concentration) was placed on some of the lumps. No reaction was seen. Therefore, it was determined that these are clay materials that were no disaggregated properly after the drying process.

The four fractions were re-sieved to determine the impact of clay materials the on the mass of each fraction. The initial mass of each fraction was measured. The first fraction was then placed in a sieve with a mesh size of 250 μm, disaggregated using the base of a beaker, and sieved. The remaining material was collected, and weighed. The process was repeated for the other two samples using sieves with mesh sizes of 125 μm and 63 μm respectively. The final fraction was collected in a receiver, and weighed.

The results of the experiment are as follows:

Table 1. Mass change of re-sieved sample.

Sample Fraction (mm)	Initial Mass (g)	Final Mass (g)	Mass Change (g)	Mass Change (%)
0.25-0.50	1.3871	1.1021	-0.285	-20.55
0.125-0.250	0.3209	0.2858	-0.0351	-10.94
0.063-0.125	0.1234	0.1702	0.0468	37.93
< 0.063	0.0668	0.1982	0.1302	194.90

Table 2. Mass change in the overall sample.

Sample Fraction (mm)	Recorded Mass before Re-sieving (g)	Recorded Mass before Re-Sieving (%)	Mass after re-sieving (g)	Mass after re-sieving (%)	Mass Change in Overall Sample (%)
0.25-0.50	1.3733	17.79	1.1021	14.96	-2.83
0.125-0.250	0.3216	4.17	0.2858	3.88	-0.29
0.063-0.125	0.1201	1.56	0.1702	2.31	0.75
< 0.063	0.0736	0.95	0.1982	2.69	1.74

Table 1. shows the change in mass that occurred in each fraction after the re-sieving. The largest percentage of change can be seen in the < 0.063 mm fraction (194.90 %), whilst the 0.125-0.250 mm fraction shows the smallest amount of change (-10.94%). In Table 2, however, it may be seen that the

mass change in the overall sample is less than 3%, the highest occurring in the 0.25-0.50 mm fraction (-2.83%), and the lowest in the 0.125-0.250 mm fraction (-0.29%).
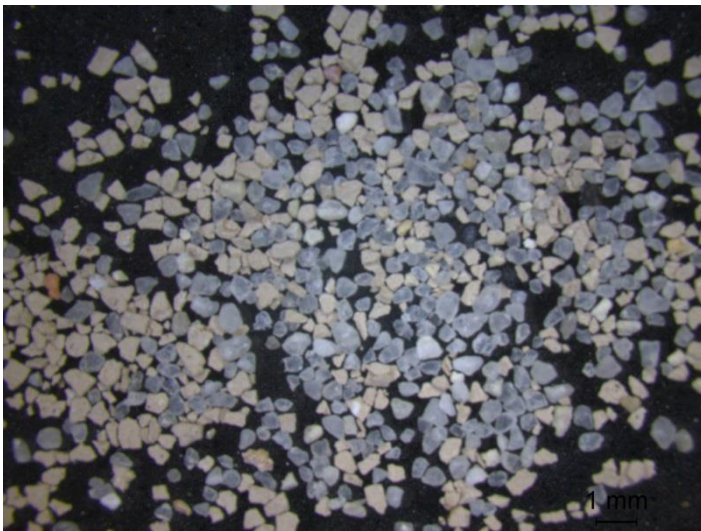
Figure 1. 0.25-0.50 mm fraction before re-sieving, observed under a stereo microscope (7.8x magnification).

Figure 2. 0.25-0.50 mm fraction after re-sieving, observed under a stereo microscope (7.8x magnification).
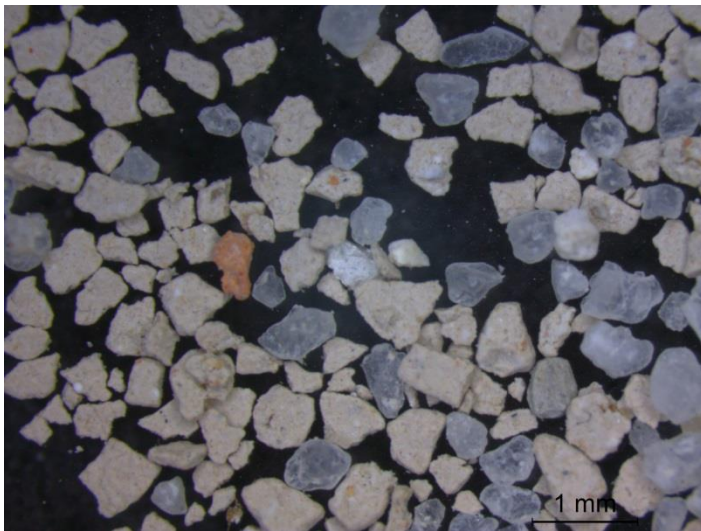
Figure 3. 0.25-0.50 mm fraction before re-sieving, observed under a stereo microscope (20x magnification).
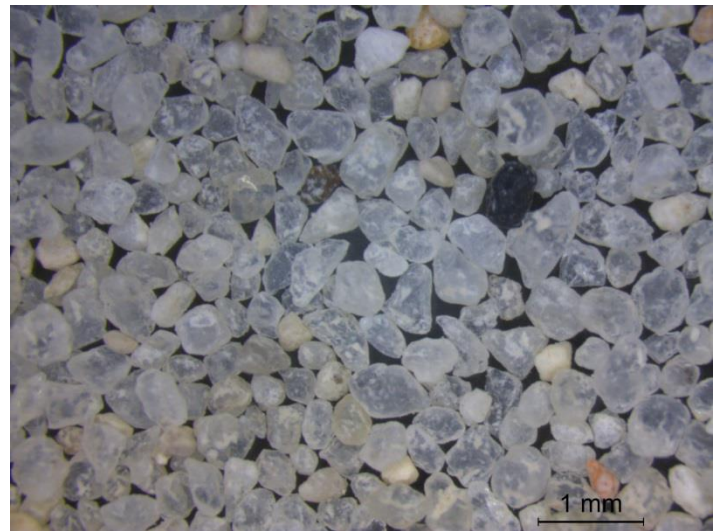
Figure 4. 0.25-0.50 mm fraction after re-sieving, observed under a stereo microscope (20x magnification).

Annex 3.5. Thermogravimetric Graphics / Thermograms
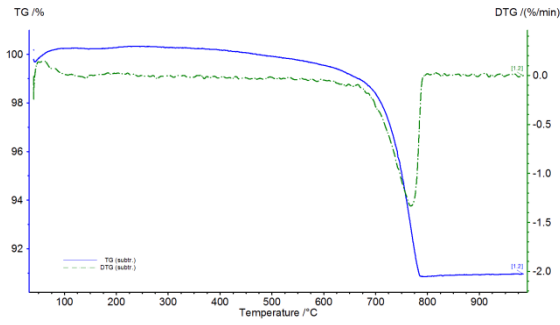
Figure 1. Thermogram of MRBT-1I.
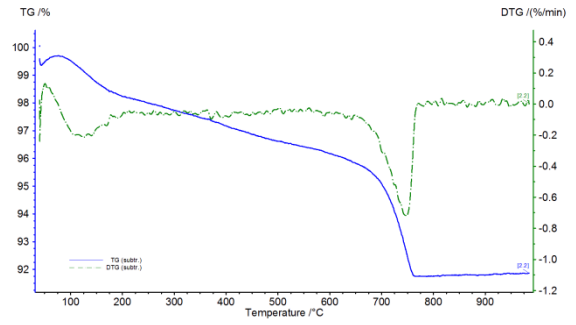
Figure2. Thermogram of MRBT-2E.
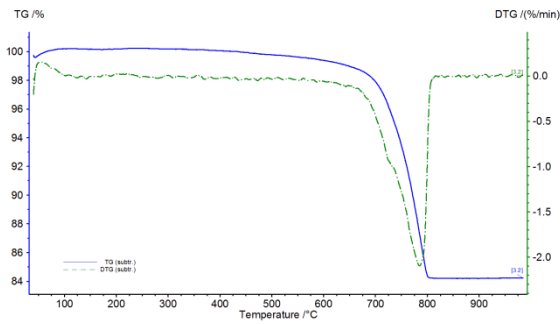
Figure 3. Thermogram of MRBT-2I.
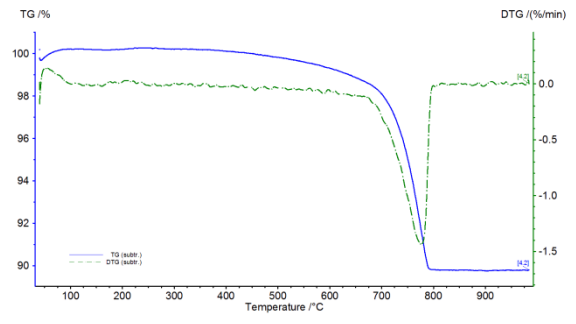
Figure 4. Thermogram of MRBD3-3.
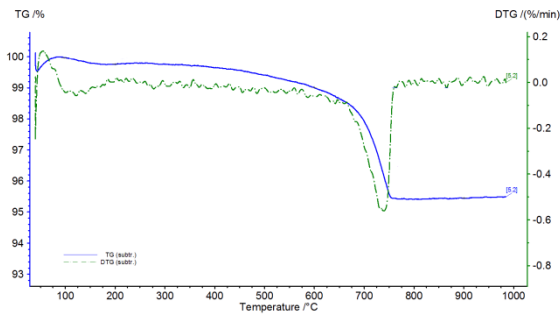
Figure 5. Thermogram of MRBD3-4.
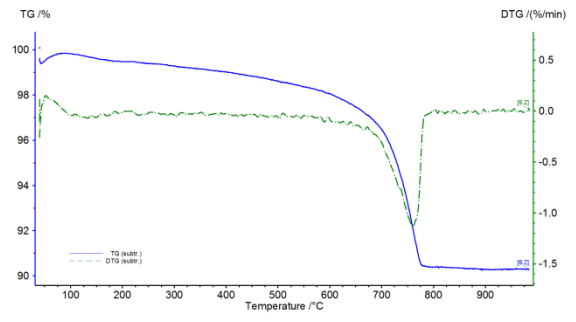
Figure 6. Thermogram of MRBD4-5.
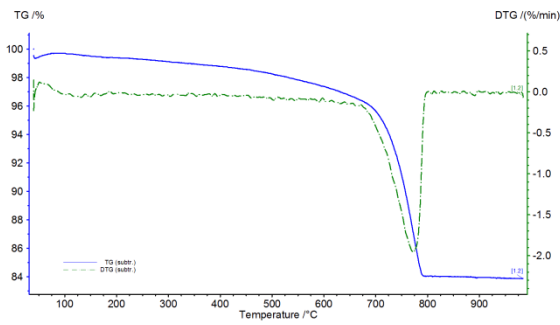
Figure 7. Thermogram of MRBD4-6.
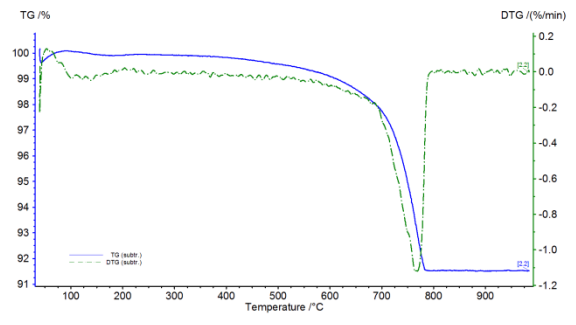
Figure 8. Thermogram of MRBTb1-7.
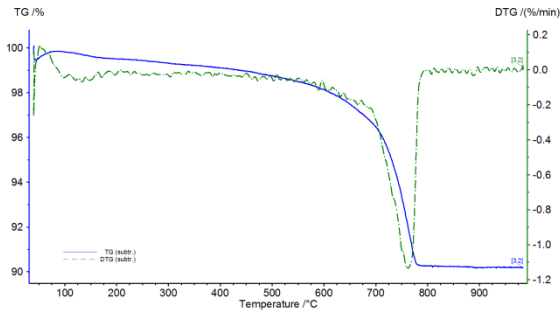
Figure 9. Thermogram of MRBTb1-8.
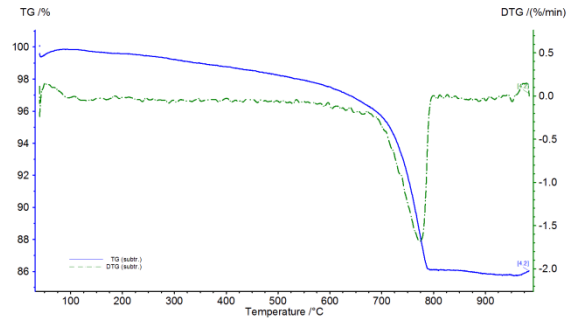
Figure 10. Thermogram of MRBTb1-9.
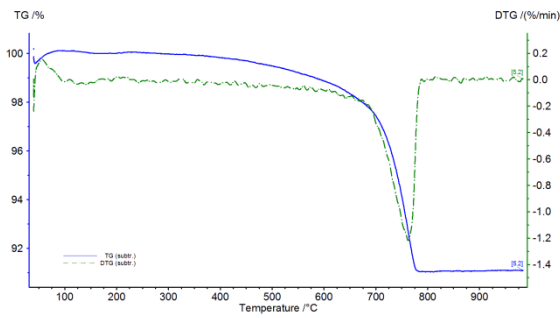
Figure 11. Thermogram of MRBTb2-10.
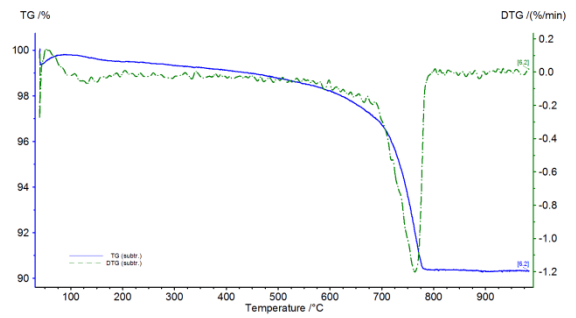
Figure 12. Thermogram of MRBTb2-11.
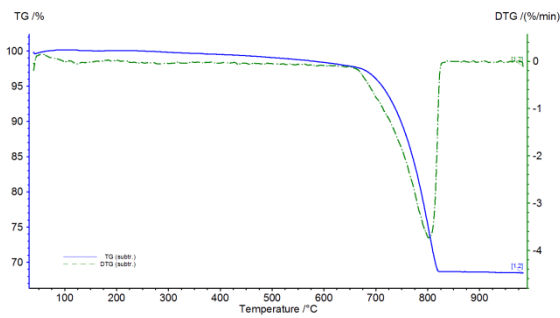
Figure 13. Thermogram of MRBH3-12E.
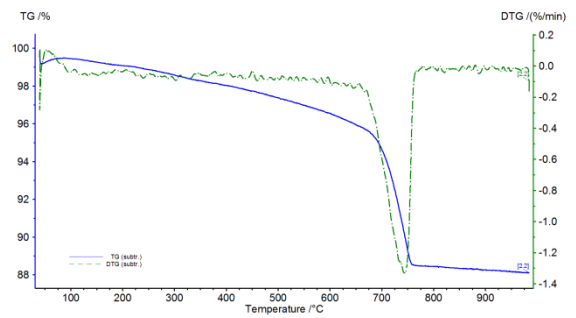
Figure 14. Thermogram of MRBH3-12I.
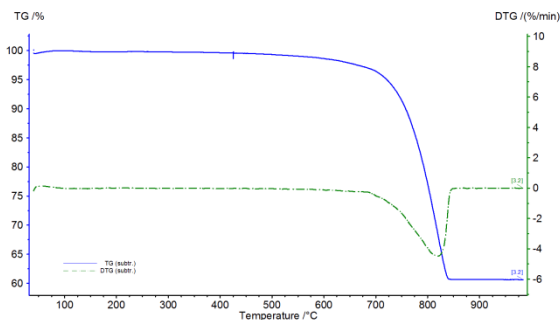
Figure 15. Thermogram of MRBH7-13BE.
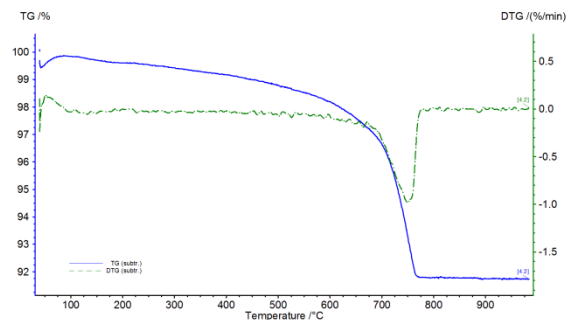
Figure 16. Thermogram of MRBH7-13BI.

78
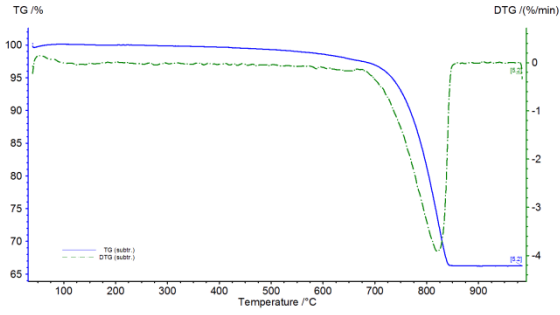
Figure 17. Thermogram of MRBH7-13VE.
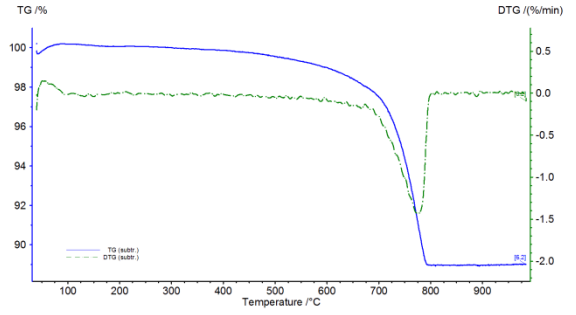
Figure 18. Thermogram of MRBH7-13VI.
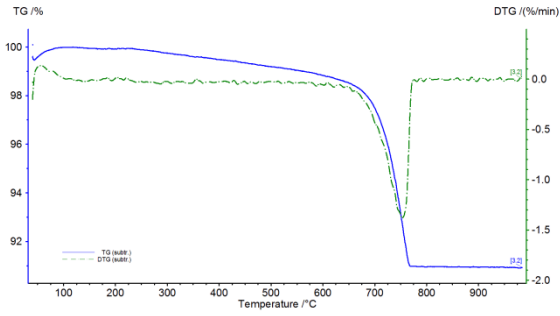
Figure 19. Thermogram of MRBH7-14.
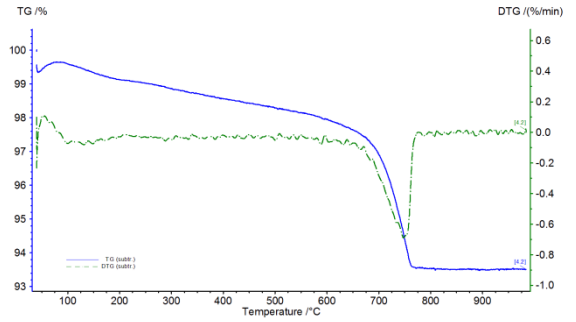
Figure 20. Thermogram of MRBM-15.
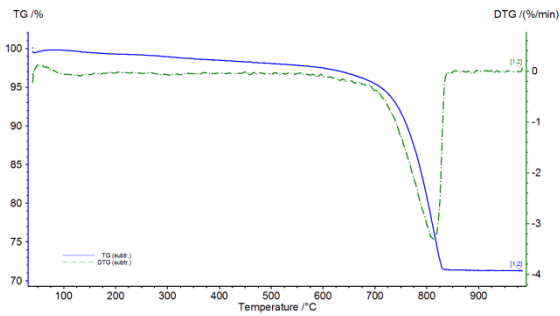
Figure 21. Thermogram of MRBF-16E.
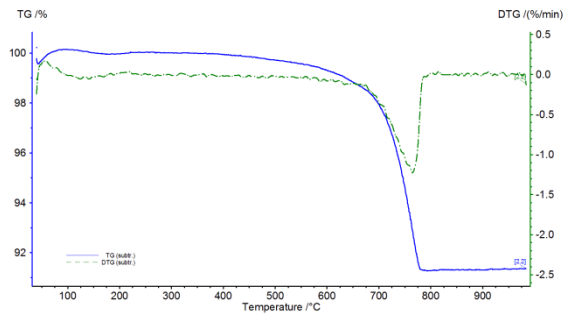
Figure 22. Thermogram of MRBF-16I.

Annex 3.6. Powder X-Ray Diffraction (XRD) Diffractograms (Global Fraction)
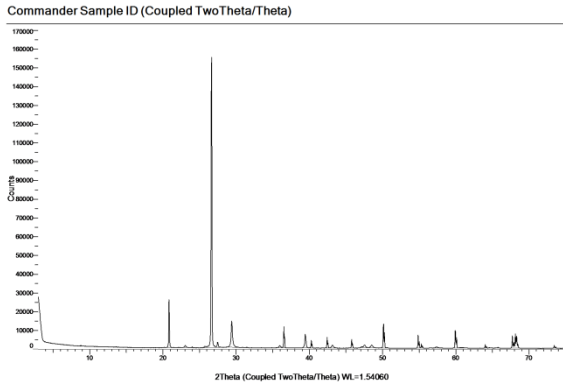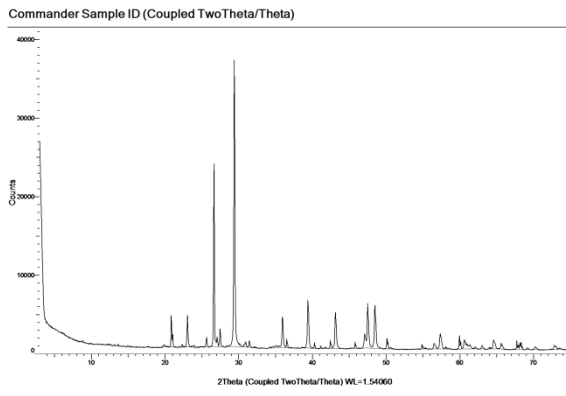

Figure 1. XRD diffractogram of MRBT-1I.
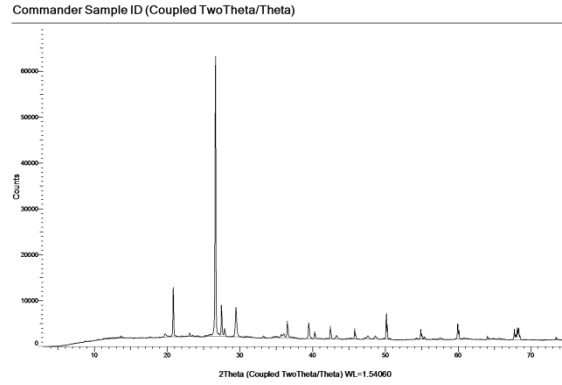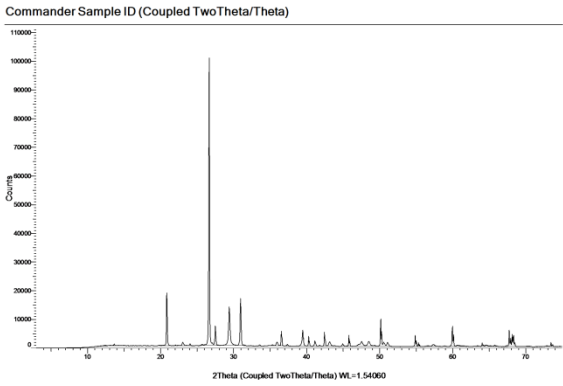
Figure 2. XRD diffractogram of MRBT-2E.

Figure 3. XRD diffractogram of MRBT-2I.
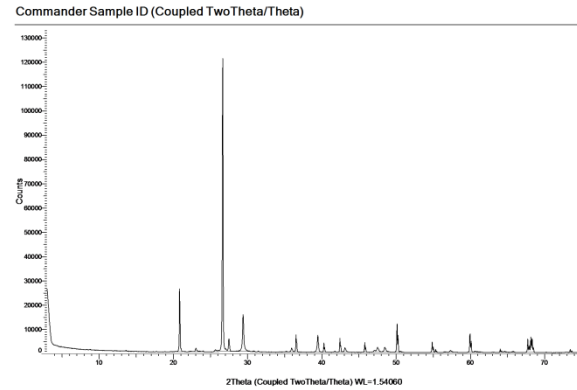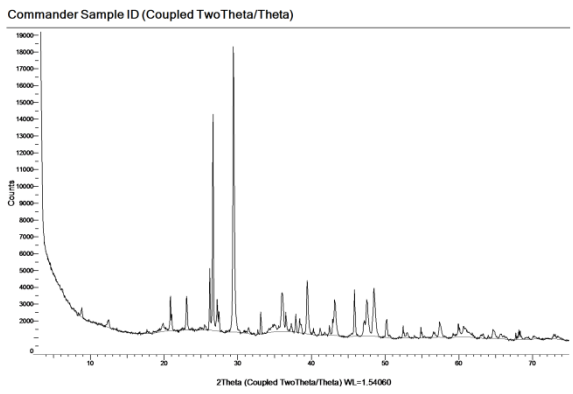

Figure 4. XRD diffractogram of MRBD3-3.
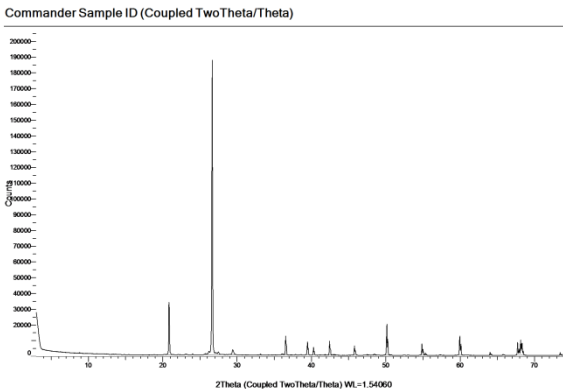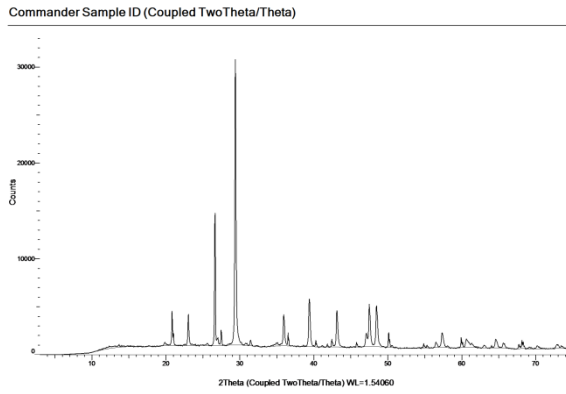

Figure 5. XRD diffractogram of MRBD3-4.
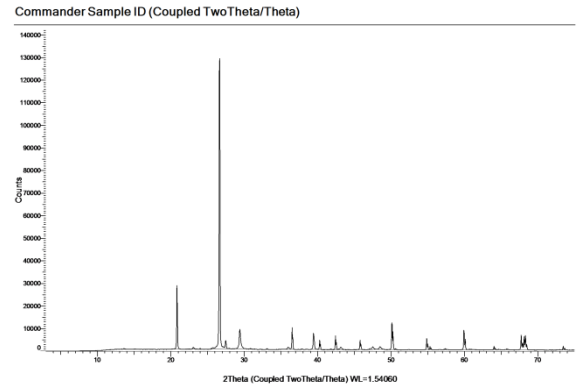
Figure 6. XRD diffractogram of MRBD4-5.
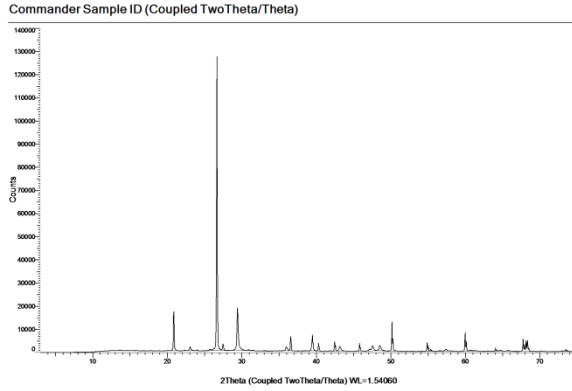
Figure 7. XRD diffractogram of MRBD4-6.
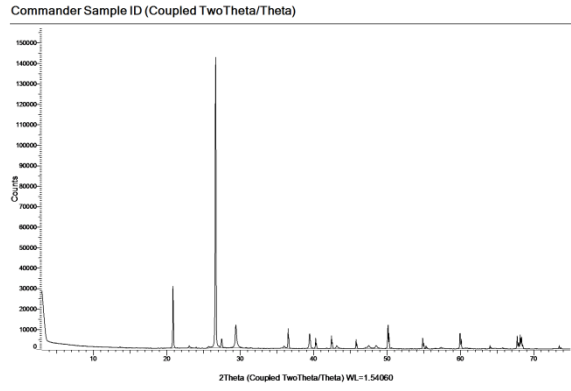
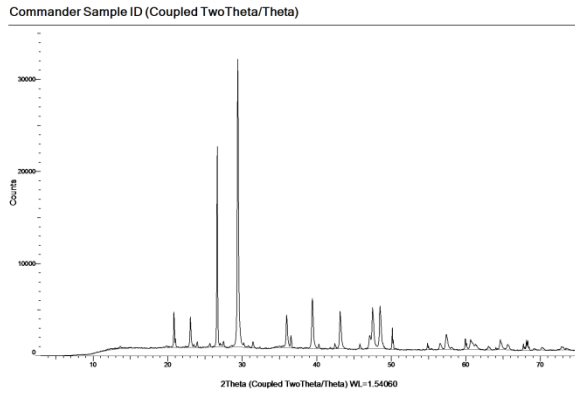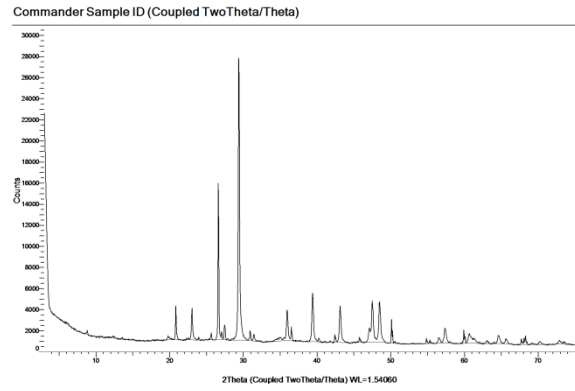Figure 8. XRD diffractogram of MRBTb1-7.
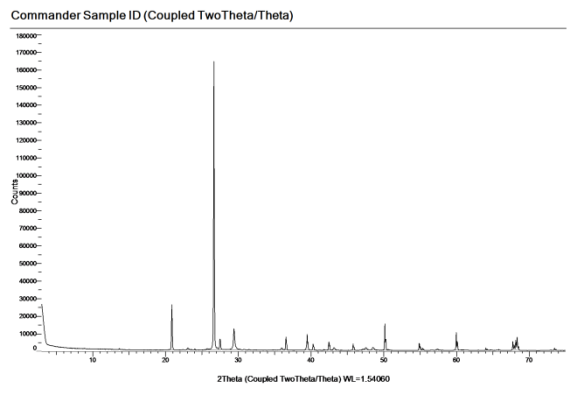
Figure 9. XRD diffractogram of MRBTb1-8.
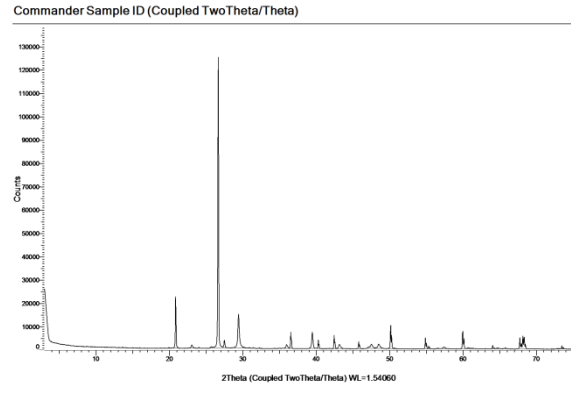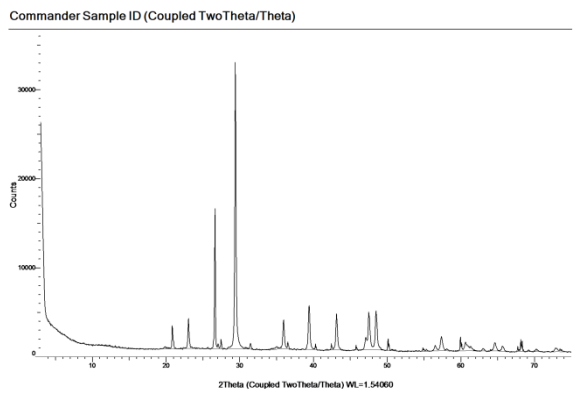

Figure 10. XRD diffractogram of MRBTb1-9.
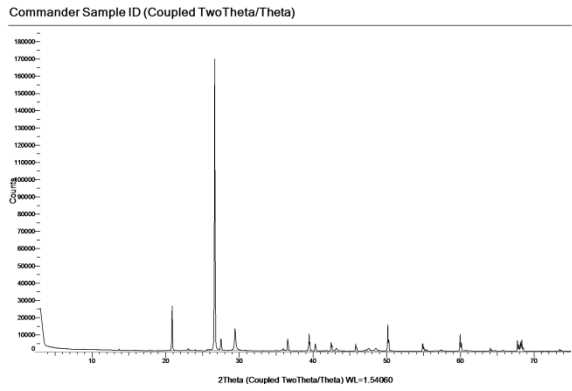
Figure 11. XRD diffractogram of MRBTb2-10.
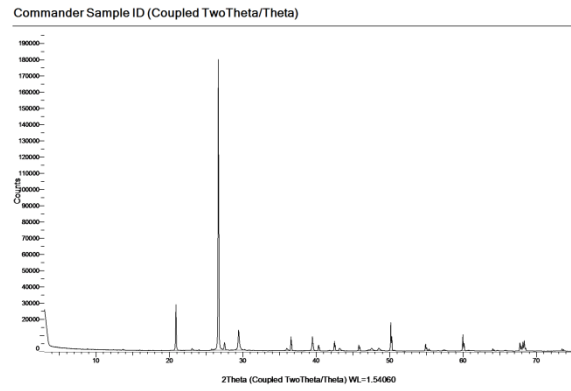
Figure 12. XRD diffractogram of MRBTb2-11.
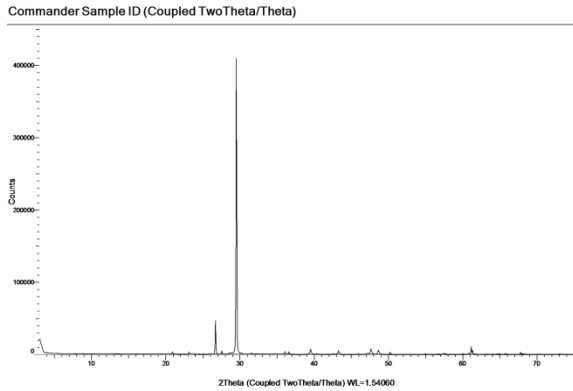
Figure 13. XRD diffractogram of MRBH3-12E.
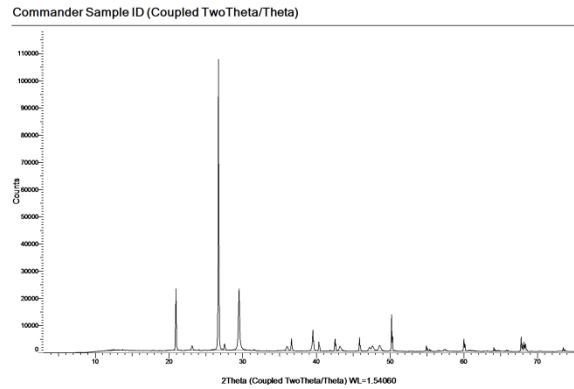
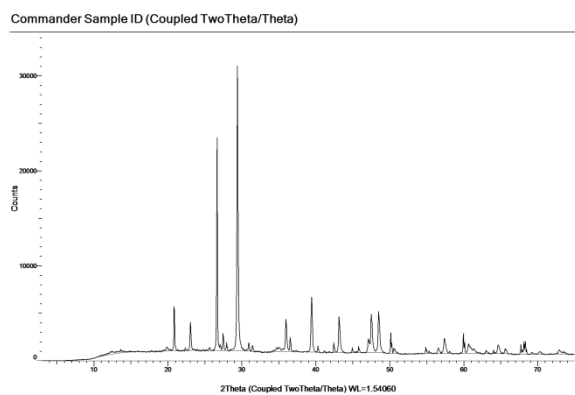Figure 14. XRD diffractogram of MRBH3-12I.
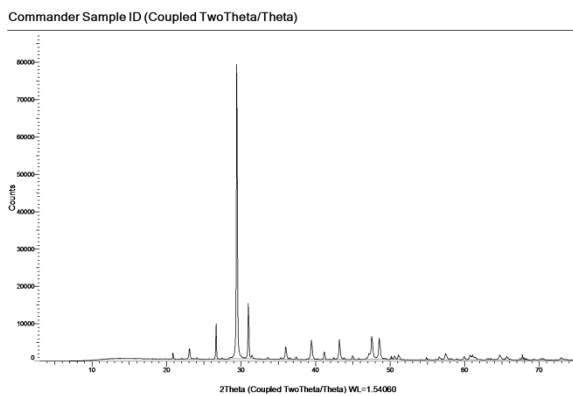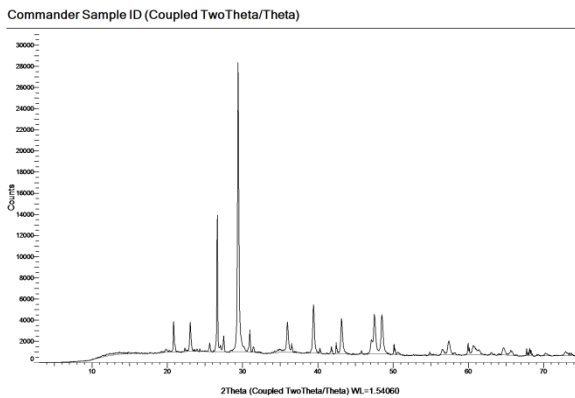

Figure 5. XRD diffractogram of MRBH7-13BE.
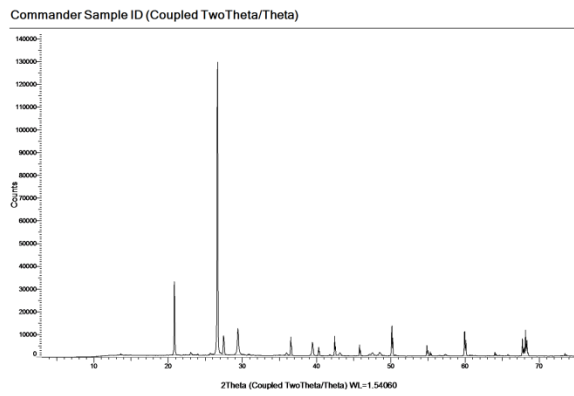
Figure 16. XRD diffractogram of MRBH7-13BI.
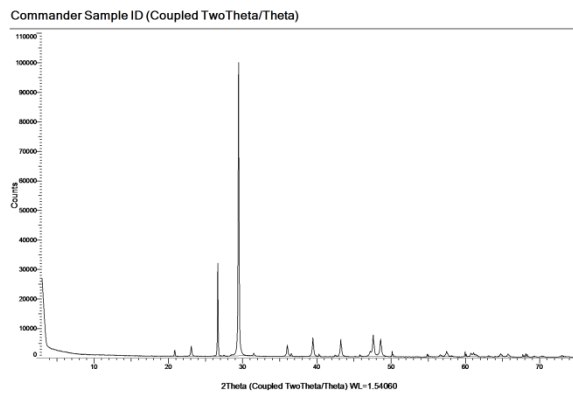
Figure 17. XRD diffractogram of MRBH7-13VE.
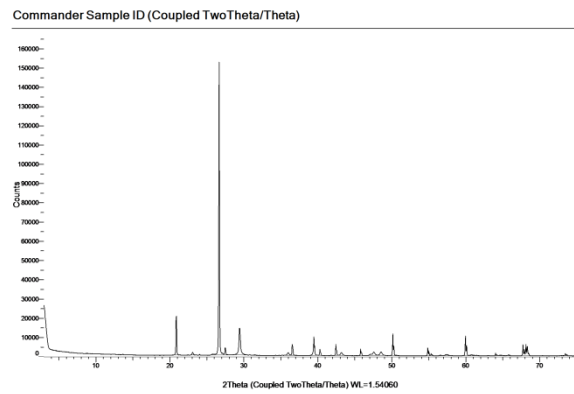
Figure 18. XRD diffractogram of MRBH7-13VI.
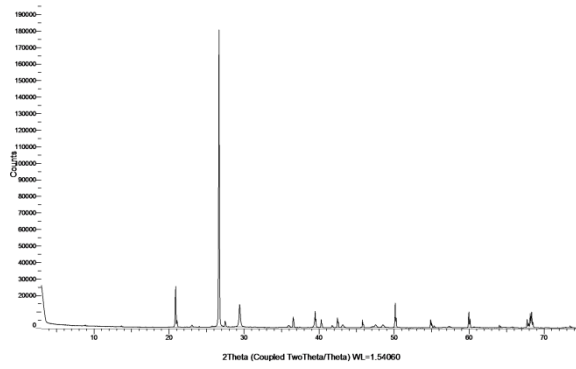
MRBH7-14
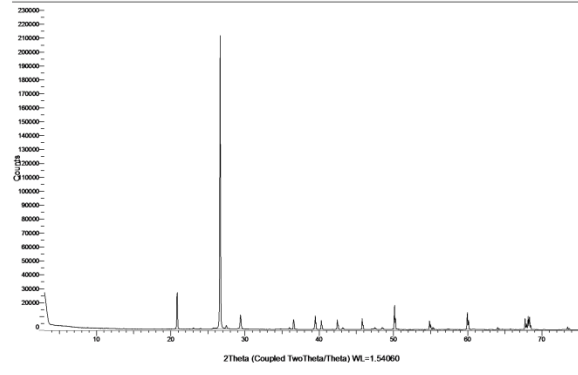
MRBM-15
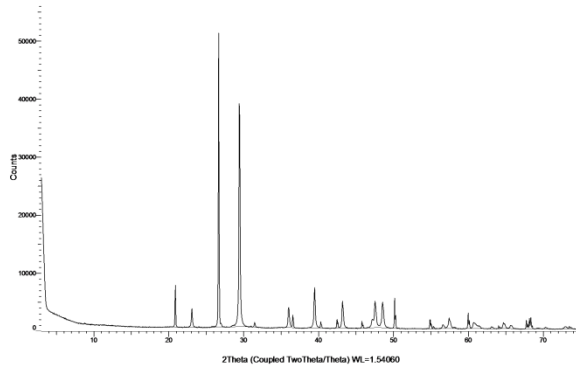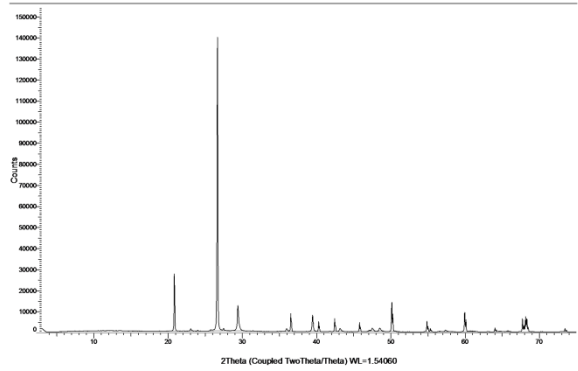
MRBF-16E

MRBF-16I

Annex 3.7. Powder X-Ray Diffraction (XRD) Diffractograms (Fine Fraction)
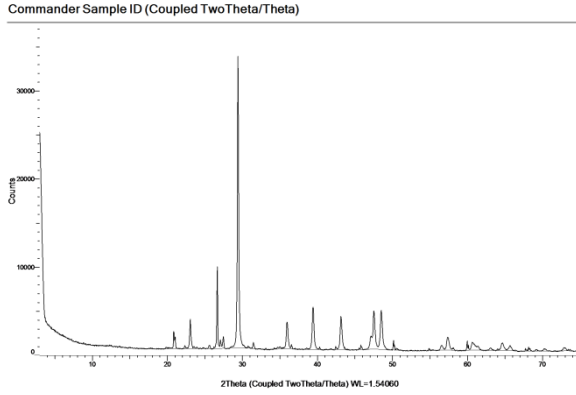
Figure 1. XRD diffractogram of MRBT-1I.
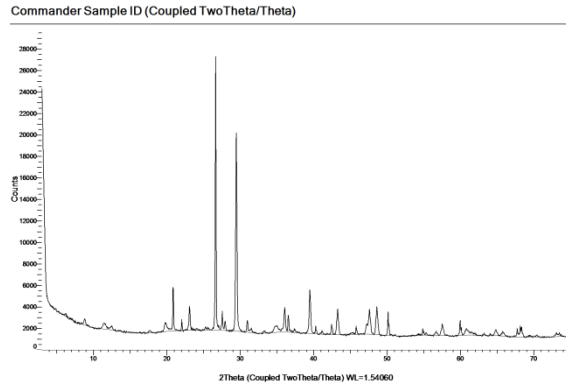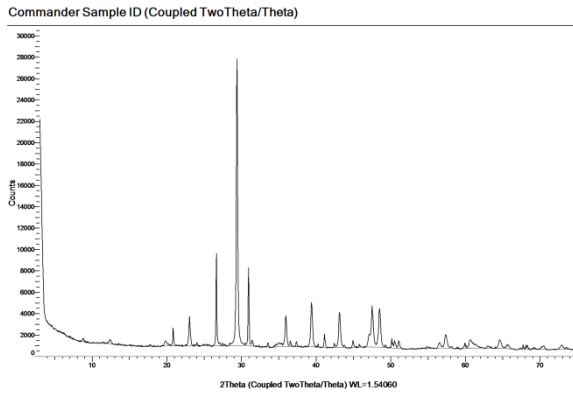
Figure 2. XRD diffractogram of MRBT-2E.

Figure 3. XRD diffractogram of MRBT-2I.

Figure 4. XRD diffractogram of MRBD3-3.

Figure 5. XRD diffractogram of MRBD3-4.

Figure 6. XRD diffractogram of MRBD4-6.

Figure 7. XRD diffractogram of MRBTb1-7.

Figure 8. XRD diffractogram of MRBTb1-8.

Figure 9. XRD diffractogram of MRBTb2-10.

Figure 10. XRD diffractogram of MRBTb2-11.
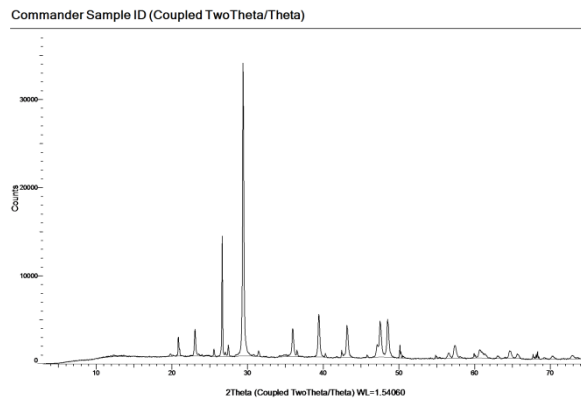

Figure 11. XRD diffractogram of MRBH7-13BI.
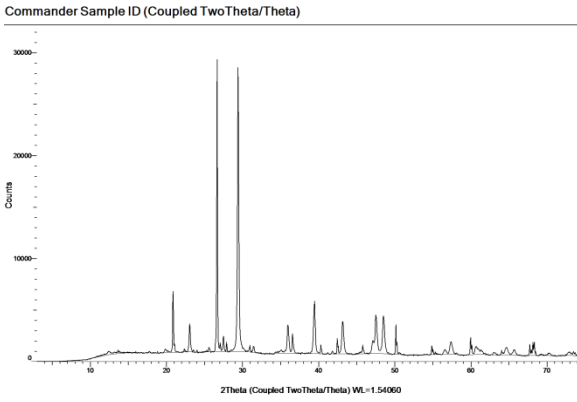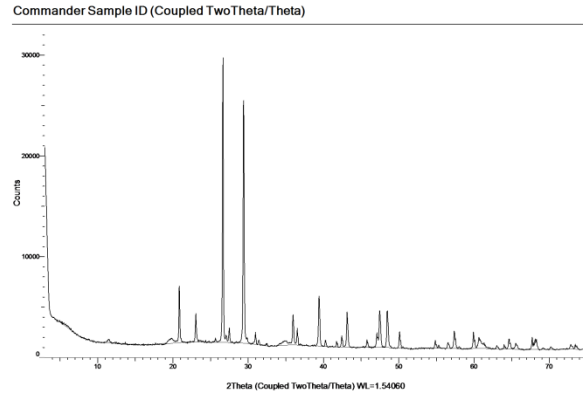

Figure 12. XRD diffractogram of MRBH7-13VI.

2Theta (Coupled TwoTheta/Theta) WL=1.54060

Figure 13. XRD diffractogram of MRBH7-14.

2Theta (Coupled TwoTheta/Theta) WL=1.54060

Figure 14. XRD diffractogram of MRBM-15.
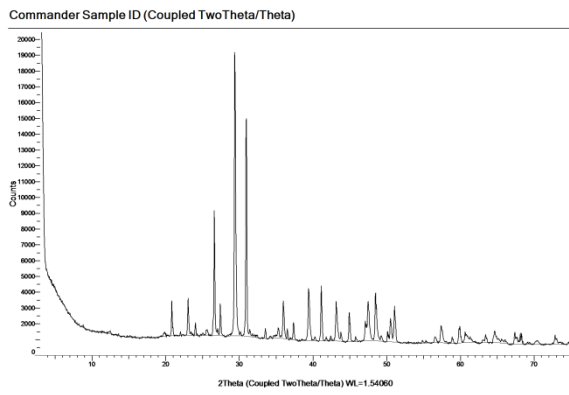
2Theta (Coupled TwoTheta/Theta) WL=1.54060
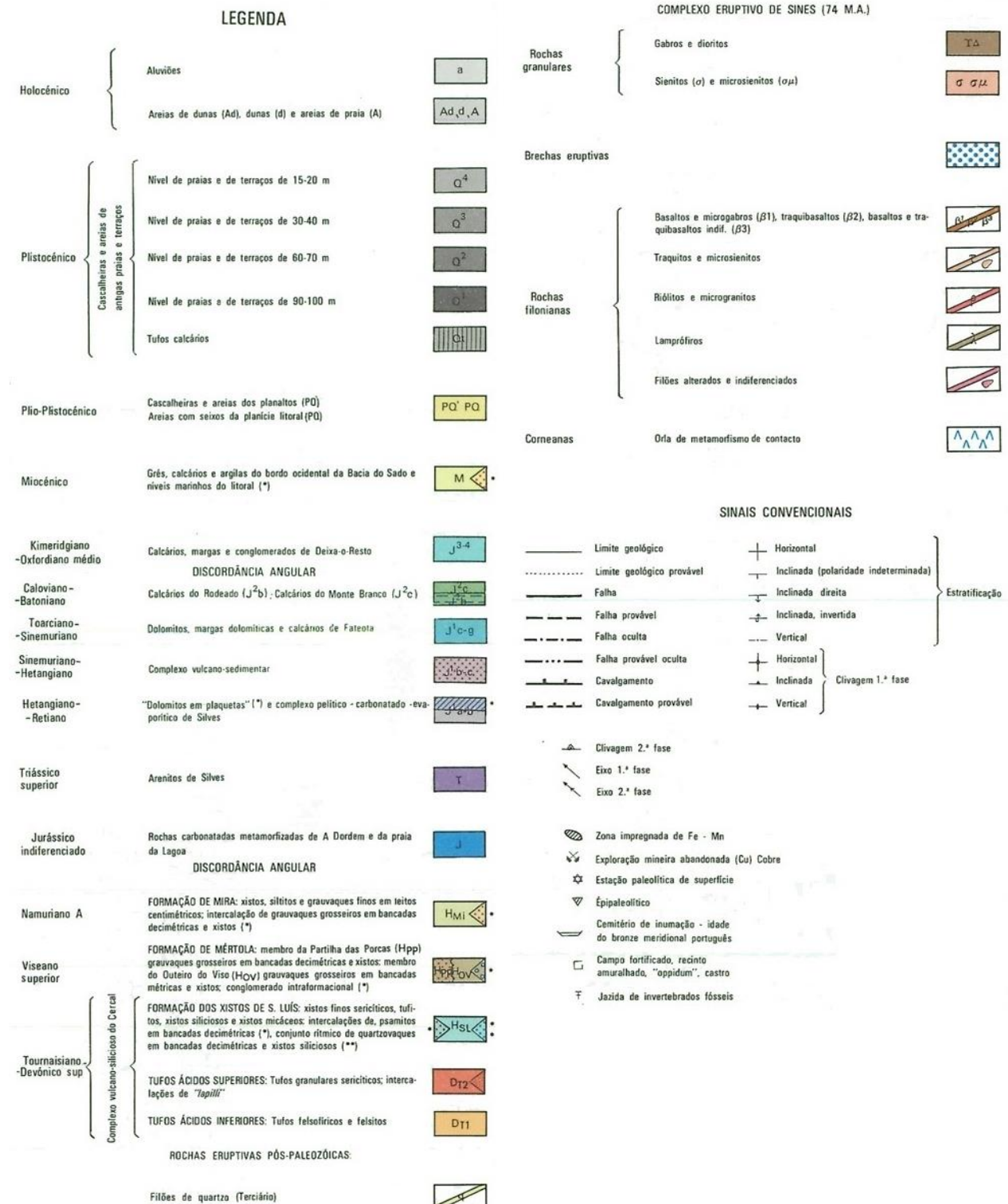
Figure 15. XRD diffractogram of MRBF-16I.

Annex 4.1. Legend for Figure 4.1.

Figure 1. Legend for Figure 4.1. [taken and adapted from *Laboratório Nacional de Energia e Geologia* (LNEG), http://geoportal.lneg.pt/geoportal/mapas/index.html]

Annex 4.2. The Chemical Characteristics of Historic Mortars as Derived from Thermogravimetric Analysis

Table 1. The Chemical Characteristics of Historic Mortars as Derived from Thermogravimetric Analysis (taken from Moropoulou, 2005, p. 297).

Table 1
Chemical characteristics of historic mortars as deriving from thermogravimetric analysis

Mortar type	Physically bound water (%)	Structurally bound water (%)	$CO_2\%$	CO_2/structurally bound water
Lime mortars	<1	<3	>32	10^a, 7.5–10^b
Lime mortars with unaltered portlandite	>1	4–12	18–34	1.5–9
Hydraulic lime Mortars	>1	3.5–6.5	24–34	4.5–9.5
Natural pozzolanic mortars	4.5–5	5–14	12–20	<3
Artificial pozzolanic mortars	1–4	3.5–8.5	22–29, 10–19^c	3–6

[a] Aggregates of calcareous nature.
[b] Aggregates of silicoaluminate nature.
[c] Byzantine "concrete".